IDENTIFYING EVIDENCE FOR EXPLOSIVE VOLCANISM ON MARS THROUGH GEOMORPHOLOGIC AND THERMOPHYSICAL OBSERVATIONS

by

Gabriel Cecilio Garcia

A thesis

submitted in partial fulfillment

of the requirements for the degree of

Master of Science in Geosciences

Boise State University

May 2018

BOISE STATE UNIVERSITY GRADUATE COLLEGE

DEFENSE COMMITTEE AND FINAL READING APPROVALS

of the thesis submitted by

Gabriel Cecilio Garcia

Thesis Title: Identifying Evidence for Explosive Volcanism on Mars through Geomorphologic and Thermophysical Observations

Date of Final Oral Examination: 24 January 2018

The following individuals read and discussed the thesis submitted by student Gabriel Cecilio Garcia, and they evaluated his presentation and response to questions during the final oral examination. They found that the student passed the final oral examination.

Brittany D. Brand, Ph.D.	Chair, Supervisory Committee
Joshua L. Bandfield, Ph.D.	Member, Supervisory Committee
Jennifer L. Pierce, Ph.D.	Member, Supervisory Committee

The final reading approval of the thesis was granted by Brittany D. Brand, Ph.D., Chair of the Supervisory Committee. The thesis was approved by the Graduate College.

DEDICATION

I dedicate this thesis to my parents. Their love and support has provided me the opportunity to strive for greatness and live a life that I can truly be proud of. No matter where I go, I will always live by your example.

ACKNOWLEDGEMENTS

I would like to thank my advisors, Brittany Brand and Joshua Bandfield, for all they have helped me with. I would not be the scientist I am now without their guidance and teachings. I would also like to thank the Idaho Space Grant Consortium for funding this research. I would like to acknowledge all the friends I have made at Boise State and the Environmental Research Building for their support and encouragement when writing seemed daunting. Lastly, I would like to thank coffee. Our love may be new, but you were always with me for the late nights and early mornings. Thank you.

ABSTRACT

Accurately identifying the products of explosive volcanism on Mars is critical for unraveling the evolution of the martian crust and interior. Recent work using high-resolution datasets suggest explosive volcanic processes may have dominated over effusive activity in early martian history. However, distinguishing the products of explosive volcanism from non-volcanic sediments remains challenging since both are similar in thermophysical and geomorphologic datasets.

The objective of this study is to identify geomorphologic and thermophysical characteristics of possible explosive volcanic deposits on Apollinaris Mons, one of the best-known candidates for explosive volcanism on Mars, using visible and thermal infrared imaging datasets. These geomorphic and thermophysical characteristics are compared to terrestrial volcanic analogs to more accurately identify evidence for explosive volcanism on Mars. Deposits that best exemplify explosive volcanism on Apollinaris Mons are then applied to Arabia Terra, an area of Mars controversially proposed to contain explosive volcanic calderas.

The primary indicators that Apollinaris Mons is volcanic are the summit caldera and surrounding edifice, which resemble caldera complexes on Earth. Thermal inertia values throughout the Apollinaris Mons region are low (~90 $J \cdot m^{-2} \cdot K^{-1} \cdot s^{-1/2}$), consistent with fine-particulate and weakly-indurated material at the surface. In addition, the flank is dissected by numerous drainages, further suggesting a composition of weakly-consolidated material. Outcrop-scale findings include planar bedding, cross-bedding, and

breccia deposits within exposed crater walls along the debris fan and within the caldera. Breccia deposits are also present along a valley wall on the southwestern flank, where boulders grade from coarser to finer with distance from the caldera wall. Planar bedding could be consistent with fall deposits, or discrete lateral flow events. Cross-bedding is consistent with traction transport in dilute mass flows, such as dilute pyroclastic density currents. However, such cross-bedding could also be formed due to truncation of earlier deposits by later erosive flows. Breccias also form during mass flows, such as concentrated pyroclastic density currents, debris avalanches or debris flows. Gradation of blocks down slope is further evidence for lateral transport since heavier blocks are dropped out of the flow at more proximal regions due to decreasing carrying capacity with distance from source. The combined evidence of a caldera with a prominent edifice, the regional low thermal inertia, and presence of extensive friable deposits with evidence of lateral transport away from the caldera supports an explosive volcanic history for Apollinaris Mons. This study revealed no evidence for past effusive activity (high strength materials), although current data limitations prevent access to the entire volcanic history.

Evidence for explosive volcanism on Apollinaris Mons is applied to three proposed calderas in Arabia Terra, named Eden, Ismenia, and Siloe Paterae, to test a previously published and controversial hypothesis that they are volcanic in origin. Like Apollinaris Mons, thermal inertia values of the proposed Arabia Terra calderas are consistently low. However, unlike Apollinaris Mons, the proposed calderas are at the same level as the surrounding topography, and lack a positive edifice. Concentric fracturing surrounding some of the proposed calderas, while consistent with ring-

fractures at volcanic calderas, is not unique to volcanic collapse. As such, while there is evidence that the Arabia Terra depressions experienced collapse, the mechanism for collapse cannot be tied directly to volcanism.

Bedding found within the proposed caldera walls and plateaus resembles those found on Apollinaris Mons in that it is friable in nature and of a similar scale. However, since the bedding was not found within an obvious edifice, it cannot be directly related to the proposed caldera or mechanism for collapse. No primary volcanic features, such as high strength materials (i.e., lava flows) are found within the proposed caldera floors. Rectilinear fracturing and chaotic terrain are identified in patches along the floor of the proposed calderas; however, neither of these morphologies are consistent with features found within Apollinaris Mons or terrestrial calderas.

The proposed calderas more closely resemble the dewatering style collapse features present within the Circum-Chryse region of Mars. Dissected, polygonal-shaped plateau structures within the proposed caldera interiors are consistent with large, fractured fault blocks common to dewatering collapse features, but not terrestrial calderas. The morphologic similarities between Circum-Chryse and Arabia Terra would suggest the proposed calderas are instead impact craters that experienced subsequent collapse following the removal of subsurface water.

This research demonstrates that geomorphologic and thermophysical observations of large-scale and fine-scale features can be combined to determine volcanic and non-volcanic origins of structures on Mars. However, without sufficient geologic context such as a volcanic edifice, distinguishing volcaniclastic materials from other sedimentary deposits on Mars remains a challenge. It is still possible that the bedded, friable deposits

exposed within Arabia Terra have a volcanic origin; however, the source has yet to be identified. In conclusion, careful and detailed geologic mapping, when compared with terrestrial analogs, can lend insight into the geologic history of Mars.

TABLE OF CONTENTS

LIST OF TABLES

LIST OF FIGURES

LIST OF ABBREVIATIONS

CTX	Context Camera
JMARS	Java Mission-planning and Analysis for Remote Sensing
MFF	Medusae Fossae Formation
HiRISE	High Resolution Imaging Science Experiment
MOLA	Mars Orbital Laser Altimeter
TES	Thermal Emission Spectrometer
THEMIS	Thermal Emission Imaging System
TIU	Thermal Inertia Units

CHAPTER ONE: INTRODUCTION

1.1 Objective

Accurately identifying the products of effusive versus explosive volcanism on Mars is critical for unraveling the evolution of the martian crust and interior. The nature of martian volcanism also has implications for the development of an early atmosphere as volcanic eruptions pump gas, such as water vapor, carbon dioxide, and sulfur dioxide, into the atmosphere (e.g., Self, 2006). On Earth, accurately identifying effusive versus explosive volcanic deposits is straightforward because we can make direct observations and measurements in the field and laboratory. On Mars, however, we rely on remote satellite measurements, which make differentiating effusive versus explosive volcanic products challenging.

The difficulty in identifying explosive volcanism is that possible volcaniclastic materials resemble non-volcanic clastic sediments in both thermophysical and geomorphologic datasets. Thus, determining the style and extent of volcanic features on Mars remains a challenge. Furthermore, dust mantles much of the martian surface, obscuring the visibility of primary surface textures and thermophysical properties of the substrate. However, geomorphologic and thermophysical observations of exposed valley and crater wall outcrops provides a technique for bypassing dust mantled surface (Bandfield et al., 2013).

The objectives of this study are to investigate large-scale morphologies and outcrop-scale deposit characteristics that can be used to identify explosive volcanic

deposits on Mars. I will then apply the distinguishing characteristics to a series of proposed calderas in the Arabia Terra region of Mars to test the hypothesis that they are volcanic in nature. My work will consist of three tasks: (1) identify possible distinguishing characteristics of explosive volcanic deposits on Mars using remote sensing data of Apollinaris Mons, a volcanic edifice on Mars with a high likelihood of an explosive eruption history (Kerber et al., 2011; Robinson et al., 1993), (2) compare terrains and surface textures on Apollinaris Mons with terrestrial analogs to further constrain the characteristics of wind-eroded volcanic deposits, and (3) apply findings from Apollinaris Mons and Earth-based analogs to test the hypothesis that anomalous depressions in the Arabia Terra region of Mars are volcanic in origin.

1.2 Previous work

Terrestrial volcanism varies between effusive lavas and explosive eruptions (e.g., Self, 2006), where eruptive style is dependent on magma composition and volatile content (e.g., Francis, 1993). Magmas with lower silica content (mafic) are less viscous (Hulme, 1974), and any exsolved volatiles in the magma can more readily escape, allowing for more effusive eruptions of lava (Vergniolle & Jaupart, 1986). Mild explosivity in mafic magmas (from increased volatile content) produce fire fountaining in what is known as Hawaiian or Strombolian eruptions (named after the locations this type of activity frequently occurs). Higher silica content within a magma (felsic) increases viscosity and hinders movement of vesiculated gasses (Woods, 1995). During ascent of these silicic magmas, bubble growth leads to rapid expansion and fragmentation of the magma, causing a more explosive eruption that produces pyroclastic materials in the form of ash columns and pyroclastic flows (Gardner et al., 1999). Explosive eruptions

also occur through magma interaction with sources of groundwater, shallow lakes, and oceans, known as phreatomagmatic eruptions (Brand & Heiken, 2009).

Volcanism on Mars is proposed to be primarily mafic in composition, based on multiple lines of morphologic and compositional evidence consistent with terrestrial mafic volcanism. Surface morphologies of volcanic terrains are consistent with effusive lavas from large shield volcanoes (Basaltic Volcanism Study Project, 1981 ;Carr, 1973; Francis & Wood, 1982; Mouginis-Mark, 1992). Satellite data has provided the mineral composition of the martian surface, indicating basaltic compositions (e.g., Bandfield, 2002). In situ measurements from rover and lander data, as well as martian meteorites, are also consistent with basaltic compositions (Baird et al., 1976; Banin et al., 1992; McSween, 1985; Ruff et al., 2006). While intermediate and high silica bearing rocks have been identified on the surface (Bandfield et al., 2000, 2004; Bandfield, 2008; Christensen et al., 2005), suggesting magma evolution processes like those on Earth, their occurrence is limited and not reflective of the dominant crust composition.

Identifying volcanic structures on Mars, or their deposits, has largely been controlled by the spatial resolution of the data available at the time. In the early years of martian research, the low spatial resolution of satellite images was primarily useful for describing large-scale features such as volcanic edifices, canyons, and smooth or cratered terrain. In 1971, Mariner 9 became the first artificial satellite to orbit Mars, providing the first glimpse of the entire martian surface at 1 km per pixel and nearly 2% of the planet at 100 m per pixel samplings (Masursky, 1973). Lacking ridges and faults that may be associated with plate tectonics, Carr (1973) suggested that Mars has a fixed crust that resulted in volcanic structures analogous to terrestrial shield volcanoes and plains

commonly found within intraplate settings. Because most current volcanic centers on Mars are large shield volcanoes, and a relative lack of features resembling terrestrial composite volcanoes, it was assumed that martian volcanic activity produced primarily effusive lavas (Basaltic Volcanism Study Project, 1981; Carr, 1973; Greeley & Spudis, 1981; Robinson et al., 1993). However, the identification of erosional channels and blanketed surfaces along volcanic flanks led some to suggest these volcanic features to be comprised of poorly-consolidated materials, consistent with explosive activity (Mouginis-Mark et al., 1982; Reimers & Komar, 1979).

Large volcanic plains characterized by shield volcanoes and complex caldera structures were recognized and grouped into two primary provinces: Tharsis and Elysium (Platz et al., 2015); isolated volcanic features also exist outside of these two provinces and have been labeled as martian paterae (Crown & Greeley, 1993; Greeley & Spudis, 1981). The reduced gravity, and lack of evidence for plate tectonics, result in volcanic features on Mars larger than their terrestrial counterparts (Carr, 1973). Morphologic similarities between Mars volcanoes and terrestrial examples of basaltic volcanoes supported the idea of primarily mafic products on Mars (Carr, 1973). Composite volcanoes, more common along plate boundaries, that typically produce felsic eruptions of lavas and pyroclasts on Earth were suggested to be absent on Mars, further implicating a fixed martian crust (Carr, 1973). Later studies eventually proposed the existence of composite volcanoes, resulting from a mix of explosive and effusive deposits (Robinson et al., 1993).

Large-volume explosive activity in mafic systems is not common on Earth because lower magma viscosities permit degassing (e.g., Wilson & Head, 1983).

However, the lower atmospheric pressures and gravity on Mars can facilitate more explosive eruptions in basaltic magmas by increasing magma ascent rates (Wilson & Head, 1983). Morphologic evidence that suggests the presence of explosive volcanism on Mars includes cones that resemble volcanic cinder cones on Earth, blanketed terrain likely resulting from ashfall, channelized volcanic flanks indicative of weakly-indurated material, flank angles interpreted to form from pyroclastic flows, and possible large-volume pyroclastic flow deposits (; Crown & Greeley, 1993; Greeley & Crown, 1990; Greeley & Spudis, 1981; Mouginis-Mark et al., 1988; Reimers & Komar, 1979; West, 1974; Wilson & Mouginis-Mark, 1987). These research efforts have led some to believe ancient volcanism on Mars was primarily explosive and transitioned to effusive later in martian history (Bandfield et al., 2013; Ivanov & Head, 2006; Mouginis-Mark et al., 1988; Reimers & Komar, 1979; Robbins et al., 2011; West, 1974).

Reimers and Komar (1979) suggest pyroclastic activity to be a dominant style of volcanism in early martian history based on morphologic similarities of some martian volcanoes to terrestrial cones and composite volcanoes. They suggest the source for explosive activity could have been phreatomagmatic in nature. For example, subsurface ice, possibly melted by regional volcanic activity, could lead to phreatomagmatic explosive volcanism. Any recycling of water back into the subsurface would have prolonged phreatomagmatic activity. Depletion of the martian hydrosphere would cause a transition of martian volcanism to a more effusive eruption style. Robbins et al. (2011) dated all major calderas on Mars and determined that volcanoes that include more friable deposits (consistent with pyroclastic deposits) pre-dated the more recent effusive activity on the large shields in Tharsis and domes in Elysium. While pyroclastic activity appears

to terminate or shift at various times, the general decrease in explosive activity occurred along the Hesperian–Amazonian boundary, ~3.5 Ga ago (Robbins et al., 2011).

Bandfield et al. (2013) test the hypothesis that early volcanism on Mars was primarily explosive by analyzing geomorphologic and thermophysical observations of the martian crust. To avoid interference from mantling dust, they observe exposed outcrops along valley and crater walls, allowing for a more direct analysis of martian crust. They find that the martian crust appears to be comprised primarily of poorly consolidated, friable materials, except within younger volcanic terrains that show evidence for dominant high strength materials. Surfaces that appear friable break up easily, preserving shallower slopes. Boulders present with bedded outcrops break up a few hundred meters down slope, suggesting they are composed of poorly consolidated material. Thermal inertia of these friable materials have low values (<600 $Jm^{-2}K^{-1}s^{-1/2}$ or thermal inertia unit, TIU), also consistent with poorly consolidated materials. Conversely, high-strength deposits have high thermal inertia (>600 TIU), and rocky surfaces marked with boulders that persist more than 1 km down slopes. Based on these observations, Bandfield et al. (2013) suggest the crust is likely dominantly volcaniclastic in nature. This is consistent with previous studies that suggest early martian volcanism was more typically explosive in nature (Reimers & Komar, 1979; Robbins et al., 2011).

Gregg and de Silva (2009) use high resolution satellite imagery to investigate surface and outcrop textures on the flanks and channels of Tyrrhena Patera. This volcano is likely comprised of pyroclastic deposits, based on low angle flanks and dissecting channels (Crown & Greeley, 1993; Greeley & Spudis, 1981; Williams et al., 2008). The attempts to identify pyroclastic deposits were based on morphologies consistent with

layering, aeolian erosional features, and variable induration (Mandt et al., 2008). Observations made by Gregg and de Silva (2009) were inconclusive, as exposed outcrops in high resolution images are too shallow and mantled with dust. Identification of primary textures within the outcrops could not be determined. While Gregg and de Silva (2009) identify layering (100s of meters thick) along fresh impact crater walls and some of the flank materials, no attempts were made to determine the origins of the layered materials.

Apollinaris Mons is another martian volcano that likely experienced phases of explosive activity (Kerber et al., 2011; Robinson et al., 1993). Apollinaris Mons is characterized by a volcanic edifice with flank slopes between 1°—35° (with the steeper slopes along the western flank), which Robinson et al. (1993) attribute to alternating effusive and explosive activity. The southern flank of the volcano is characterized by a debris apron, marked by km-wide channels that radiate from the top of the apron. These dissecting channels suggest erosion through friable materials (Gulick & Baker, 1990). The regional Medusae Fossae Formation (MFF) adjacent to the volcanic edifice is also interpreted to be pyroclastic in nature (Malin, 1979; Mandt et al., 2008; Scott & Tanaka, 1982, 1986). While the origins are still debated, some have proposed Apollinaris Mons to be a likely source for the MFF deposits (Kerber et al., 2011).

Arabia Terra is an ancient landscape on Mars that dates to the mid- to late Noachian Era, ~3.7—3.9 Ga (Michael, 2013; Tanaka et al., 2014). The morphology of Arabia Terra is characterized by degraded craters and linear ridges within the intra-crater plains. These linear ridges, also known as wrinkle ridges, are a common feature on Mars and have been interpreted to represent tectonic deformation of the surface (Greeley & Spudis, 1981). Dust mantles much of the highland material in the central region of Arabia

Terra, based on the high albedo and low thermal inertia (e.g., Fergason & Christensen, 2008).

Layered deposits are common within the Arabia Terra region, which have been proposed to originate from accumulated dust deposits, ocean sediments, or volcanic sills (e.g., Edgett & Parker, 1997; Grant & Schultz, 1990; Greeley & Guest, 1987; Moore, 1990; Schultz & Lutz, 1988; Wilhelms & Baldwin, 1988). Other studies suggest the source of these layered deposits may originate from explosive volcanism, such as volcanic ash fall (e.g., Fassett & Head, 2007; Hynek et al., 2003; Kerber et al., 2012; Michalski & Bleacher, 2013; Moore, 1990; Scott & Tanaka, 1986). Of these works, Michalski and Bleacher (2013) suggest the source of the layered deposits resulted from explosive volcanic calderas within the Arabia Terra region. The proposed calderas in Arabia Terra are large depressions 10s of kilometers wide, with depths greater than 1 km. These proposed calderas lack a defining edifice structure, and are interpreted by Michalski and Bleacher (2013) to represent a new class of martian volcanic construct, plains-style calderas.

1.3 Motivation

While previous research has identified thermophysical and large-scale evidence for explosive volcanism on Mars (Bandfield et al., 2013; Reimers & Komar, 1979; Robbins et al., 2011), few attempts have been made to identify outcrop-scale evidence for volcaniclastic materials on known martian volcanoes (Gregg & de Silva, 2009). The objective of this study is to investigate large-scale morphologies and outcrop-scale deposit characteristics of Apollinaris Mons that can be used to identify explosive volcanic deposits on Mars. The steeper flanks of Apollinaris Mons are likely to provide good

valley- and crater wall exposures that are relatively dust free. Bandfield et al. (2013) have shown that thermal inertia can be used to distinguish high-strength material from potential pyroclastic debris. These exposures offer more direct thermophysical and geomorphologic observations of the Apollinaris Mons subsurface, and thus volcanic history.

I will apply the distinguishing characteristics identified on Apollinaris Mons to a series of proposed calderas in the Arabia Terra region of Mars to test the hypothesis that they are volcanic in nature. High resolution datasets have provided the opportunity to study surface features in greater detail that was previously unavailable when preliminary evidence for martian explosive volcanism was identified. With little regional evidence for volcanism in Arabia Terra, comparative analyses will lend insight into the characteristics of explosive volcanic deposits in martian remote sensing datasets, and if they differ from terrestrial deposits that form from explosive volcanism.

1.4 Methods

1.4.1 Instrumentation and analytical techniques

Four satellite instruments onboard three different spacecrafts make up the bulk of analytical tools used for morphologic observations. The Mars Orbiter Laser Altimeter (MOLA), on the Mars Global Surveyor spacecraft, provides quantitative elevation data at 256 pixels per degree (Smith et al., 2001). The Thermal Emission Imaging System (THEMIS) aboard the Mars Odyssey spacecraft provides day and night global infrared mosaics for large-scale regional observations at 100 m per pixel sampling (Christensen et al., 2004). Two instruments on the Mars Reconnaissance orbiter, Context Camera (CTX) and High-Resolution Imaging Science Experiment (HiRISE), are used to describe fine-

scale surface texture and morphology (Malin et al., 2007; McEwen et al., 2007). Spatial sampling of CTX and HiRISE are ~5.5 m and ~0.25—0.5 m per pixel sampling respectively. These datasets are viewed and analyzed using Arizona State University's Java Mission-planning and Analysis for Remote Sensing software (JMARS; Christensen et al., 2009).

Thermophysical data is derived from THEMIS nighttime infrared temperature data to measure thermal inertia. Thermal inertia is defined as resistance to changes in temperature of a material, with respect to energy input, and is dependent on the particle size and degree of consolidation within the top few centimeters of the subsurface (Fergason et al., 2006; Presley, 2002). Thermal inertia is expressed quantitatively as: $I=(\kappa\rho c)^{1/2}$, where I is thermal inertia, k is thermal conductivity, ρ is bulk density, and c is specific heat capacity of a material. Units of thermal inertia are given in $J/m^2s^{1/2}K$, which are referred to as TIU (thermal inertia units) through this paper.

Surfaces with high thermal inertia values are comprised of high-strength, well-consolidated materials (>600 TIU), while weakly-consolidated, particulate material have low thermal inertias (<600 TIU). For example, mantling dust has a low thermal inertia, while reworked materials from impact-crater ejecta can have either a high or low thermal inertia, depending on the properties of the impacted surface. Figure 1.1 is an example of low thermal inertia impact-crater ejecta, embaying high-strength bedrock. The Thermal Emission Spectrometer (TES; Christensen et al., 1992) onboard Mars Global Surveyor will provide global thermal inertia maps, at lower thermal inertia spatial resolutions (Mellon et al., 2000). Thermophysical data from THEMIS and TES also provide context

to the relative abundance of dust on a surface within each image (Bandfield, 2002; Fergason et al., 2006).

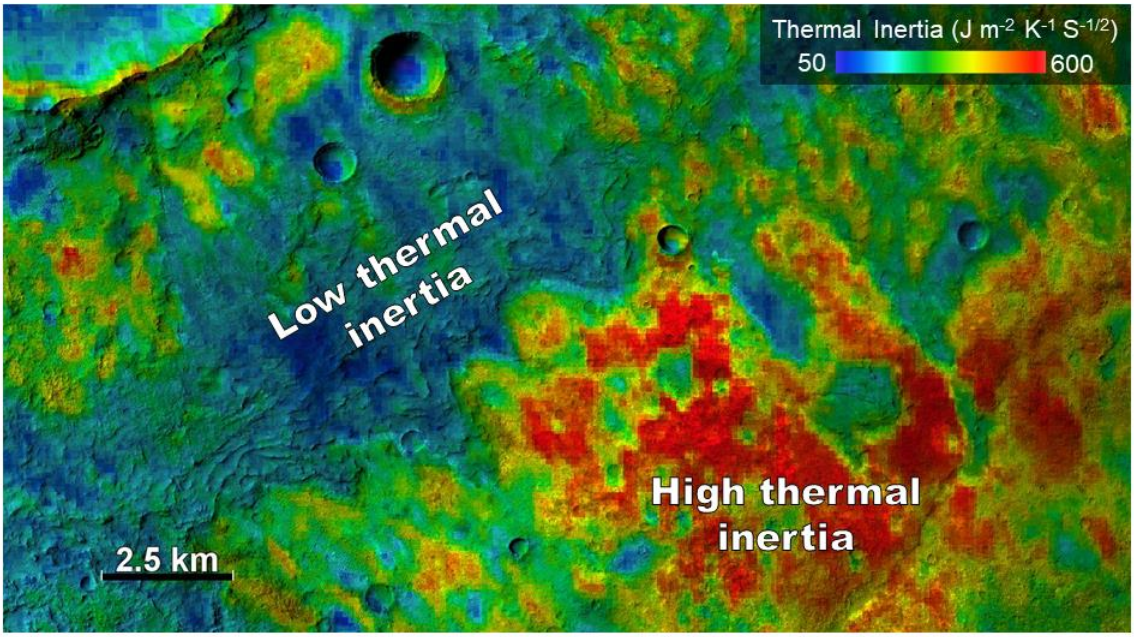

Figure 1.1 THEMIS derived thermal inertia data with CTX data used for shading. Impact crater ejecta is comprised of reworked materials, that are poorly-consolidated. Thermal inertia of the ejecta deposit is low, and contrasts the high thermal inertia of the bedrock surface that the impact-crater (upper left) is embayed in.

Thermophysical and morphologic data are combined to more accurately determine surface textures and degree of induration. MOLA elevation data are used to determine slope angles that further constrain deposit consolidation; crater and valley walls comprised of coherent bedrock and lavas will maintain steeper slope angles than poorly-consolidated, friable deposits (Schultz, 2002). Average slope angles in images below MOLA resolution are calculated by taking the inverse tangent of relief over distance (Figure 1.2). Fine-scale feature dimensions (10s—100s of meters) are calculated from solar incidence angles in CTX and HiRISE images, by measuring cast shadows

(Figure 1.2). Percent coverage of terrains or features are measured using the point counting technique.

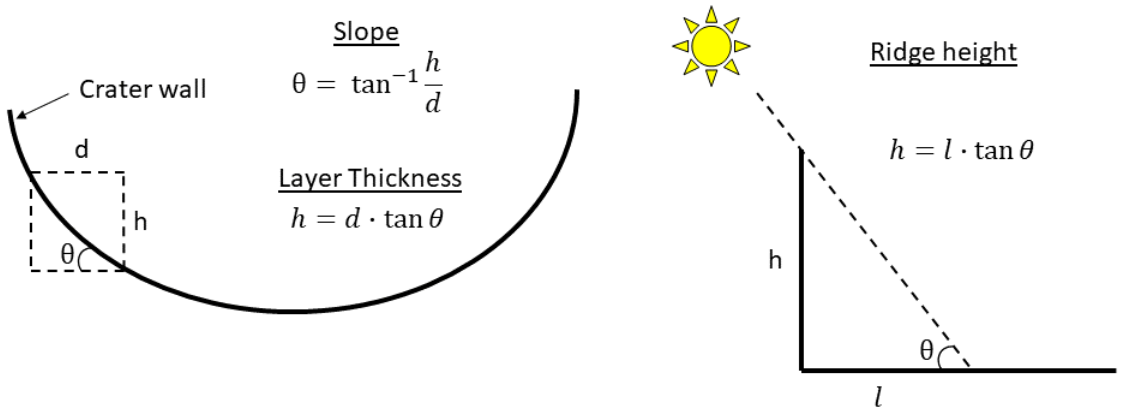

Figure 1.2 Illustration demonstrating the analytical techniques used to determine slope, layer thickness, and ridge height from images below MOLA resolution. As illustrated in the figure, the slope of a crater wall, for example, are not always constant. Thus, slope refers to the average slope between two points along the wall.

1.4.2 Definition of terminology

Some of the terms used to describe morphology, throughout this thesis, are genetic terms that imply a specific formational process on Earth. For our purposes, these terms are merely descriptive and meant only to aid in visualizing the features being described. For example, the term ‘terrace’ refers to remnants of stream or river floodplains, that often form flat step-like surfaces on Earth. Terrace is used in this thesis to describe broad, flat, step-like surfaces, not implying fluvial origins. The terms ‘mesa’ and ‘plateau’ are also used descriptively, and refer to isolated flat-topped hills or mounds. The difference between these features is the scale, with mesas refereeing to features 10’s of meters tall, and plateaus being 100’s of meters to 10’s of kilometers in size.

Aeolian activity is currently the most pervasive geologic process on Mars. Remote sensing datasets have provided evidence for both erosional and depositional

features on the martian surface including yardangs, dunes, ripples, and other aeolian features (Mccauley, 1973; Sagan et al., 1972). The main factors that control whether a feature is erosional or depositional is sediment size and availability, degree of induration or compaction, and strength and direction of local wind regimes. Because explosive volcanic deposits are comprised of rock of variable sizes (from meter sized boulders to ash sized particles) volcanic and non-volcanic terrains can be similarly modified by aeolian processes. All the deposits and features described in this thesis are erosional features, likely modifying deposits formed by other processes. For example, yardangs, elongated wind sculpted ridges carved into weakly-indurated material (Ward, 1979), are erosional features common on Mars, carved into deposits that may be volcanic in origin (Kerber et al., 2011; Malin, 1979; Mandt et al., 2008; Scott & Tanaka, 1982, 1986;). Examples of depositional aeolian features include dunes and ripples which can bury pre-existing surfaces.

CHAPTER TWO: IDENTIFYING EVIDENCE FOR EXPLOSIVE VOLCANISM

2.1 Introduction

2.1.1 Objective

Based on the easily erodible nature of the edifice, Apollinaris Mons is considered one of the most likely candidates for a dominantly explosive volcanic center on Mars (Kerber et al., 2011; Robinson et al., 1993). While large scale features have been mapped (Krysak, 2011; Robinson et al., 1993; Scott et al., 1993), there have been no attempts to identify outcrop scale (10s—100s of meters) evidence for explosive volcanic deposits.

The objective of this work is to test the hypothesis that Apollinaris Mons is an explosive eruptive center by identifying evidence consistent with pyroclastic deposits on the edifice at the large scale and outcrop scale (10's—100's of meters). I use geomorphologic and thermophysical observations to identity possible volcaniclastic deposits within the caldera and along the flanks of Apollinaris Mons. Morphologic and outcrop-scale features are compared to terrestrial pyroclastic deposits to constrain the similarities and differences between known volcanic terrains and proposed volcaniclastics on Mars. The deposits that best exemplify explosive activity can then be used as a standard for identifying explosive volcanism elsewhere on Mars (namely, Arabia Terra, discussed in greater detail in Chapter 3). Identifying explosive volcanism on Mars would suggest early Mars had more water in the lithosphere since water is one of the main volatiles that drives explosive volcanism on Earth (Self, 2006). This has

implications for the development an early martian atmosphere and may also further our understanding of the martian hydrosphere.

2.1.2 Apollinaris Mons

Apollinaris Mons is a volcano located along the dichotomy boundary, the transition zone between the young, smooth, northern lowlands and the ancient, cratered, southern highlands, at 174.1°E, 8.6°S (Figure 2.1A). Crater-based ages of Apollinaris Mons suggest the last eruptive activity occurred ~3.5—3.7 Ga, placing it between the late Noachian and early Hesperian boundary (Greeley et al., 2005; Hartmann, 2005; Robinson et al., 1993). The volcano covers an area of ~46,000 km^2, and consists of a caldera complex and an edifice. Apollinaris Mons is ~5 km tall and bound by a basal scarp an all sides, except along the southern flank, which is covered by a debris apron (Krysak, 2011). The slope of the flanks from the caldera rim to the basal scarp ranges from 3°—7°. Wide, semi-linear valleys dissect the flanks of Apollinaris Mons, especially along the large apron south of the caldera. The northeastern flank of the volcano displays plateau-like features, interpreted to represent remnants of groundwater sapping (El Maarry et al., 2012).

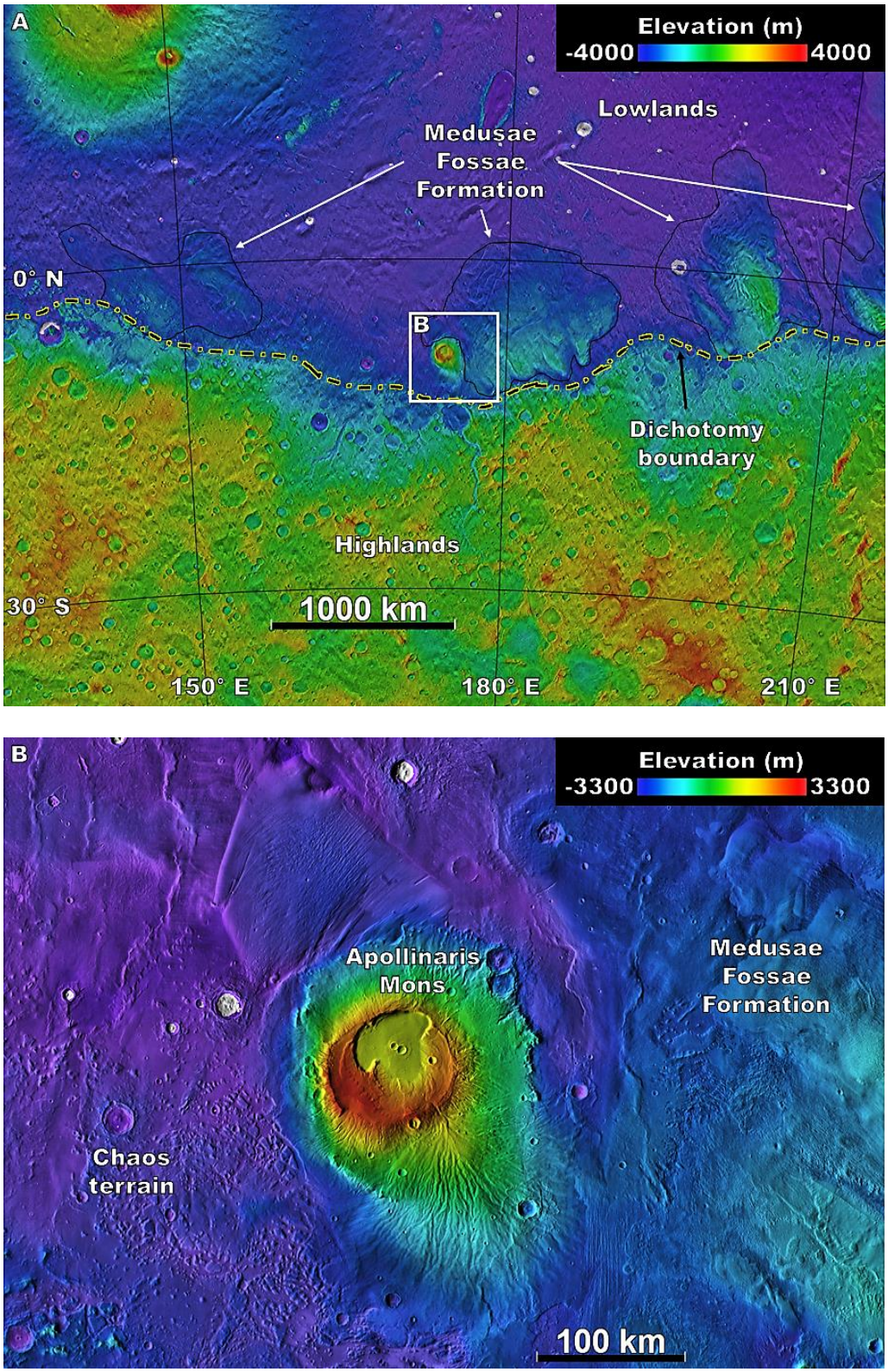

Figure 2.1 (A) Colorized MOLA elevation data draped over THEMIS daytime infrared global mosaic of Mars, surrounding Apollinaris Mons, showing Medusae Fossae Formation. (B) Regional map of Apollinaris Mons, surrounded by chaos terrain to the west, and the Medusae Fossae Formation to the east.

The Apollinaris Mons caldera is ~80 km in diameter and is divided into an inner and outer caldera floor unit (Figure 2.2); the inner caldera unit is nested within the outer caldera unit, and is bound by a scarp (Robinson et al., 1993). The outer caldera floor unit is between 2250—3150 m in elevation (above the Mars datum, or average elevation), and the inner caldera floor unit elevation is ~1350 m. The maximum caldera rim-to-inner floor depth is ~1.9 km. The outer caldera shows curvilinear fracturing in an amphitheater shaped depression that occupies the eastern half of the outer caldera (Figure 2.2; Outer caldera depression). The western region of the outer caldera displays a flat-topped plateau that has scalloped rims on the eastern side (Figure 2.2; Outer caldera plateau 2). The inner caldera is flat and smooth at a scale of 10s of meters, and marked only by impact craters. The outer caldera is interpreted as a scarp related to an older caldera, later altered by subsidence, and infilling; the inner caldera is interpreted as more substantial subsidence, followed by infilling (Robinson et al., 1993).

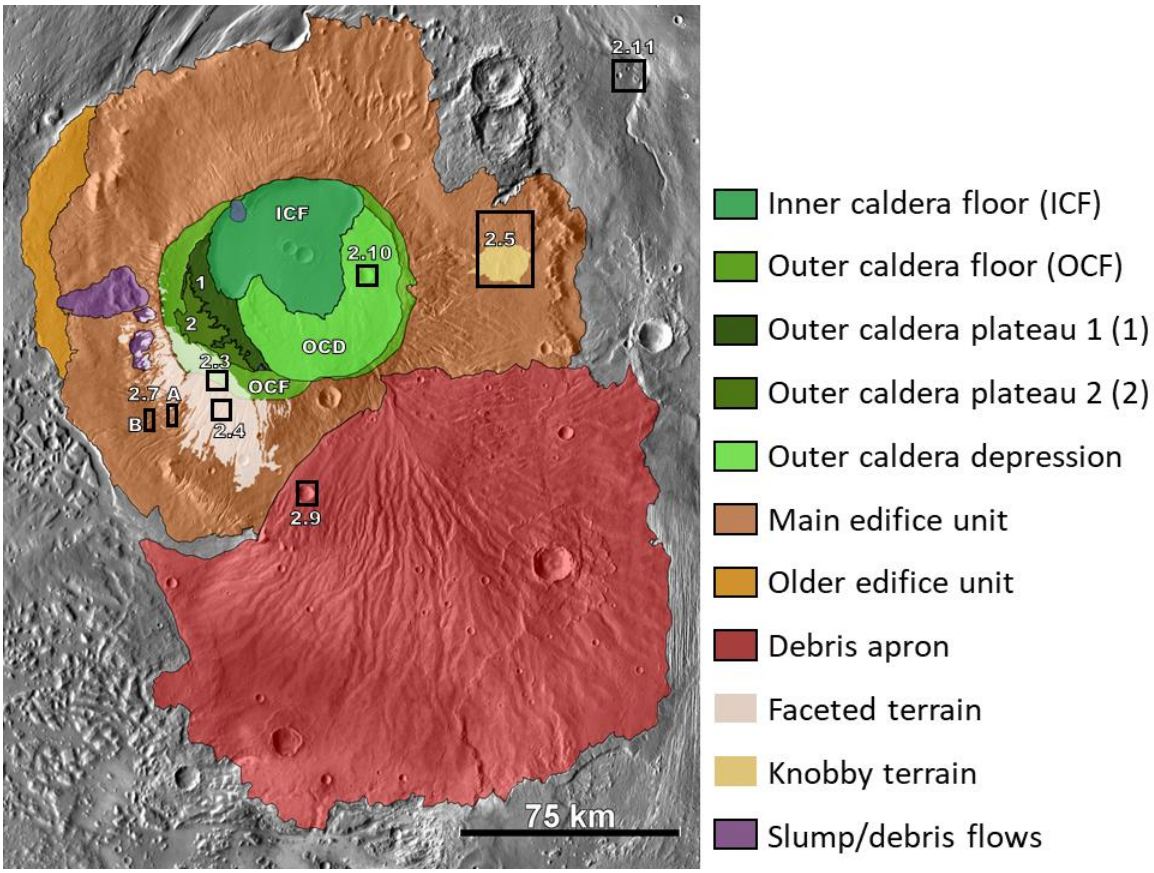

Figure 2.2 THEMIS daytime global mosaic of Apollinaris Mons with mapped units. Figure reference of portions of the edifice are outlined by black boxes.

Based on CTX and HiRISE images, many of the craters of the inner caldera floor are pedestal craters, characterized by raised ejecta deposits 10's of meters above the surrounding plains (e.g., Schultz & Lutz, 1988). Pedestal craters are believed to originate from impactors that strike volatile-rich terrain, where the ejecta becomes indurated (post-impact), armoring the ejecta from erosion (Kadish et al., 2008; Schultz & Lutz, 1988; Wrobel et al., 2006). As such, these crater morphologies suggest water was present within the caldera floor (El Maarry et al., 2012).

The southern flank of Apollinaris Mons is characterized by a debris apron which radiates from a valley that breaches the caldera rim (Figure 2.2). The slope of the apron is ~2°, and is 100—130 km in length from the apex at the rim. Dissecting valleys are 2—3

km wide and span the length of the apron from the apex at the rim. Kerber et al. (2011) interpret these channels to have formed by erosion though weak, friable material, and thus are interpreted to represent a flank comprised of explosive volcanic products. Most of the valleys do not extend to the basal scarp, and only travel ~20 km down the ~50 km long flank. The exception to this is the western flank; this region of the volcano also displays slumps and landslide debris lobes (Figure 2.2). The largest valleys on Apollinaris Mons dissect the southwestern flank of the volcano, with valleys ~0.5—1 km wide, and extend to the basal scarp.

Arrays of fractured polygonal plateau structures, known as chaos terrain (Figure 2.1B; Chapman & Tanaka, 2002; Sharp, 1973), are present beyond the western flank of the volcano, and further along the dichotomy boundary. These chaos terrains are interpreted to represent partial collapse of the surface by the removal of subsurface ice or water (e.g., Sharp, 1973).

The northern and eastern scarps of Apollinaris Mons are surrounded by the Medusae Fossae Formation (MFF), a large-volume friable deposit that has been interpreted as sourced from volcanic activity (Figure 2.1B; e.g., Kerber et al., 2011; Malin, 1979; Mandt et al., 2008; Scott & Tanaka, 1982, 1986;). Yardangs, elongated wind sculpted ridges carved into weakly-indurated material (Ward, 1979), are common in the MFF. Yardangs are erosional features that modify depositional materials. On Earth, morphologically similar yardangs are found within large-volume ignimbrite (pyroclastic flow) deposits in the Altiplano-Puno Volcanic Complex (APVC) in Chile (de Silva et al., 2010), further supporting the hypothesis that the MFF may represent weakly-indurated, explosive volcanic deposits.

Gulick and Baker (1990) studied the flanks of Apollinaris Mons to understand the origin and evolution of volcanic valleys on Mars. All valleys along the flanks originate at the caldera and have a rill-like form. Valleys on the southern fan appear degraded and wide compared to the more incising, rill-like channels along the northern, eastern, and western flanks. Gulick and Baker (1990) suggest that the valleys on the flanks may be pyroclastic in nature, indicative of weakly-indurated flank material. Valleys dissecting the fan are interpreted as possible lava channels since they are more subdued than valleys on the flanks. Gulick and Baker (1990) note that lobate morphologies associated with lava flows are not visible on the fan deposit, and suggest the fan to be mantled. However, the pervasiveness of fluvial morphologies that is also consistent with the observed valley morphologies suggest fluvial processes have since obscured primary characteristics for volcanism, and imprinted more fluvial evidence for valley formation. Gulick and Baker (1990) ultimately conclude that valley formation on Apollinaris Mons is suggestive of mixed fluvial and lava origins.

Robinson et al. (1993) and Scott et al. (1993) were the first to map Apollinaris Mons in its entirety. The map produced by Robinson et al. (1993) is divided into a main edifice unit (m), an inner and outer caldera unit (cf2 and cf1), a fan unit (f), and a visible and inferred basal scarp. The caldera units are split into two units based on a scarp that bounds the inner caldera, and raised rim that borders the outer caldera, suggesting subsidence and lava infilling activity.

The fan deposit extends 150 km from the caldera and is likely sourced from a channel the breaches the caldera rim at the apex of the fan (Robinson et al., 1993; Scott et al., 1993). Morphologic differences between valleys on the fan and the volcanic flanks

(i.e., shallower, more subdued fan channels) suggest the fan material comprises effusive materials. Robinson et al. (1993) suggest the fan has a blockier structure than the edifice based on relatively higher thermal inertia measurements made using the Viking Infrared Thermal Mapper. The authors assert that the edifice is composed of friable material, based on the presence of radial channels incising the flanks from the caldera rim and slumping features on the western flank of the edifice (consistent with observations made by Gulick and Baker, 1990).

The map produced by Scott et al. (1993) splits Apollinaris Mons into four lava units which differ from the units proposed by Robinson et al. (1993). Scott et al. (1993) suggest the inner caldera and fan units comprise the same lava flow materials which formed in the latest episodes of activity at Apollinaris Mons. Radial channels along the fan are interpreted as either fluvial or lava channels. The outer caldera unit and a portion of the main edifice unit are also interpreted as the same materials, formed from lavas and pyroclastic deposits. The distal portion of the main edifice unit, along the western flank, is interpreted as more lava materials, likely formed during the earliest modes of activity at Apollinaris Mons. Scott et al. (1993) assert that explosive volcanism occurred sometime between early and late effusive activity at Apollinaris Mons. These interpretations agree with Gulick and Baker (1990) and Robinson et al. (1993), claiming the main edifice unit was built by both effusive and explosive deposits, with the fan and inner caldera units comprised of lavas.

More recently, Farrell and Lang (2010) used high-resolution datasets to investigate the distribution of explosive and effusive deposits on Apollinaris Mons. Much like previous efforts, Farrell and Lang (2010) concluded that Apollinaris Mons

experienced an explosive phase responsible for building the edifice, and ended with an effusive phase that produced a flat inner caldera floor. Farrell and Lang (2010) claim Apollinaris Mons experienced at least two phases of explosive activity; the formation of the caldera complex is likely associated with the first phase, and the fan deposit representing a second phase. However, they argue that the fan deposit was likely produced from volcaniclastic products, contrasting earlier interpretations made by Gulick and Baker (1990), Robinson et al. (1993), and Scott et al. (1993). They conclude by stating Apollinaris Mons displays evidence consistent with a dominant explosive history. Their interpretations are based on morphologic characteristics of friable terrains described by Greeley and Crown (1990) and Crown and Greeley (1993).

Following previous mapping efforts, Krysak (2011) conducted a detailed analysis of Apollinaris Mons that investigated possible origins for the debris apron, caldera, and timing of volcanic activity and modification of the edifice. Krysak (2011) claims the debris apron is comprised of pyroclastic materials based on a lack of distributaries channels; they state effusive lava flows and channels on alluvial fans will usually spread outward. Channels incised in the fan only display tributaries, consistent with channels carved by water. Layers identified within impact crater walls in the debris apron also suggest multiple depositional events.

Krysak (2011) interprets the caldera as both pyroclastic and lava materials, based on impact crater densities. The inner caldera is likely a lava deposit based on higher impact crater densities, compared to the outer caldera; they state more durable materials can retain more impact craters. Impact crater densities are also higher within the outer caldera than on the fan, suggesting the fan is younger than the outer caldera material.

Interpretations for a dominantly explosive history agree with Farrell and Lang (2010). Prior to the crater analysis made by Krysak (2011), previous efforts likely suggested the inner caldera to be comprised of lavas based on the presence on the flat and level surface (Farrell & Lang, 2010; Robinson et al., 1993; Scott et al., 1993).

Kerber et al. (2011) examined deposits within the MFF, beyond the flanks of Apollinaris Mons, to test the hypothesis that the MFF was sourced from the volcano. The methods used to determine a depositional origin include geomorphologic observations that would suggest weakly-indurated deposits, stratigraphic relationships with Apollinaris Mons that would indicate volcanic activity during emplacement of the MFF, and ash distribution models from Apollinaris Mons that correlate with the current extent of the MFF. The volcanoes proximity to the MFF make it an ideal source for the observed weakly-indurated deposits. However, Apollinaris Mons was believed to have formed during the early to mid-Hesperian (Scott et al., 1993), with the MFF being dated as Amazonian in age (Bradley et al., 2002; Greeley & Guest, 1987; Scott & Tanaka, 1982). These discrepancies in age suggested the volcano was active before the MFF was emplaced. Stratigraphic relationships identified by Kerber and Head (2010) more recently propose an older age for the MFF that is consistent with volcanic activity at Apollinaris Mons. Distribution models made by Kerber et al., (2011) also correlate with chlorine concentrations around Apollinaris Mons, commonly produced from volcanic outgassing (Keller et al., 2007). This research suggests that Apollinaris Mons was a primarily explosive volcano, responsible for edifice construction, and potential deposition of pyroclastic materials beyond the edifice.

2.2 Research questions and approach

The following observations suggest that Apollinaris Mons is a primarily explosive volcano: (1) a lack of identified lava flow morphologies and high strength materials, (2) valley formations that suggest erosion through poorly consolidated materials, and (3) regional large-volume friable deposits that may have been sourced from Apollinaris Mons. Even with the onset of improved spatial sampling by CTX and HiRISE instruments, no attempts have been made to identify outcrop scale (10's to 100's of meters) evidence for explosive volcanism on Apollinaris Mons. As such, the objectives of my work are to identify the extent of effusive and explosive materials on the surface and within exposed outcrops within impact craters and valley walls. Detailed thermophysical and geomorphologic observations of exposed outcrops provide a window into the eruptive history of Apollinaris Mons. The outcrops and deposits identified on the volcano are compared to terrestrial examples of explosive volcanic deposits for more accurate interpretations.

In addition to morphologic units and features identified by previous researchers (Robinson et al., 1993; Scott et al., 1993; Krysak, 2011), I have identified unique surface textures that may be linked with the nature of the deposits that comprise them. These include a faceted terrain on the southwestern rim and flank of Apollinaris Mons and a knobby terrain on the eastern flank. To further explore the nature of the Apollinaris Mons subsurface, I use HiRISE images to better characterize outcrop exposures within the craters and cliff walls along the caldera and edifice. Features in outcrops include breccia deposits and layered materials. Lastly, I describe an anomalous crater northeast of Apollinaris Mons that may have formed from explosive volcanic activity.

2.3 Results

2.3.1 Weakly-indurated surface deposits

Friable surface deposits are defined as low thermal inertia features that preserve erosional characteristics suggestive of poorly consolidated materials. For example, terrains that can be carved by aeolian and/or fluvial processes are considered weakly-indurated. Morphologic observations of weakly-indurated materials preserve surfaces and exposures that indicate carved surfaces, or deposits that appear to break apart easily. On Apollinaris Mons, weakly-indurated terrains are found either along the surface of the volcano, or in outcrops (caldera walls and impact craters). Weakly-indurated surface deposits include faceted terrain (diamond shaped pits carved between angular ridges), knobby terrain (resistant mounds preserved in friable materials that has since eroded out), bedding, and breccia deposits.

2.3.1.1 Faceted terrain along the southwestern flank and interior caldera rim

More than 1,200 km^2 of material covering the southwestern flank and interior caldera rim of Apollinaris Mons displays a pattern of sharp ridges above a scalloped interior (Figure 2.2 and 2.3), termed here as faceted terrain. The northern boundary of the deposit, located within the caldera, has a sharp contact with the dust mantled surface. The faceted terrain has a thermal inertia ~50 TIU higher than the smooth dust covered surface (THEMIS image ID: I07478012).

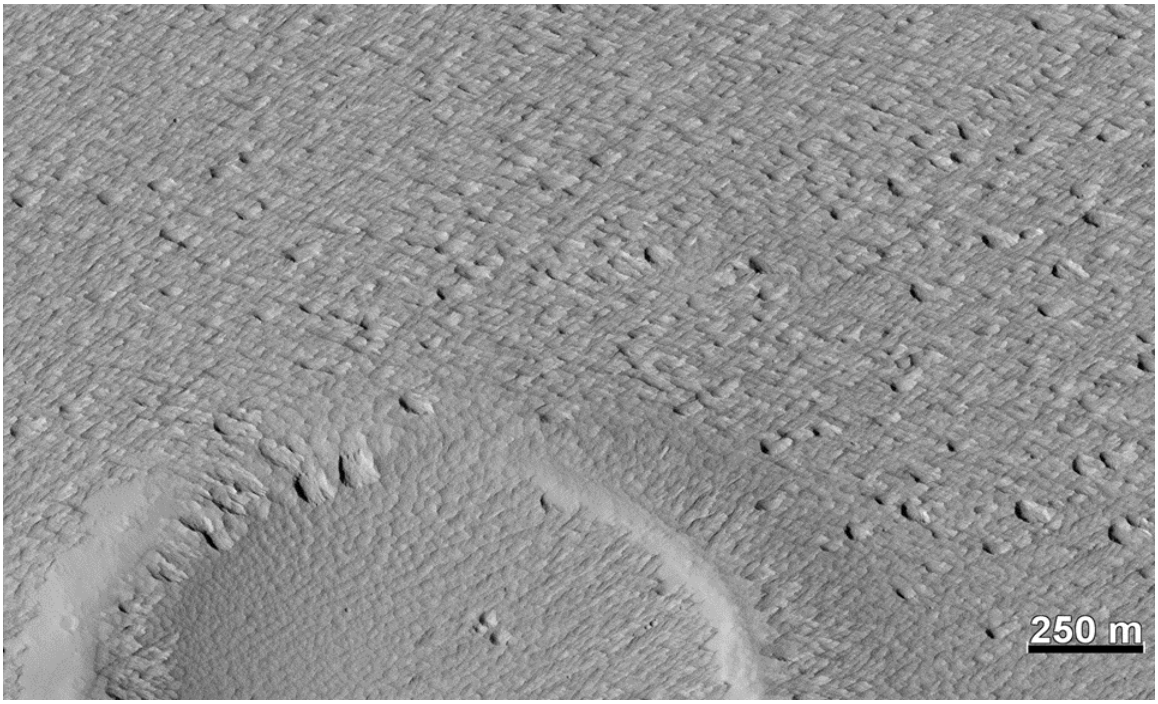

Figure 2.3 Faceted terrain within the caldera shows ridge orientations that trend NW-SE and NE-SW. Scour pits embay the faceted terrain, and are large enough to produce shadows (but not large enough to measure cast shadows). A portion of an impact crater near the bottom left shows a crater rim mostly free of faceted terrain. HiRISE image ID: ESP_029481_1705.

Within the caldera, the facets cover an area of 210 km^2 and have two dominant ridge orientations, NW-SE and NE-SW (Figure 2.3). The intersection angle between the ridges of each facet, which creates the interference pattern, averages at 56°. Facet long axes average 43 m in length with the short axis averaging 25 m.

Pits 100 m long and 50 m wide are present within the caldera and along valley ridges down flank; they are oriented in a NW-SE direction (Figure 2.3). They share a similar morphology to the faceted surface, but are deeper and more ovate. Pit concentrations within the caldera grade from 9% in the eastern portion to 1% going westward based on point counts.

Beyond the caldera rim, faceted terrain transitions to a NE-SW oriented linear pattern (Figure 2.2 and 2.4). Although the length of each facet remains similar down

flank, intersection angles between the ridges of each facet decreases from 56° in the caldera to 37°. Farther down the flank where the deposit begins to thin and becomes discontinuous, the terrain forms linear ridges similar to yardangs. Along the boundaries of the faceted terrain, the deposit is present in isolated patches, often located along the western edge of topographic lows.

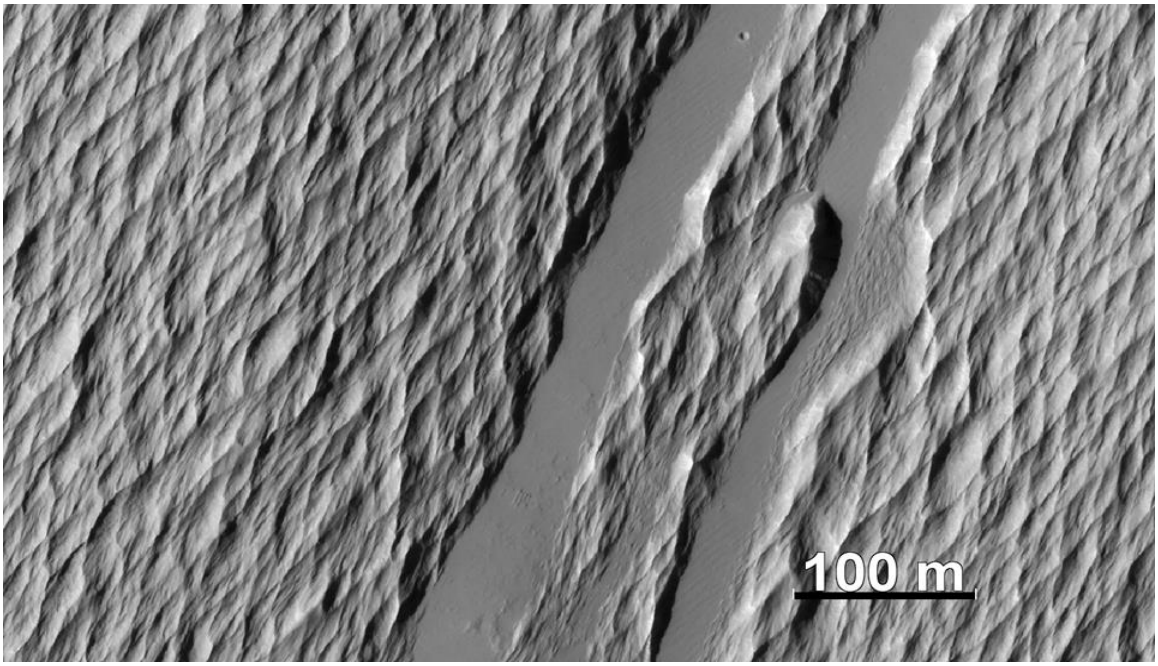

Figure 2.4 Faceted terrain along the flank of Apollinaris Mons display more linear facets, compared to those present in the caldera. Smooth linear valleys are present between the faceted terrain and show ripple-like features on the surface with wavelengths of less than 10 meters, suggesting valleys filled with windblown dust. HiRISE image ID: ESP_029481_1705.

2.3.1.2 Knobby terrain

A knobby surface terrain is present on the eastern flank of Apollinaris Mons near 175.5° E, 8.5° S, covering an area of 330 km^2 (Figure 2.2 and 2.5A). The region that contains the knobby terrain slopes toward the south at an average slope of 1° into a local, ~100 m deep depression. The knobs within the region of lower topography are taller and more prominent, and comprise 7% of the surface area (based on point counts). Knob

widths vary from 30 to 500 m and are commonly ~50 m tall. Larger knobs have flat topped surfaces resembling mesas, and smaller knobs display a more rounded, mound-like appearance. Angular ridge structures are emplaced in the terrain between knobs (Figure 2.6). These ridges have a fracture pattern that resemble desiccation cracks, but are positive features. The knobs in the region of higher topography are less prominent and appear more mound-like (Figure 2.5).

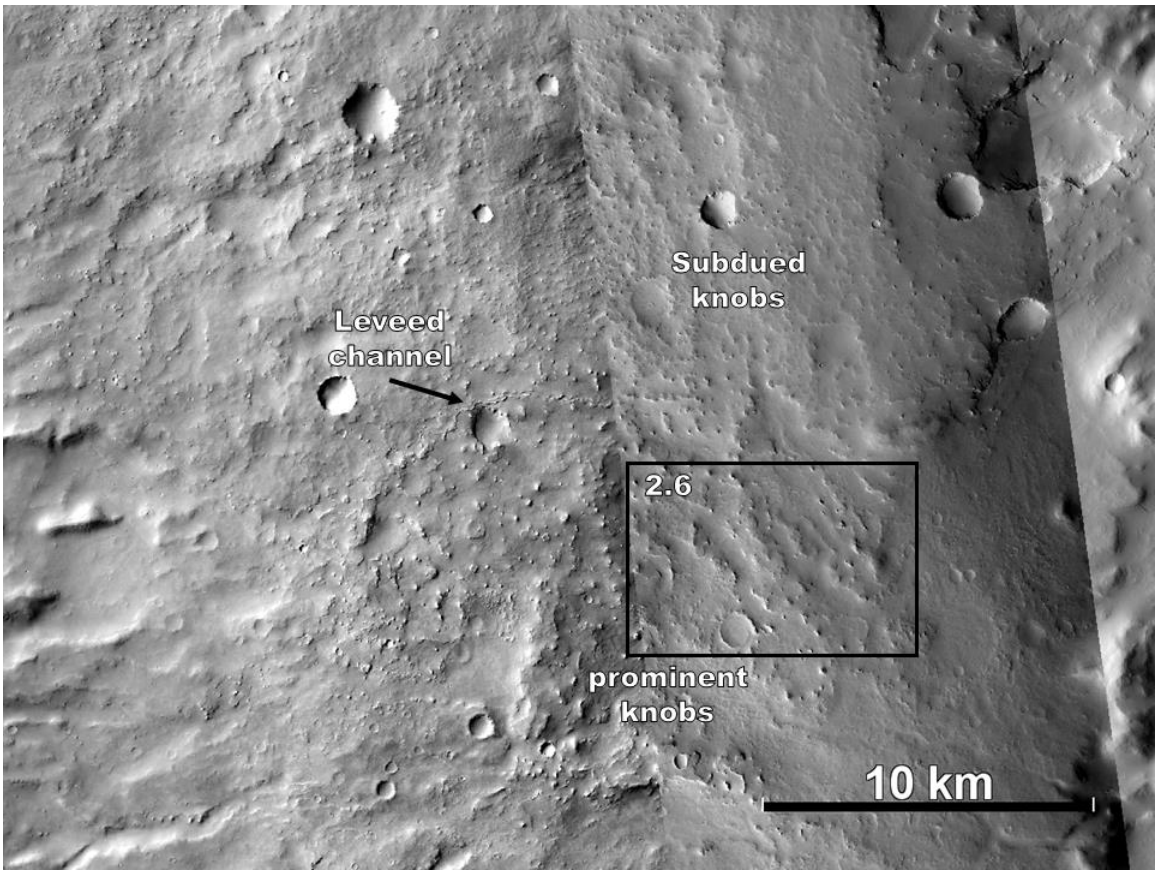

Figure 2.5 Knobby terrain within a shallow, 100 m depression shows prominent knobs and mesas. Knobby terrain to the north is present on the surface, and appears more subdued. A sinuous channel-like feature separates the two knobby regions. Solar incidence is from the west. The Location of Figure 2.6 is represented by a black box. CTX image ID: P16_007381_1694_XN_10S184W, B08_012932_1703_XN_09S184W, G05_020224_1704_XN_09S184W.

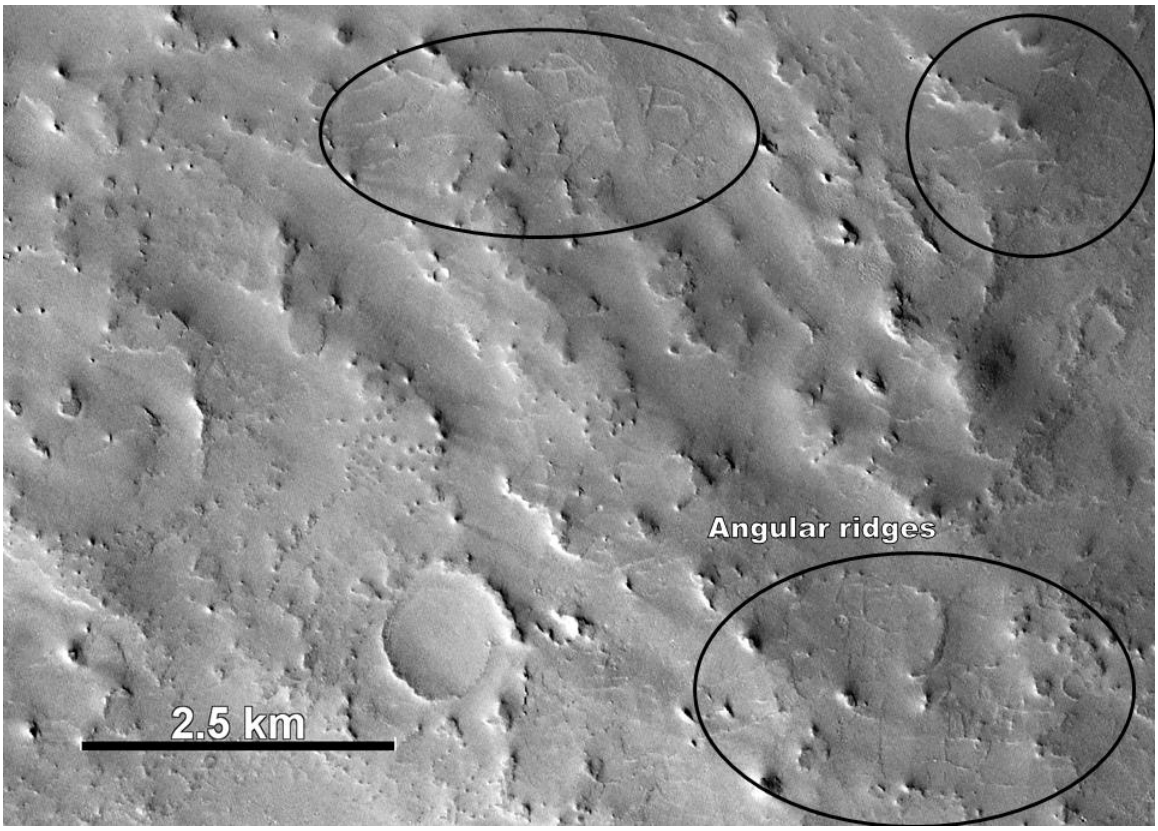

Figure 2.6 Angular ridges are visible between knobs. Black ovals indicate the separate clusters of angular ridges present in the more prominent region of knobby terrain. Solar incidence is from the west. CTX image ID: B08_012932_1703_XN_09S184W.

2.3.2 Bedding and breccia deposits in crater and valley wall outcrops

Exposed crater and valley wall outcrops provide a history of deposition by exposing layers of material in the substrate. Along the southwestern flank of Apollinaris Mons, boulders are visible in the wall of one of the largest valleys on the edifice (Figure 2.2 and 2.7). The slope of the valley wall ranges from 12° to 15°. The wall deposits are boulder rich and appear massive (lacking any bedding orientation). Boulder sizes grade laterally down slope, getting smaller with distance from the caldera rim. HiRISE coverage of the valley at a spacing of 11 km shows that the average boulder size at each outcrop (from long-axis measurements of 100 boulders at each site) is 3.2 m up slope and 1.8 m down slope (Figure 2.7).

Six craters with HiRISE coverage were studied at 0.25–0.5 m/pixel sampling, all of which are larger than 5 km in diameter (Figure 2.8). Four of the craters are located within the debris apron, one between the debris apron and the southern portion of the caldera rim, and the last in the eastern portion of the caldera. Crater wall slopes vary between 11° and 30°, with the steepest wall slope belonging to the intra-caldera crater (Figure 2.8, #1). Thermal inertia of the crater walls varies between ~110—250 TIU (THEMIS image ID: I13768005, I07478012, I01511006, I01873002, I06729006, I05955006).

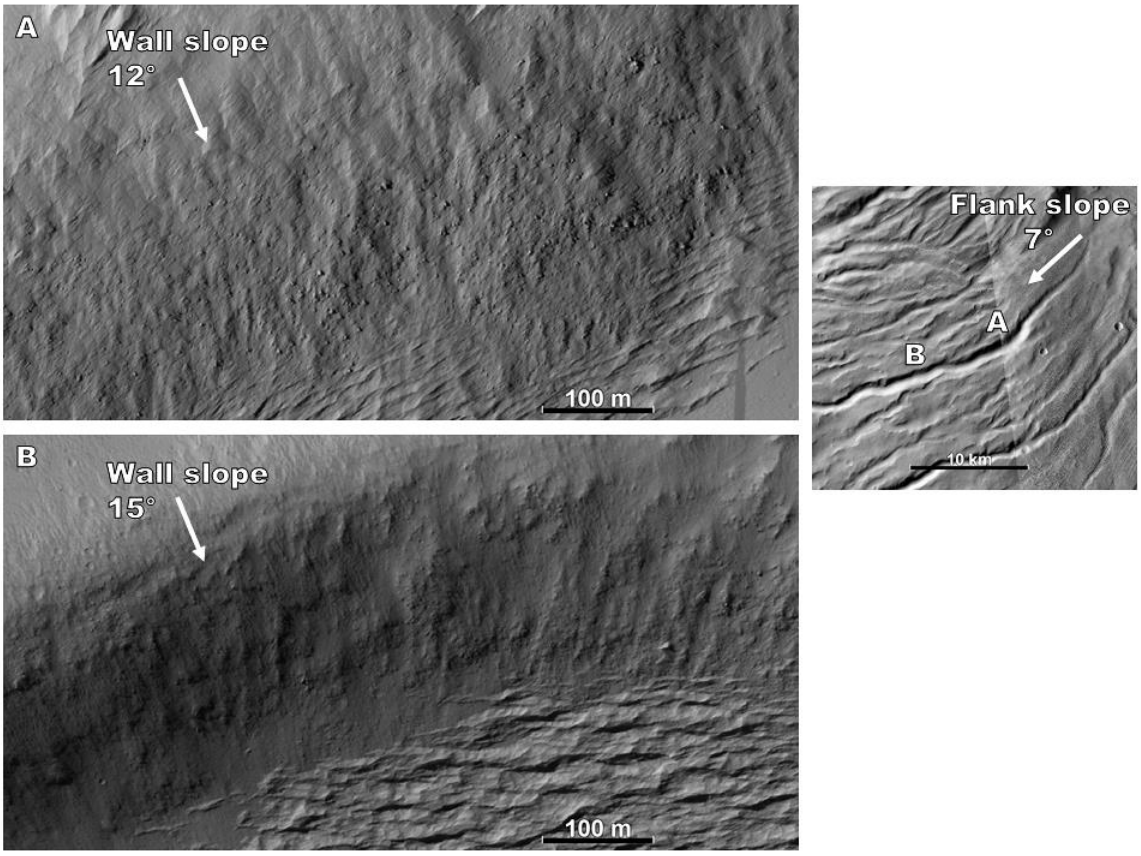

Figure 2.7 Outcrops along the northern wall of a valley on the southwestern flank of Apollinaris Mons (upper right). The outcrops are boulders rich, and massive in texture. The outcrops are 11 km apart, with (A) up slope, and (B) down slope. Boulders in the outcrop become visibly smaller down slope, from 3.2 to 1.8 m. Faceted terrain is visible at the base of the wall in both images. HiRISE image ID: PSP_009596_1705, ESP_029125_1705.

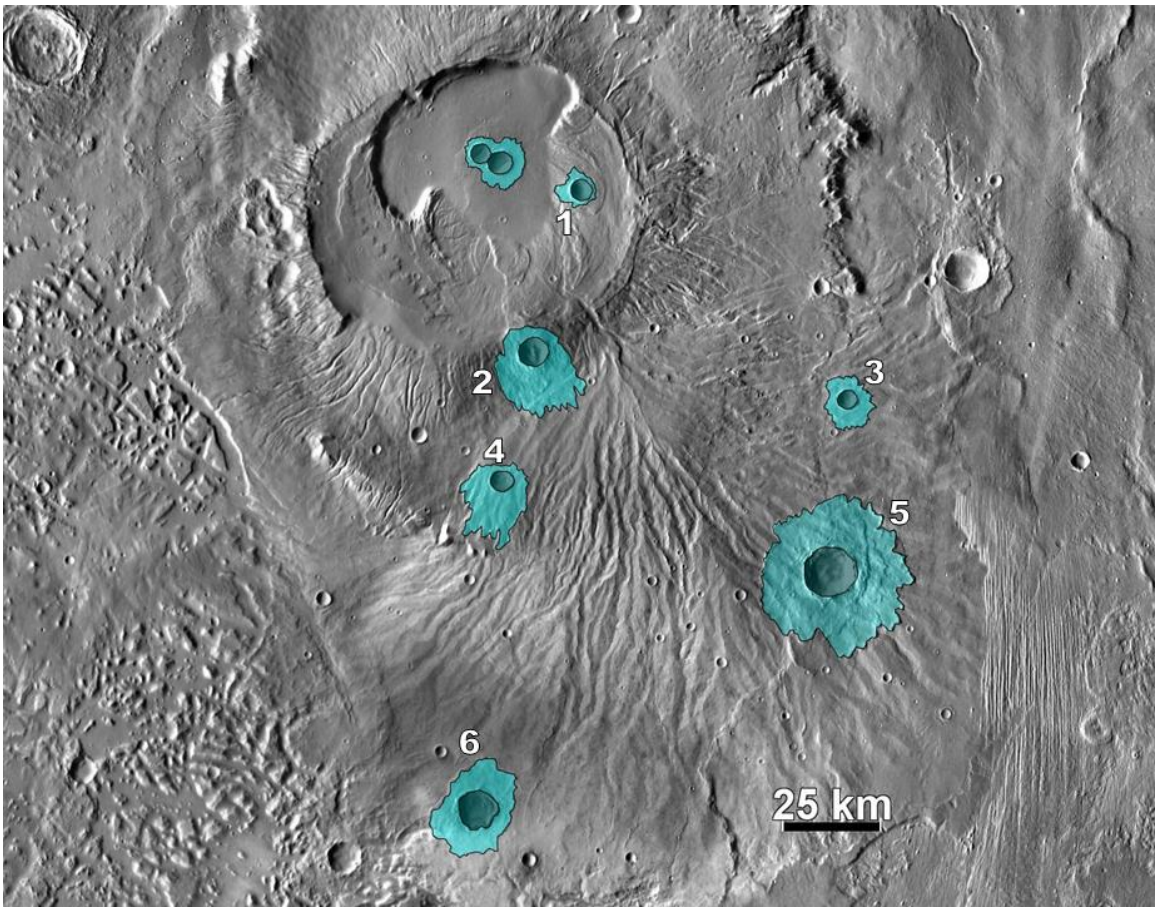

Figure 2.8 THEMIS day IR global mosaic of Apollinaris Mons, showing the locations of craters with HiRISE coverage on crater wall exposures. Numbered craters have exposed walls that preserve bedding structures.

The crater located on the western region of the debris apron shows at least four distinct layers between 5–10 m thick, containing 1–2 m thick sublayers (Figure 2.8, #4, and 2.9; 174.3° E, 9.8° S). Many layers are planar, but most layers appear to truncate other. The surface appears smooth with shallow, incised valleys. Boulders are present along the layers and visibly persist only 50 m down slope. Patches of faceted terrain are present at the base of the northern wall of the crater and obscure the view of the crater floor preventing identification of boulders at the wall base (Figure 2.9). The slope of the wall is 25° based on MOLA elevation data. Thermal inertia of the layered deposits is ~150 TIU (THEMIS image ID: I07840015, I01873002). Impact craters 2, 3, 5, and 6

from Figure 2.8 show similar planar bedding deposits as those in Figure 2.9, but do not have layer truncations.

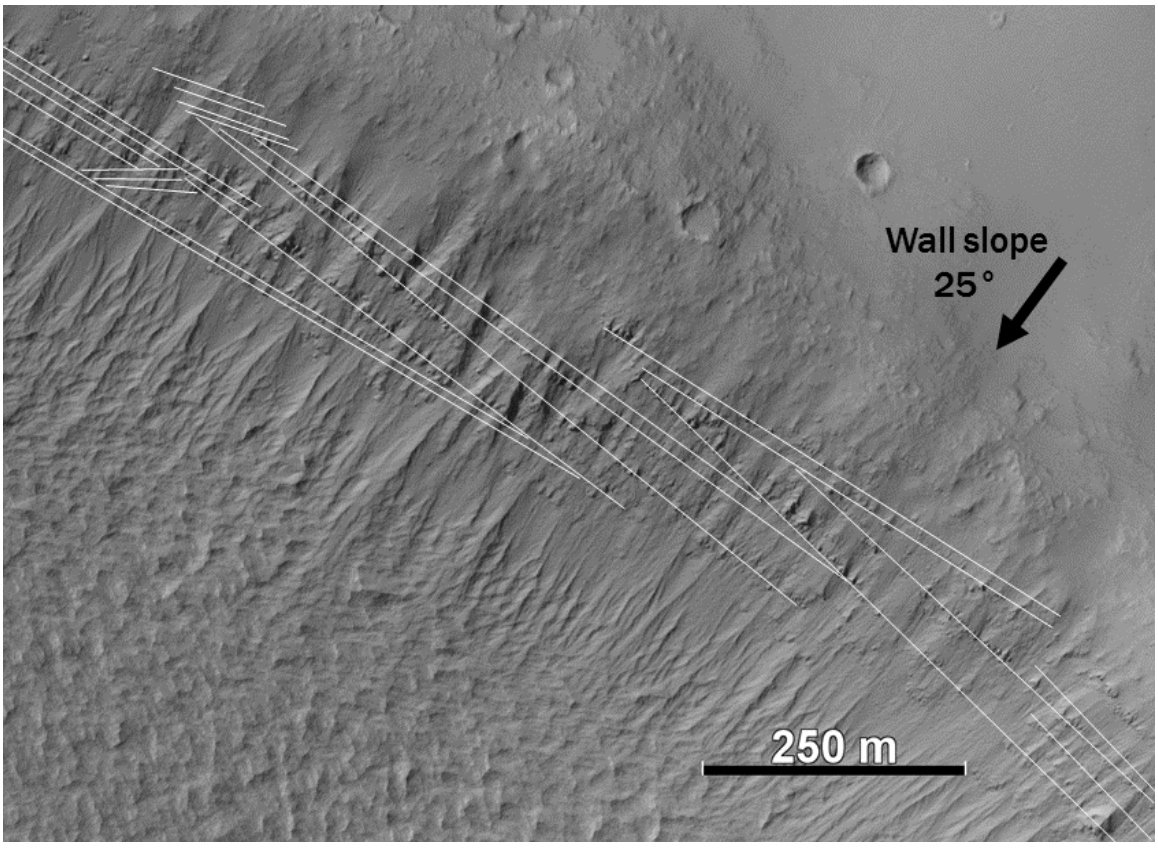

Figure 2.9 The northeastern wall of a crater in the debris apron shows planar and truncated bedding. The slope of the wall is ~25°, and faceted terrain is observable at the base of the wall. White lines trace the more prominent bedded layers. HiRISE image ID: ESP_035797_1700.

In contrast to the planar and truncated bedding identified within the debris apron, the crater located in the eastern portion of the caldera shows a massive boulder rich deposit (Figure 2.8, #1, and 2.10; 174.64° E, 8.5° S). With a slope of ~30°, the inner crater walls are blocky with boulders persisting more than 1 km down slope (reaching the crater floor). THEMIS derived thermal inertia of the crater wall is ~250 TIU (THEMIS image ID: I01511006, I07453004, I08589007, I16551011, I13793007). Although this thermal inertia value is low compared to bedrock and lava flow materials on Mars, this is

the highest observed value on Apollinaris Mons and is consistent with poorly consolidated deposits (Bandfield et al., 2013).

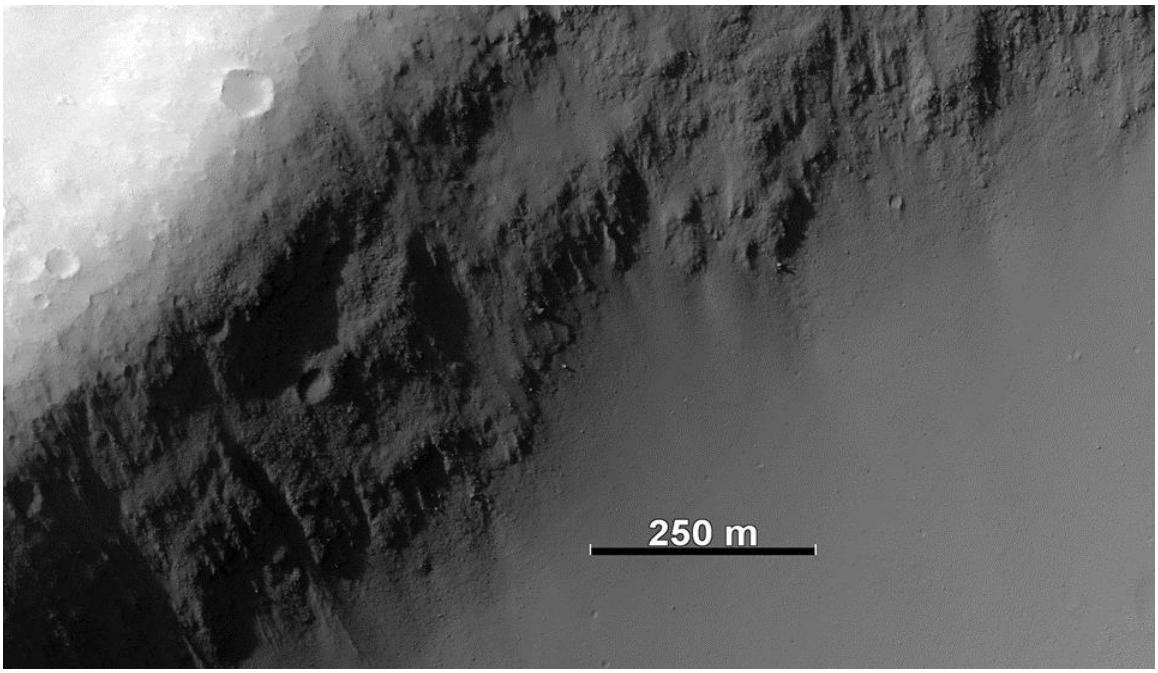

Figure 2.10 The exposed substrate texture of the Outer caldera depression is boulder rich, and shows no defined layers. Boulder persist more than 1 km. Solar incidence is from the northwest. HiRISE image ID: ESP_028136_1710.

2.3.3 Anomalous structure near Apollinaris Mons

Northeast of Apollinaris Mons at 176.2° E and 7.3° S, a heart-shaped structure stands out from the typical bowl-shaped craters observed on Mars (Figure 2.2 and 2.11). The heart-shaped structure is 2 km across at its widest point and shows a breach in the northeastern wall exposing a flat crater floor at the same elevation as the surrounding topography. The western wall is ~65 m tall and the rim is sharp. The outer rim slopes away from the crater at 12° based on MOLA elevation data. The inner wall slope, though seemingly steep, is too small to resolve with MOLA. The minimum wall slope based on solar incidence is ~56°. Horizontal layering is present on the northern outer rim. For comparison, an impact crater with a similar diameter is adjacent to the heart-shaped

structure, and is marked by a raised crater rim and a floor ~600 m below the level of surrounding topography (Figure 2.11).

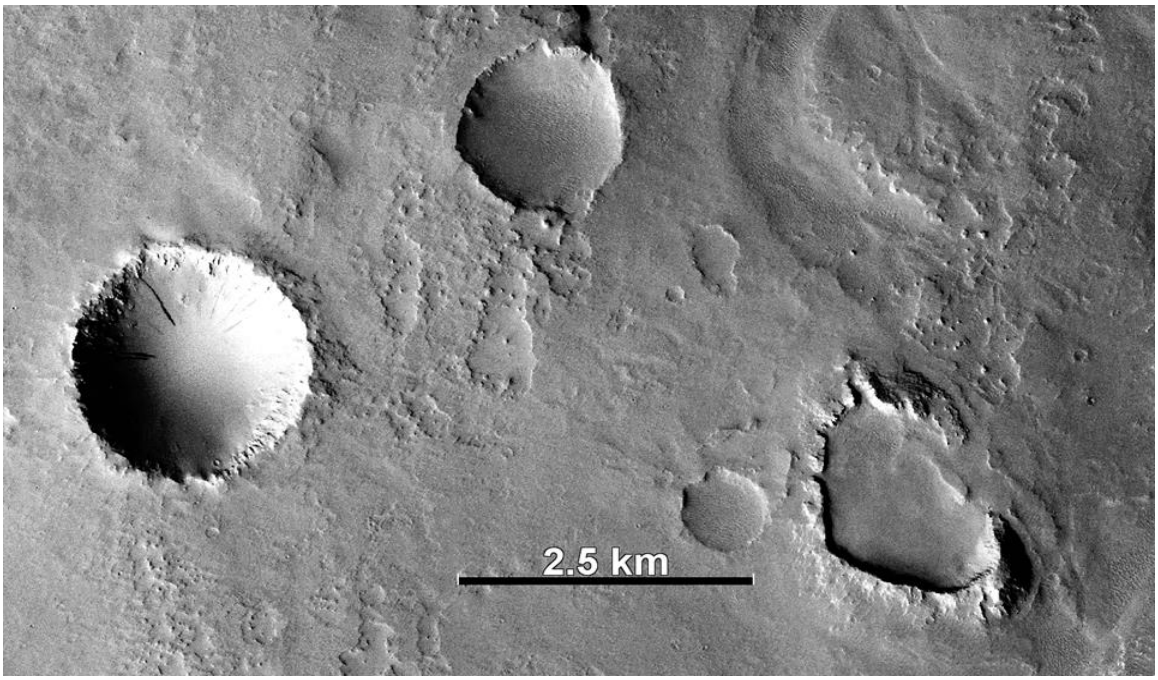

Figure 2.11 A heart-shaped crater northeast of Apollinaris Mons contrasts the typical impact crater bowl-shape. The floor of the heart-shaped crater is at the level of surrounding topography. Solar incidence is from the southwest. CTX image ID: B09_013288_1724_XN_07S184W.

2.4 Discussion

2.4.1 Evidence consistent with weakly-indurated deposits

2.4.1.1 Faceted terrain

Like yardang fields on Earth, faceted terrains form in weakly-indurated, friable deposits, such as lithified sedimentary or volcaniclastic deposits (Ward, 1979). Previously interpreted as bidirectional yardangs (Bradley et al., 2002; Mandt et al., 2008), the faceted terrain shares a morphology with similar structures within the MFF formed from the abrasion of windblown sediments (Zimbelman & Griffin, 2010). Bradley et al. (2002) suggest that the bidirectional nature of some yardang fields is attributed to jointing

within the deposit, possibly from cooling and contraction of pyroclastic materials. They suggest that the observed commonality in ridge intersectional angle (~30°—45°) of bidirectional yardangs within the MFF, but variable orientation directions, indicates that funneled winds are exposing joints within the deposit. The intersection angles observed within the faceted terrain on Apollinaris Mons are similar to those determined by Bradley et al. (2002), which may support a pyroclastic origin for the faceted terrain, given its location on the flank of a volcano. However, there is a discrepancy between the intersection angles between the faceted terrains observed within the caldera (~50°; Figure 2.3), and along the flanks (~37°; Figure 2.4) of Apollinaris Mons. It seems more likely that these differences could be explained by variations in local wind regime between the caldera and the flanks, and not by jointing within the deposit.

Indurated deposits modified by aeolian erosion of one orientation can be eroded over time to preserve a different wind orientation, suggesting bidirectional yardangs and faceted terrains to be intermediate steps in this erosional process. This also suggests that the preserved facets and ridges are dominated more by wind direction and induration rather than jointing. Kerber and Head (2012) suggest that faceted terrains and other wind-carved terrains in the MFF are part a cycle of erosional stages in indurated terrains that can vary based on wind regime and sediment availability. Similar to accumulations of transverse aeolian ridges (aeolian bedforms; Bourke et al., 2003), bidirectional yardangs and faceted terrains usually appear to be thin (10’s of meters) erosional deposits covering a preexisting surface, and not erosional remnants of that preexisting terrain (Kerber & Head, 2012). Faceted terrains described by Kerber and Head (2012) elsewhere in the MFF show similar morphologies and distributions to the faceted terrains on Apollinaris

Mons, and similarly drape and curve around preexisting topography. These observed similarities between the faceted terrains on Apollinaris Mons and in the MFF suggests the faceted terrain may be weakly-indurated volcaniclastic deposits sourced from the Apollinaris Mons volcano, and later eroded by aeolian activity.

Pits within the caldera portion of the faceted terrain resemble blowout features in Chilean ignimbrite deposits. Within the APVC, pits are present in linear rows (Figure 2.12; Bailey et al., 2007). The pits formed from complex aeolian activity over uneven topography (blowouts). However, the pits on Apollinaris Mons are more angular in their appearance relative to the circular blowout depressions of the APVC. While both terrains share similar sizes (50—100 m), it is likely that differences in substrate properties, such as particle size, cohesion, and age, are affecting the morphology of the erosional surface. As such, the pits within the caldera region of the faceted terrain on Apollinaris Mons are interpreted as blowout features, formed by similar aeolian excavation mechanism as those found in the APVC. Similar pit features are present elsewhere in the MFF, and are also interpreted to be the result of complex wind regimes over uneven topography (Kerber & Head, 2012). The occurrence of the pits suggests a more chaotic wind regime in the caldera, based on morphologic similarities with terrestrial blowouts, which is also evident by the more orthogonal faceted terrain intersectional angle. Channelized winds down slope can explain the more linear shape of the faceted terrain along the flanks (Figure 2.4), and decreased intersection angle.

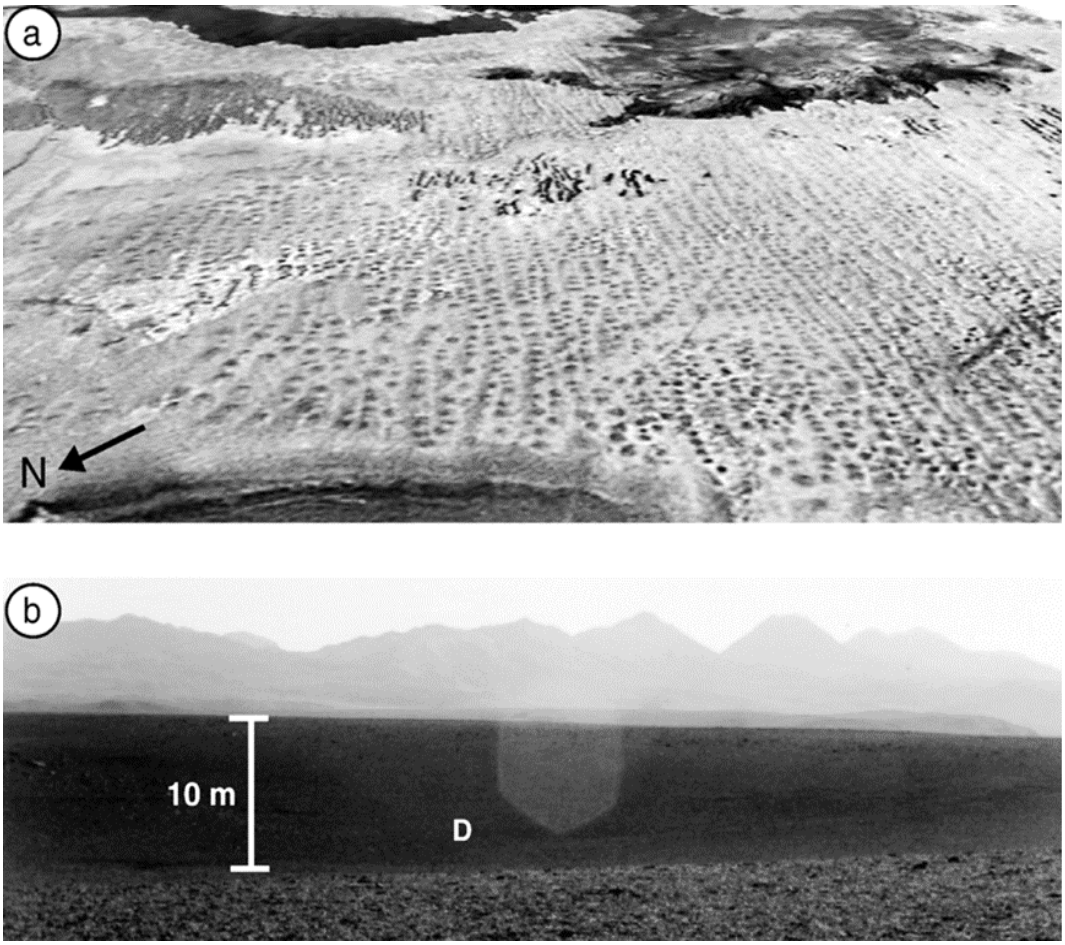

Figure 2.12 Blowout features in the APVC (A) are the result of aeolian activity over uneven topography. The pits here are ~10 m deep (B) and between 50—100 m wide. The "D" represents the center of the depression in (B). Figure modified from Bailey et al. (2007).

The presence of downslope boulders and boulder trails is further evidence to suggest that the faceted terrain is weakly-indurated. Boulders that break off the wall outcrop in Figure 2.7 tumble down the wall and deposit at the base of the slope, leaving a trail behind in any unconsolidated materials (Figure 2.13). The trails present in Figure 2.13 only begin on the distal edge of the faceted terrain against the wall. In this case, the boulder trail closest to the wall was either buried by the faceted terrain, or the boulders began to leave trails upon encountering the loose dust mantled surface of the valley floor. Considering the pervasiveness of eroding winds on Mars, the preservation of boulder

trails following deposition and erosion of the faceted terrain is unlikely, suggesting the faceted terrain is indurated.

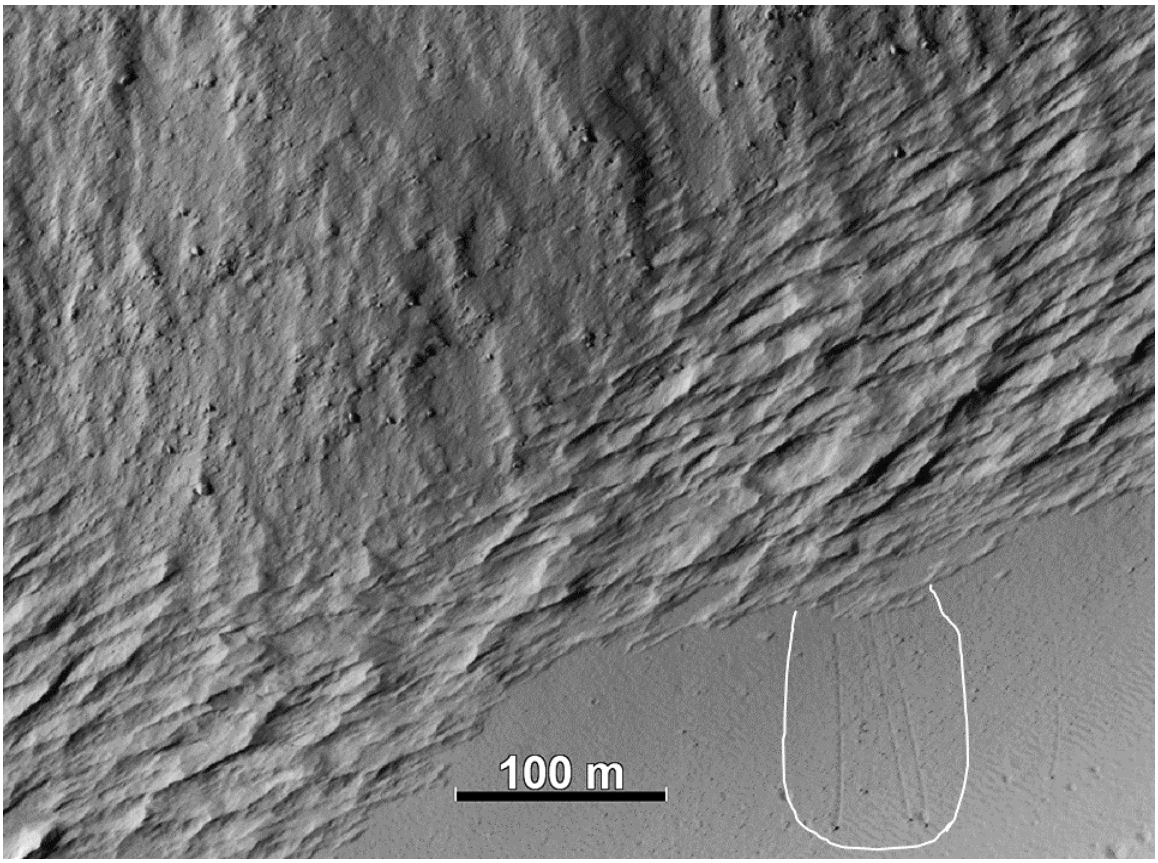

Figure 2.13 Boulder trails are observed at the base of the valley in Figure 2.6. The trails (outlined by the white line) only begin at the edge of the faceted terrain, suggesting the boulders broke off the wall outcrop, and bounced off the indurated faceted terrain. HiRISE image ID: ESP_029125_1705.

The carved nature of the faceted terrain suggests the deposit is indurated enough to preserve sharp edges, but friable enough to erode over time. Although it is difficult to constrain the origin of the faceted terrain and other bidirectional yardang features within the MFF, the proximity of the deposits to a volcano and the similarities to terrestrial ignimbrites (and the nearby MFF) suggest the faceted terrain on Apollinaris Mons could be an indurated pyroclastic deposit. Observed depositional characteristics (thin, 10's of meters, layers that appear to drape over pre-existing topography; Kerber et al., 2011) of

faceted terrain on Apollinaris Mons combined with similar erosional forms as terrestrial ignimbrite yardangs is further evidence to support the faceted terrains within the MFF and along Apollinaris Mons as being volcaniclastic in origin. However, since lithification and induration of fine-grained sediment can occur by non-volcanic sedimentary processes, such features found without an obvious volcanic edifice are difficult to interpret as volcanic in origin.

2.4.1.2 Knobby terrain

Much like yardangs and faceted terrains, the presence of knobby terrain on the eastern flank of Apollinaris Mons suggests the knobs and mounds are more indurated than the surrounding terrain, and more resistant to erosion. The terrain surrounding the knobs is interpreted as more friable, and thus more easily eroded away over time. In sedimentary environments, induration processes that form more resistant knobs can occur from mineral precipitation and cementation, burial and compaction, or a combination of the two processes (Assaad & LaMoreaux, 2004). Induration within volcanic ignimbrites is often associated with chemical and thermal hardening, resulting from vapor phase crystallization post-emplacement (de Silva & Bailey, 2017). Variability in surface erosion, either from aeolian or fluvial process, can also preserve remnants of preexisting terrains.

Sheridan (1970) describes similar knobby terrain within the Bishop Tuff ignimbrite, California, USA (Figure 2.14A). The Bishop Tuff mounds are interpreted as the result of fumaroles (Sheridan, 1970). Hot gases escaping from the ignimbrite just after deposition promote localized mineral precipitation in the upper, non-welded portion of the ash flow deposit, causing cementation and induration of the deposit around the

fumaroles (de Silva & Bailey, 2017). Erosion of the unconsolidated tuff surrounding the fumaroles exposes the more resistant mounds. Such fumarolic activity is common in ash flow deposits, and interpreted to cause similar induration in the Valley of Ten Thousand Smokes (Sheridan, 1970) and in Crater Lake ignimbrites (Pinnacles; Williams et al., 1942).

The knobs, which are more mound-like in the Bishop Tuff, are up to 20 m tall and 60 m wide. They comprise 5% of the total surface, although with locally variable concentrations because the knobs often form in clusters. The Bishop Tuff mounds resemble the Apollinaris Mons knobby terrain both in terms of distribution and size. Individual knobs on Apollinaris Mons may vary in size more than those in the Bishop Tuff, but the distribution is similar (7% surface coverage).

Emplaced between the fumarolic mounds in the Bishop Tuff are angular ridges that preserve desiccation-like fracture patterns (Figure 2.14B). The ridges are 10's of meters in length, and have a similar surface morphology as the fumarolic mounds. These ridges are interpreted to also form by escaping gasses, but along joints within the ignimbrite (Sheridan, 1970; de Silva & Bailey, 2017). Similarly, angular ridges are present within the knobby terrain on Apollinaris Mons, further supporting the interpretation of cementation by fumarolic gasses, consistent with degassing pyroclastic deposits.

The presence of knobby terrain on Apollinaris Mons suggests the deposit has variability in induration, which is common in volcaniclastic materials due to fumarolic activity. The mounds resisted erosion, whereas the surrounding materials were more weakly-indurated and easier to erode. The similarity to other mounds and filled-fracture

features in terrestrial ignimbrites further support the interpretation that the knobby terrain on Apollinaris Mons is pyroclastic in nature, and indurated via post-deposition fumarolic processes. However, induration by other sedimentary precipitation processes cannot be ruled out without sampling of the material.

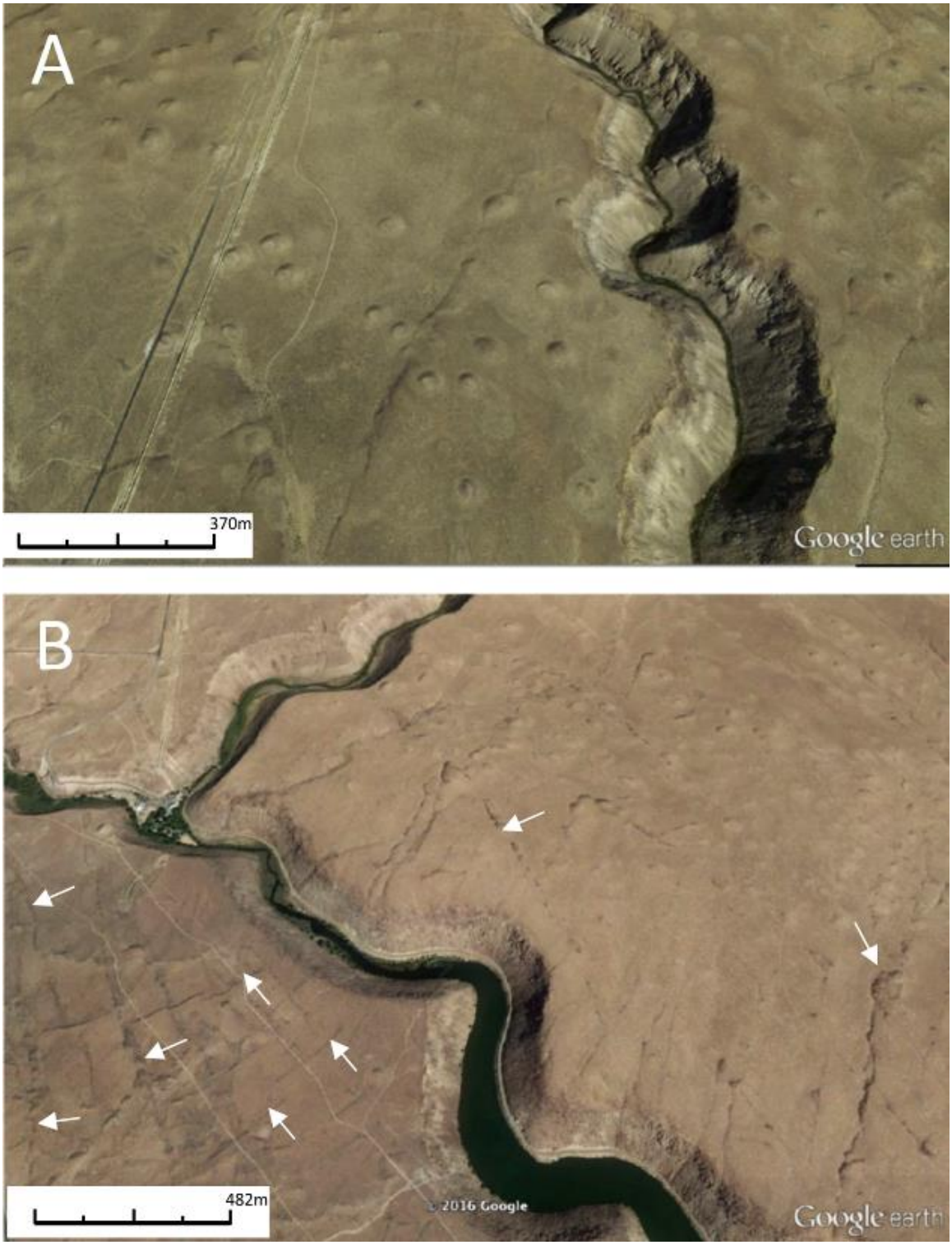

Figure 2.14 Fumarolic mounds within the Bishop Tuff, California, described by Sheridan (1970). As the ignimbrite eroded away, more resistant ridges were revealed. (A) The knobs formed from escaping gasses within the ignimbrite, post deposition, locally indurating portions of the deposit. (B) Fumarolic ridges are also emplaced within the ignimbrite (White arrow). Solar incidence for both images is from the southeast. Image modified from de Silva and Bailey (2017).

2.4.1.3 Outcrop features on the southwestern flank of Apollinaris Mons

Along the southwestern flank of Apollinaris Mons, a deep channel exposes boulder rich outcrops along the valley walls (Figure 2.7 and 2.13). The boulders do not preserve any preferred orientation, and the deposit in which they are in is massive. HiRISE images of the valley, ~11 km apart, show decreasing boulder diameters with distance from the caldera, suggesting lateral grading down slope. Such lateral grading suggests deposition by mass flow, such as a debris flow or pyroclastic flow. As flows travel down slope, they progressively lose energy. As such, the larger boulders will drop out of suspension, while smaller blocks will get carried farther from source (Palladino & Valentine, 1995).

The source of mass flow could be from a flank collapse debris avalanche, a debris flow, or pyroclastic flows following an eruption. For example, similar lateral grading from debris flows is found in lahar deposits (Giordano et al., 2002), and pyroclastic flow deposits (Brand et al., 2014). The subdued rim of the caldera upstream from the boulder-rich deposits could have facilitated collapse or overflow of debris during an eruption (Figure 2.15). However, the deposit features alone are not sufficient to distinguish between debris versus pyroclastic mass flow processes. It is possible that laterally graded deposits are more widespread on Apollinaris Mons, but the limited HiRISE image coverage does not allow for a detailed investigation of substrate texture along incised valleys on the flanks or debris apron. Additionally, a volcaniclastic interpretation would not be possible if the deposit was not emplaced along a volcanic edifice.

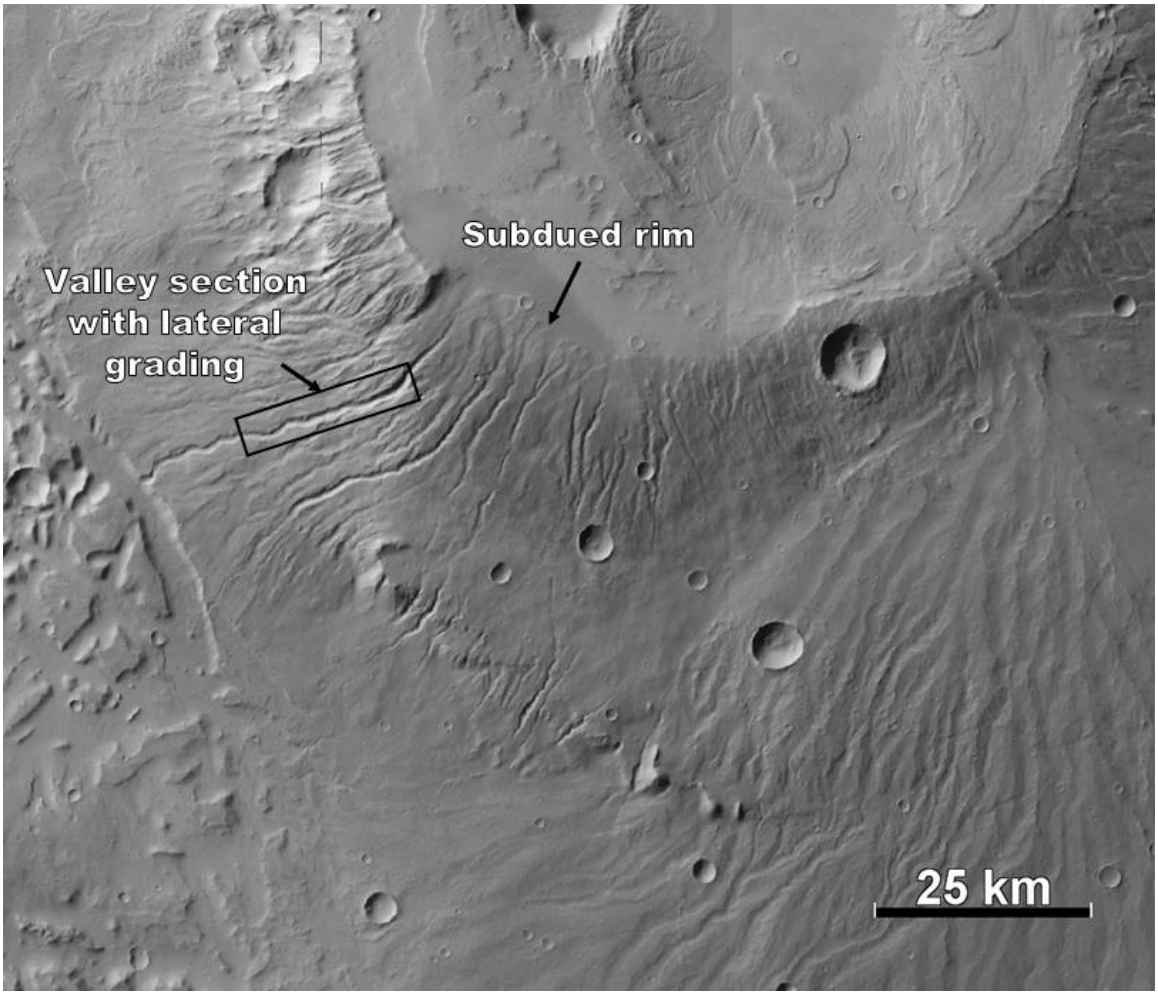

Figure 2.15 A portion of the Apollinaris Mons caldera rim appears subdued, contrasting the more raised appearance to the west. The valley exposures with lateral grading are present down flank of the subdued rim. HRSC image ID H1009_0009_ND3, H0998_0000_ND3, H0987_0000_ND3.

2.4.1.4 Outcrop features within the debris apron

Along the walls of impact craters in the debris apron, planar and truncated bedding is present. The crater walls have low thermal inertia values (<200 TIU; THEMIS image ID: I16838008, I13768005, I05955006, I06729006). The surface morphology of the bedding is smooth. Boulders falling from the bedding are not abundant, and any blocks that break off a layer do not persist more than a few hundred meters down slope. This suggests the boulders are not comprised of coherent material, and break apart easily

(e.g., Bandfield et al., 2013; Malin & Edgett, 2000). This series of properties suggests that the bedded deposits are weakly-indurated, and sedimentary or volcaniclastic in nature.

The presence of layered deposits is indicative of lateral flow. For example, pyroclastic flow deposits from the May 18, 1980 eruption of Mt. St Helens preserve a range of features including massive, planar, and truncated bedding (Figure 2.16). The pumice plain north of Mt. St. Helens preserve multiple bedding facies reflecting multiple eruptive phases (Brand et al., 2014; Mackaman-Lofland et al., 2014). Variability in mass flux and eruption explosivity can affect clast sizes within flow units, making each unit more distinct from one another. While image resolution does not allow for detailed textural analysis of the exposed layers in the Apollinaris Mons debris apron, their presence on the flank of a volcano suggests that they may be volcaniclastic in nature.

In addition to planar bedding, truncated bedding is present in a crater wall in the northwestern region of the debris apron (Figure 2.7). The orientation of the bedding shows truncation perpendicular to flow, assuming radial flow from the breach at the apex of the debris apron. Truncated bedding observed in pyroclastic flows deposits from Mt. St. Helens are usually associated with an erosive flow that is cutting older units or substrate materials (Figure 2.16; Brand et al., 2014). Truncated bedding planes also exist in lava flow deposits when pahoehoe lobes overlap one another. However, the observed truncations in the debris apron occur within friable material, based on low thermal inertia values and a lack of coherent lava morphologies, and are likely not reflective of effusive deposits. Cross-bedding and truncation of bedding is also a common feature in lithified aeolian deposits. Because the truncated bedding on Apollinaris Mons is present on a

volcanic edifice, we infer the truncations to be volcanic in origin, forming from lateral flows (pyroclastic flows or debris flows).

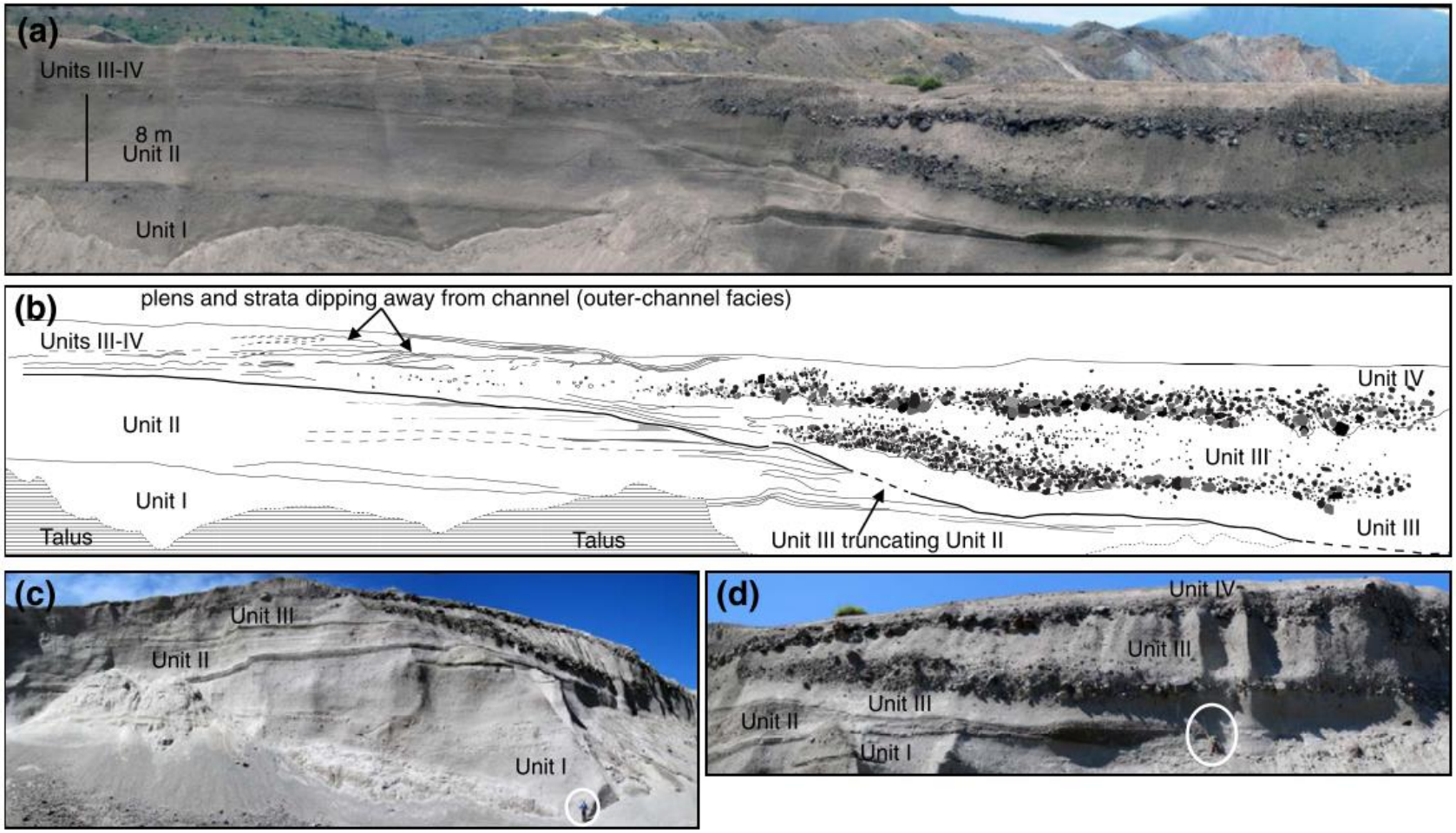

Figure 2.16 Examples of massive, planar, and truncated bedding within the pyroclastic flow deposits from the May 18, 1980 eruption of Mount. St. Helens. (a) A portion of an exposed outcrop that shows different facies layers (Unit I-IV). (b) A label illustration of (a) marks the contacts between different flow units. (c) and (d) are close-up photos of (a). Figure modified from Brand et al. (2014)

2.4.1.5 Outcrop features in the caldera

Consolidated boulder-rich deposits are exposed within an impact crater on the eastern side of the Apollinaris Mons caldera (Figure 2.8). The blocks persist more than 1 km down slope, suggesting they are comprised of solid, durable material. However, the deposit in total has a low thermal inertia (~250 TIU), well below what is considered high-strength, blocky material (>~600 TIU's; Bandfield et al., 2013). The complete lack of high thermal inertia values is surprising considering high strength materials would be expected to be present within a volcanic caldera. For example, many explosive eruptions on Earth are followed by an effusive phase (Jaupart & Allègre, 1991).

The impact crater with the exposed boulder outcrop is emplaced in an amphitheater-shaped terrace. The surface of the terrace is characterized by curvilinear and concentric fracturing, suggestive of collapse. It is possible that collapse of this portion of the caldera produced a breccia of high-strength boulders originally sourced from effusive lavas or welded tuffs. For example, blocks of welded tuff breccias resulting from caldera collapse are found within the Sapinero Mesa Tuff of the San Juan caldera, in southwestern Colorado, USA (Lipman, 1976).

Additionally, the observed breccia deposits could have formed from impact craters, or explosive volcanic activity. Regardless of reworking mechanisms, the observed thermal inertia is likely a mix of high-strength rocks and fine grained friable material. Assuming a TIU of 1200 for consolidated rock (Christensen et al., 2003), and the observed TIU of ~250 for the breccia deposit, the wall can contain ~10-15% of coherent rock.

For comparison to craters in Apollinaris Mons, a crater located within the Tharsis region (257.5° E, 3.9° N) displays both rough surface textures and defined layering (Figure 2.17). The crater wall is characterized by sharp spurs that appear resistant to erosion. Boulders present on the slopes of the crater wall persist more than 1 km down to the crater floor. Although the crater wall thermal inertia value is ~200 TIU, similar to the blocky crater wall located within the caldera of Apollinaris Mons, the amount of dust mantling in this region is greater than at Apollinaris Mons (Bandfield, 2002). Higher dust accumulations are likely lowering the average thermal inertia value within the Tharsis region. The crater is clearly emplaced within a lava field based on the lobate flow features present in the terrain around the crater (Figure 2.17; Theilig & Greeley, 1986). Additionally, the minimum slope of the crater wall is calculated to be 36°, which is greater than any of the measurable craters on Apollinaris Mons, consistent with more coherent wall material (Schultz, 2002).

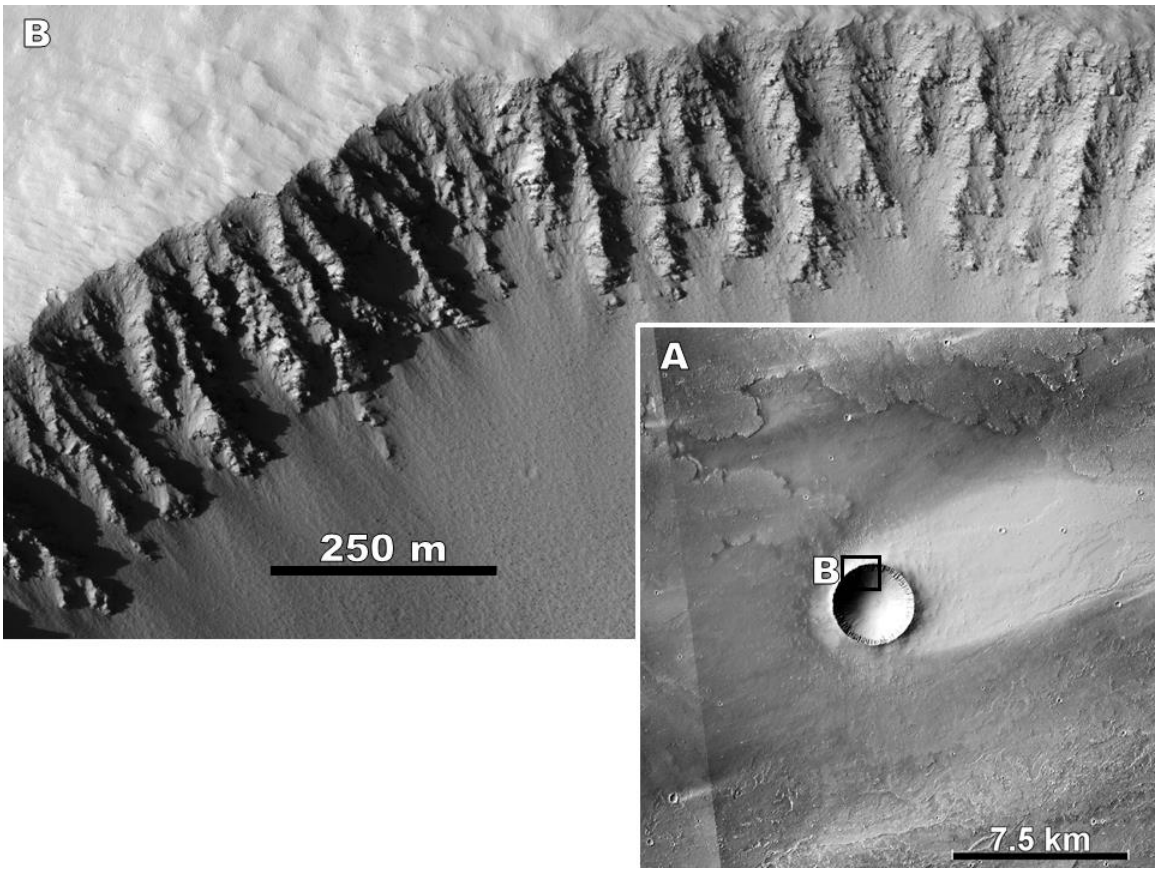

Figure 2.17 An impact crater in the Tharsis region preserves a rough crater wall characterized by numerous bedded lavas. The crater is emplaced in a lava flow field (A), and shows a resistant crater wall with a slope of ~36° (B). The thermal inertia of the bedded lava is ~ 200 TIU, which is likely more reflective of the greater dust mantling in the Tharsis region. CTX image ID: D04_028779_1840_XN_04N102W. HiRISE image ID: ESP_028779_1840.

2.4.2 Anomalous crater east of Apollinaris Mons

An anomalous crater is present beyond the eastern flank of Apollinaris Mons (Figure 2.11). From morphologic observations alone, the anomalous heart-shaped structure more closely resembles a terrestrial tuff ring than an impact-crater. A potential terrestrial analog to the heart-shaped structure is Fort Rock tuff ring (Figure 2.18) in Oregon, USA, which formed through the interaction of magma with a shallow lake (Brand & Heiken, 2009). Both the martian structure and Fort Rock have similar height/width ratios (0.044 for Fort Rock and 0.05 for the heart-shaped crater), horizontal

layering around the outer rim, and flank slopes below 30°. Tuff rings also have interior floors that are at or slightly above the level of surrounding topography, which is observed within the martian structure. The similarity with terrestrial tuff rings suggests that the martian heart-shaped structure is the result of phreatomagmatic activity, where magma encounters groundwater, resulting in an explosive eruption (Brand & Heiken, 2009). This may suggest volcanic activity beyond the flanks of Apollinaris Mons, as well as from the caldera, as is common in terrestrial caldera complexes (e.g., Newberry Caldera, Oregon, USA, MacLeod et al., 1995).

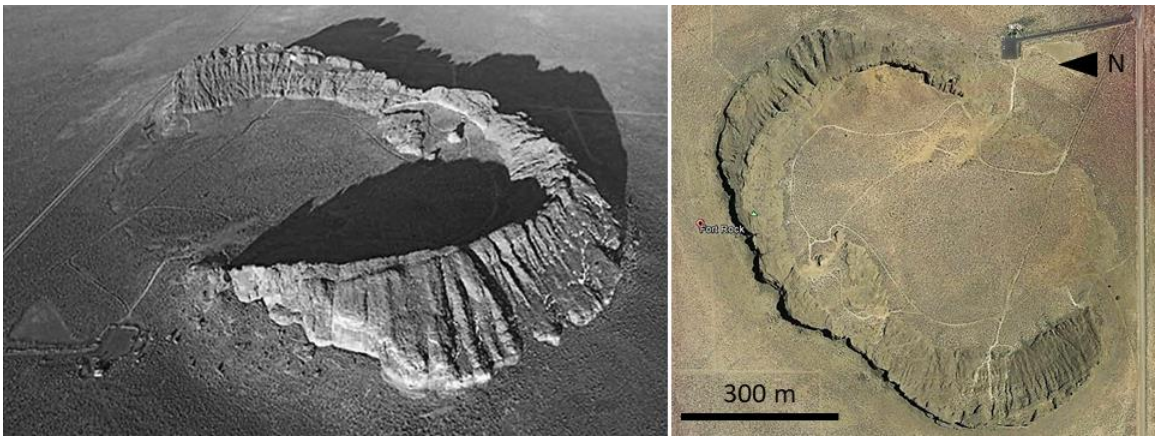

Figure 2.18 Fort Rock tuff ring in Fort Rock, Oregon, USA, shows a similar morphology to the heart-shaped structure near Apollinaris Mons. Both features share height/width ratios, and an interior at the level of surrounding topography. Solar incidence for the photo on the right is from the south (with respect to north in the image).

2.5 Conclusion

All morphologic and thermophysical data collected at Apollinaris Mons suggests the volcano is primarily composed of weakly-indurated, friable materials. Low thermal inertia values throughout the region (under 250 TIU's) are inconsistent with the presence of effusive volcanism. There is no clear morphological or thermophysical evidence for effusive volcanism at Apollinaris Mons aside from reworked blocks identified within the

caldera and along the southwestern flank. Though we do not have access the entire volcanic record at Apollinaris Mons, the abundance of friable materials on the surface and within exposed regions of the substrate point to a volcano dominated by volcaniclastic materials rather than high-strength, blocky lavas from effusive activity. These morphologic observations support the hypothesis that Apollinaris Mons primarily experienced explosive volcanic activity.

The deposits identified on Apollinaris Mons share morphologies with terrestrial volcanic terrains, and can be used as standards for identifying explosive volcanism elsewhere on Mars. While the purpose of this research was not aimed at determining the eruptive style of the volcano, the outcrop scale deposits identified in this study support an explosive history for Apollinaris Mons. One of the more important observations that help interpret an explosive volcanic origin for the deposits described in this research, is the fact that they are all emplaced on a volcanic edifice. Planar bedding, breccia deposits, and friable surface terrains are common sedimentary features; without the presence of a volcanic edifice, it would be difficult to interpret these features as volcanic in nature.

CHAPTER THREE: PROPOSED CALDERAS IN ARABIA TERRA

3.1 Introduction

3.1.1 Objective

Seven craters in Arabia Terra are proposed to be volcanic calderas (Michalski & Bleacher, 2013), based on their unusual morphological characteristics relative to typical impact craters. The objective of this research is to apply the distinguishing characteristics for martian explosive volcanism identified at Apollinaris Mons to test the hypothesis that the unusual craters in Arabia Terra are volcanic calderas.

In this chapter, I investigate the potential for explosive volcanism in Arabia Terra through the analysis of morphological and thermophysical datasets. I compare the morphologies of the proposed calderas to known volcanic collapse structures on Earth and Mars, and dewatering collapse features on Mars. This work has implications for the possible identification of a previously unrecognized volcanic province on Mars. If the unusually shaped craters are volcanic, their identification can help recognize a major source for layered deposits within Arabia Terra. This work can also further our understanding of Mars climate history by identifying new explosive volcanic centers that could have contributed gases to an early martian atmosphere.

3.1.2 Arabia Terra

Arabia Terra is a cratered region of Mars that has been dated to the mid- to late Noachian Era (~3.7—3.9 Ga; Michael, 2013; Tanaka et al., 2014). Arabia Terra covers an area of ~12,000,000 km^2 and is the northern-most extent of the martian highlands (Figure

3.1A; Anguita et al., 1997). The morphology of Arabia Terra is characterized by degraded craters and linear ridges within the intra-crater plains. These linear ridges, also known as wrinkle ridges, are a common feature on Mars and have been interpreted to represent tectonic deformation of the surface (Greeley & Spudis, 1981). Dust mantles much of the highland material in the central region of Arabia Terra, based on the high albedo and low thermal inertia (e.g., Fergason & Christensen, 2008).

Further to the north, the terrain transitions from the cratered highlands into the younger, relatively crater-free lowlands (Figure 3.1A). The transition zone between these two regions is known as the dichotomy boundary, and spans the circumference of Mars in an E-W orientation. The northern boundary of Arabia Terra, along the dichotomy boundary, is characterized by fractured (chaotic) terrain and irregular plateau structures. Chaotic terrain is interpreted as remnants of ice or water-related collapse (Sharp, 1973).

Layered deposits are common within the Arabia Terra region, which have been proposed to originate from accumulated dust deposits, ocean sediments, or volcanic sills (e.g., ; Edgett & Parker, 1997; Grant & Schultz, 1990; Greeley & Guest, 1987; Moore, 1990; Schultz & Lutz, 1988; Wilhelms & Baldwin, 1988). Other studies suggest the source of these layered deposits may originate from explosive volcanism, such as volcanic ash fall (e.g., Fassett & Head, 2007; Hynek et al., 2003; Kerber et al., 2012; Michalski & Bleacher, 2013; Moore, 1990; Scott & Tanaka, 1986). Of these works, Michalski and Bleacher (2013) suggest the source of the layered deposits resulted from explosive volcanic calderas within the Arabia Terra region (Figure 3.2).

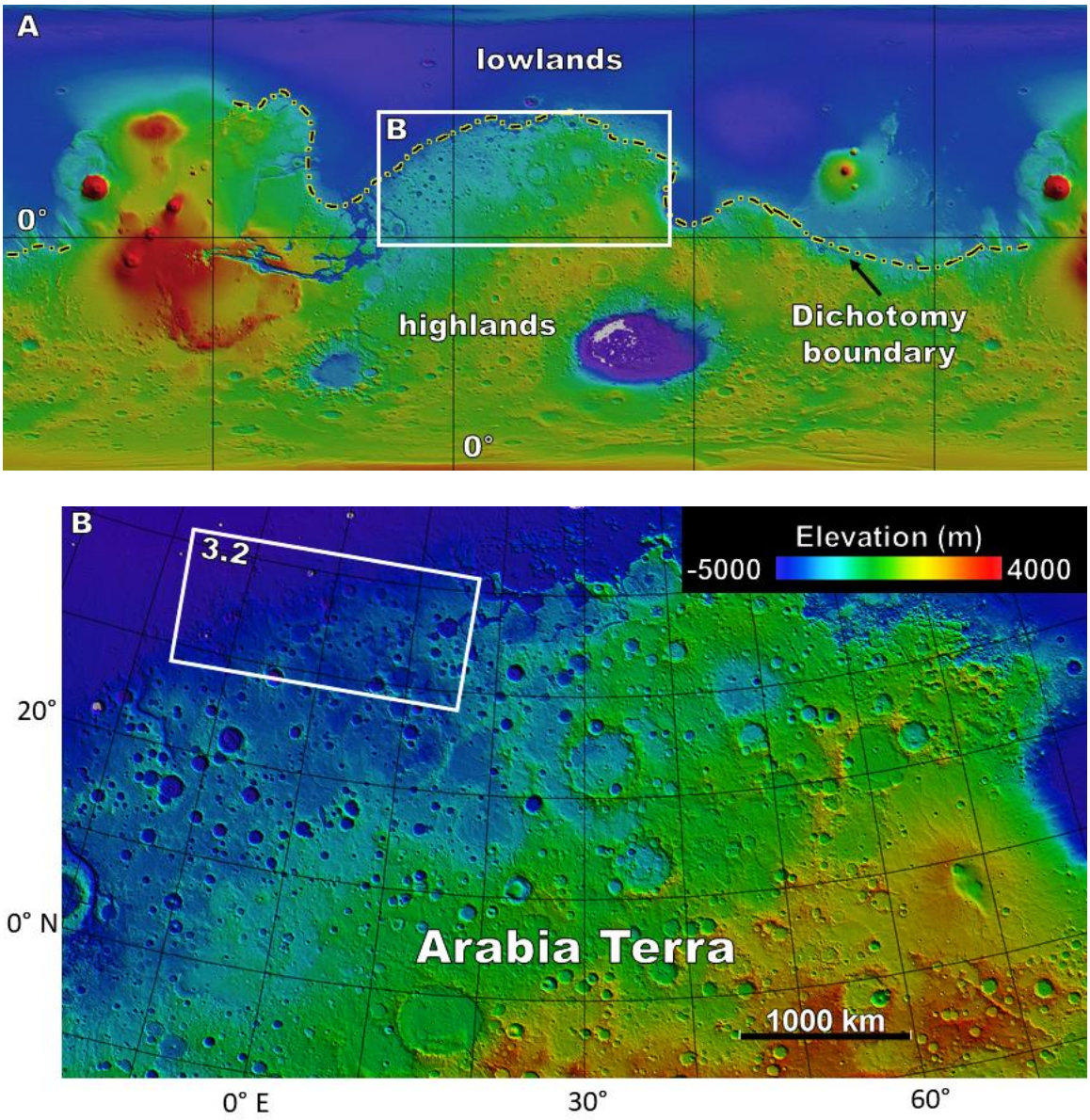

Figure 3.1 (A) MOLA colorized elevation global map of Mars with (B) the location of Arabia Terra. The northwestern region of Arabia Terra that this study focuses on is noted by the white box in (B), and expanded in Figure 3.2.

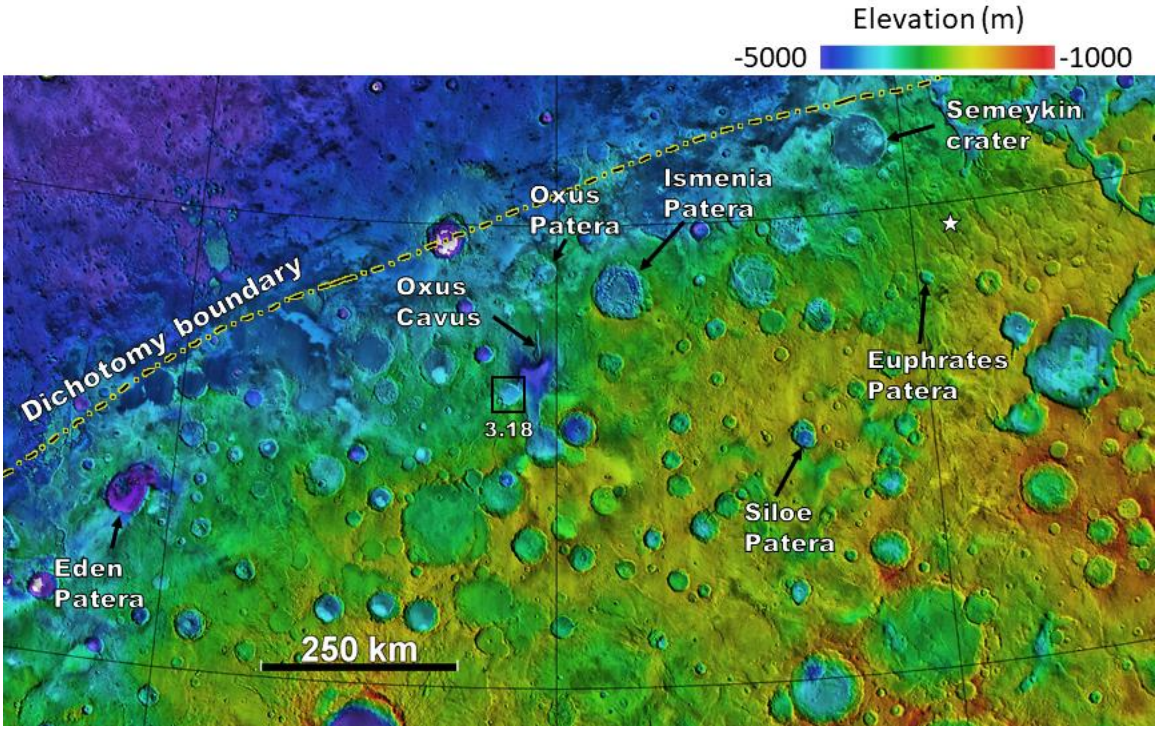

Figure 3.2 Proposed calderas in northwestern Arabia Terra. Modified from Michalski and Bleacher (2013). The star north of Euphrates Patera represents an example of some wrinkle ridges in Arabia Terra.

3.2 Background

3.2.1 Proposed calderas in Arabia Terra

3.2.1.1 Identifying anomalous depressions

Michalski and Bleacher (2013) propose a new style of plains-style volcanism to be the source of layered deposits within Arabia Terra. This new type of volcanism includes calderas with low topographic relief, collapse features, and evidence for both friable ash and blocky lava deposits. Seven anomalous depressions within northwestern Arabia Terra are proposed to represent this new class of volcanic caldera (Figure 3.2): Eden Patera, Oxus Patera, Oxus Cavus, Ismenia Patera, Siloe Patera, Euphrates Patera, and Semeykin crater. The proposed calderas were identified because they exhibit high depth-to-diameter ratios that are not typical for impact craters of similar diameters and

preservation states within Arabia Terra. While all the proposed calderas in Arabia Terra are suggested to have morphologic characteristics of terrestrial calderas (e.g., concentric fracturing, a depth greater than 2 km, and a sub-circular shape), Michalski and Bleacher (2013) identify the most evidence for volcanism within Eden Patera. Thus, the most detailed morphologic observations they present come from Eden Patera (Figure 3.3a).

3.2.1.2 Eden Patera

The Eden Patera complex is proposed to represent three caldera collapse events (Figure 3.3b). Michalski and Bleacher (2013) also identify two fault-bound blocks within Eden Patera that they suggest preserve ridge plains lavas on the surface (wrinkle ridges; Figure 3.3c). They interpret the other fault feature in Caldera 2 to be a graben-related vent structure based on a topographic high peak near the middle of the structure (Figure 3.3d). Looking at smaller scale deposits, Michalski and Bleacher (2013) identify a terrace and fractured mound within caldera 3 (Figure 3.3e) of Eden Patera. They interpret these features to be remnants of a lava lake high stand that were preserved during drainage of the lava lake. However, aside from the presence of wrinkle ridges that have been associated with volcanic plains on the plateaus, there are no identifiable lava flow features (i.e., lobate flow features).

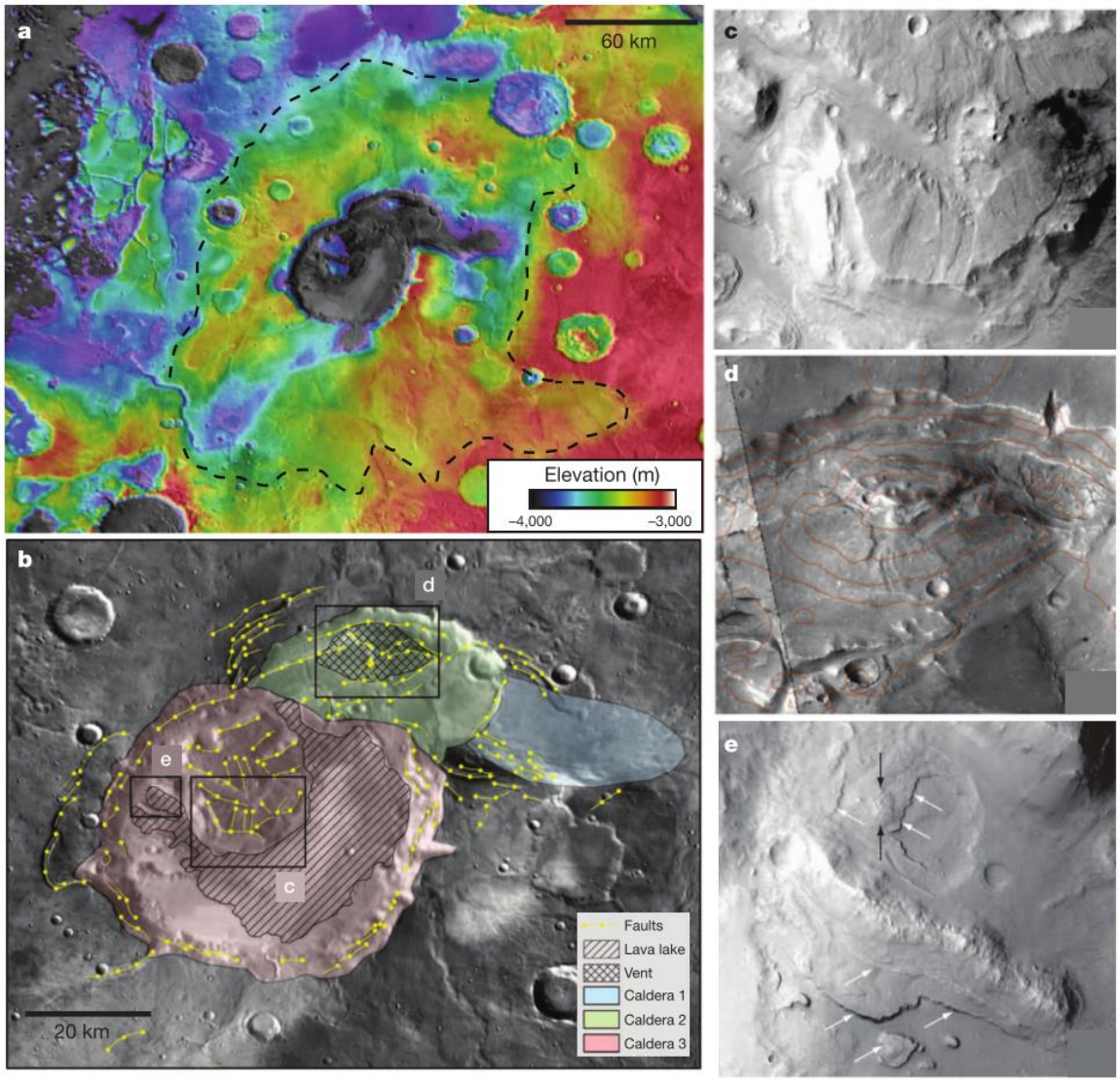

Figure 3.3 This figure is adapted from Michalski and Bleacher (2013). (a) The proposed caldera, Eden Patera, in northwestern Arabia Terra. (b) zoomed in image of Eden Patera, highlighting the proposed caldera depressions from Michalski and Bleacher. Note wrinkle ridges are visible to the southeast of Caldera 3. (c) Interpreted fault block structure in Caldera 3, which also preserves wrinkle ridge structures. (d) Michalski and Bleacher interpret a graben-related volcanic vent structure in Caldera 2. (e) White and black arrows point to a terrace and fractured mound, respectively, which are interpreted by Michalski and Bleacher as remnants of a lava lake.

3.2.1.3 Siloe Patera

Siloe Patera (Figure 3.4) is sub-circular in shape and has a high depth-to-diameter ratio that distinguishes it from other craters in the immediate vicinity. Michalski and Bleacher (2013) suggest a lobate feature off the southwestern rim of Siloe Patera to be

either a lava or pyroclastic flow feature (Figure 3.4). The interior of the proposed caldera also has a plateau along the northern wall with an irregular topography characterized by flat and hummocky fretted terrains, surrounded by ridges hundreds of meters tall (Figure 3.4). Michalski and Bleacher (2013) suggest this plateau surface is composed of pyroclastic materials based on its friable nature.

3.2.1.4 Depression dimensions

Michalski and Bleacher (2013) evaluate the depth-to-diameter ratios of Siloe, Euphrates, and Eden Patera (Figure 3.5) with all the craters in Figure 3.2. Trendlines are fit to the data in four classes: class 1 represents the most degraded and class 4 represents the least degraded (Robbins & Hynek, 2012). The proposed calderas fit closest to class 2 as modified craters. With this data, Michalski and Bleacher (2013) suggest that class 2 craters should still preserve morphological details from the impact, such as well-defined crater rims and ejecta deposits; the lack of this evidence at the proposed calderas leads them to believe they are not formed by impacts.

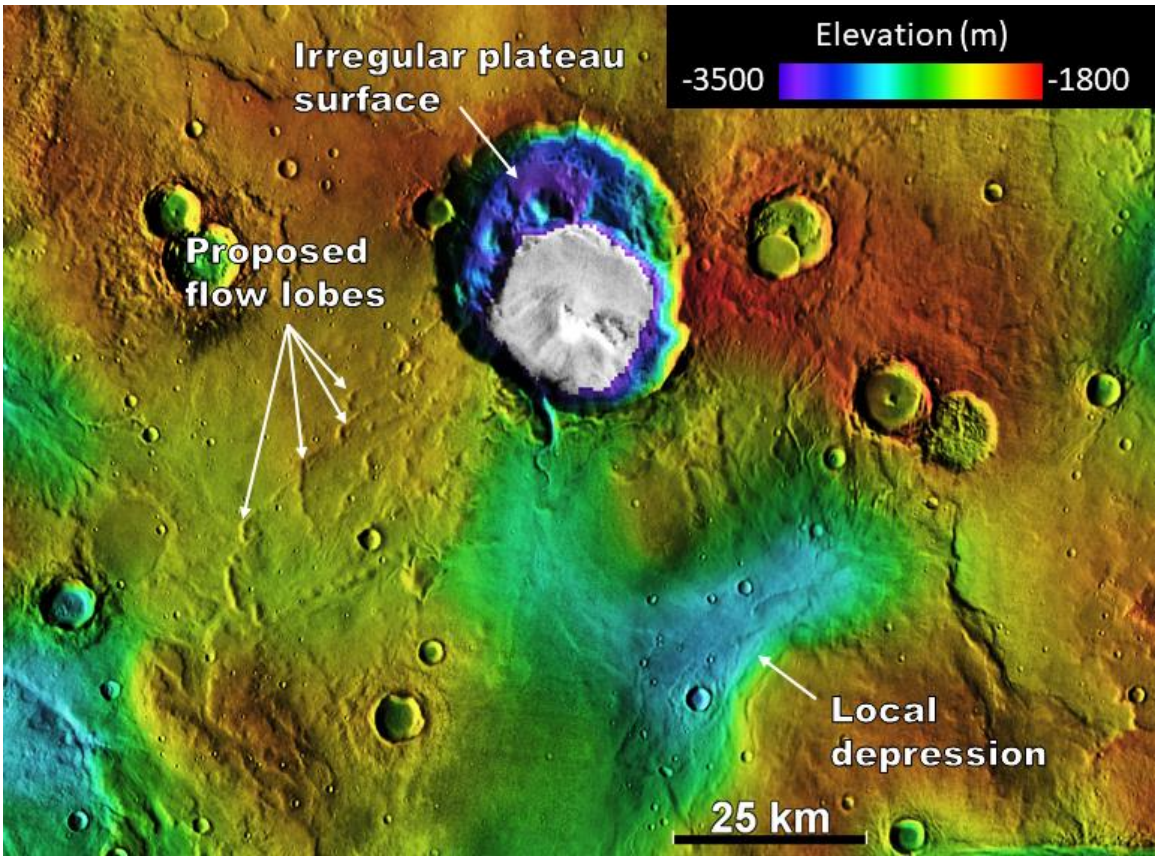

Figure 3.4 Colorized MOLA elevation data draped over THEMIS daytime global mosaic of Siloe Patera. Michalski and Bleacher (2013) propose the lobate deposit off Siloe Pateras southwestern rim to be a volcanic flow, and the irregular plateau surface along the northern wall to be comprised of friable materials. Note the uneven surface topography Siloe Patera is emplaced in, especially the depression south of Siloe Patera.

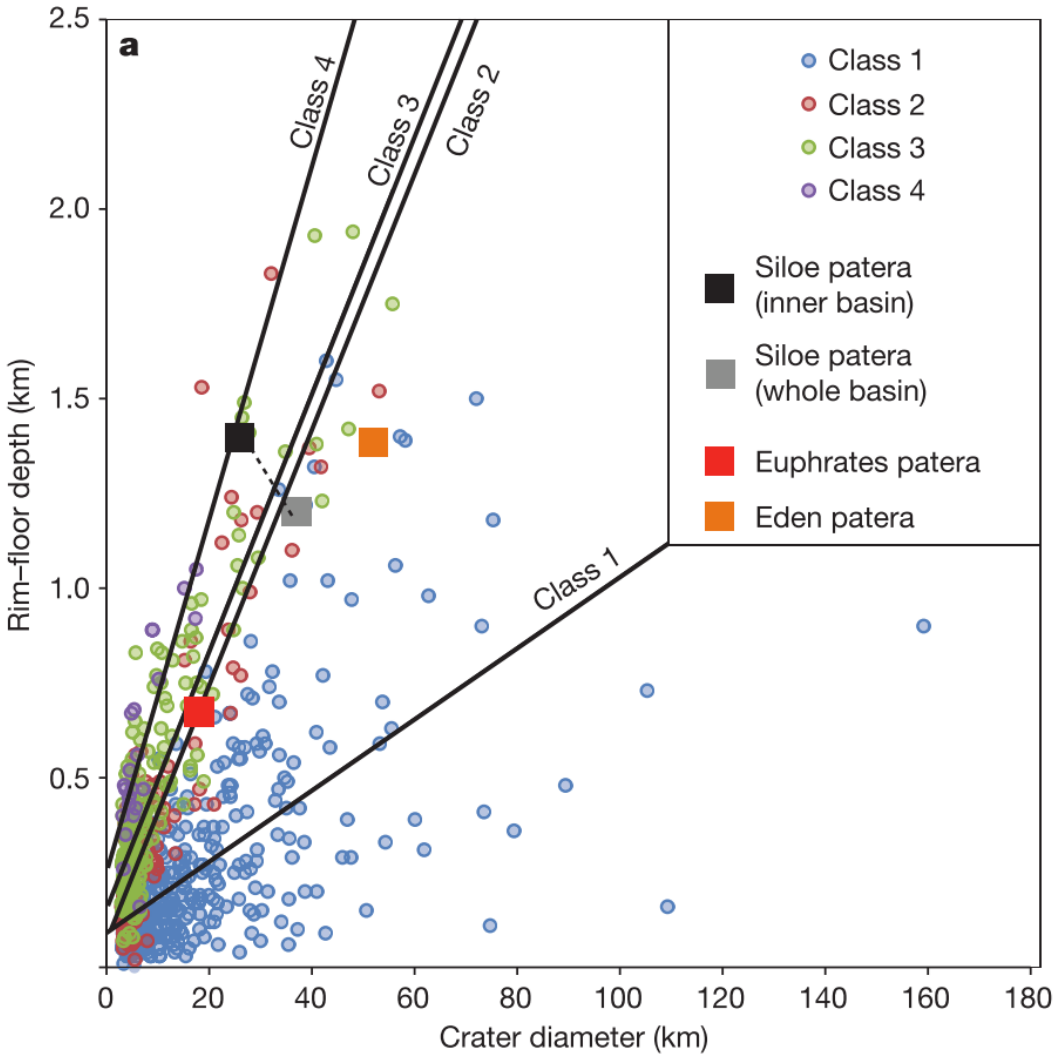

Figure 3.5 Depth-to-diameter plot of all craters in Figure 3.2. Three of the proposed calderas fit in line with class 2 craters, which are degraded craters, suggested to preserve some evidence for impacting. Figure adapted from Michalski and Bleacher (2013).

Michalski and Bleacher (2013) calculate the major and minor axis dimensions of Eden, Euphrates, Oxus, and Siloe Paterae for comparison to terrestrial supervolcanoes, thermokarsts, and martian scalloped terrains (a feature suggested to represent martian thermokarsts; Costard & Kargel, 1995; Séjourné et al., 2011). The proposed calderas show areal dimensions consistent with terrestrial supervolcanoes (Figure 3.6). Michalski and Bleacher (2013) use this to suggest that the proposed calderas are closer in size and

shape to terrestrial supervolcanoes than to thermokarst features. In addition, terrestrial supervolcanoes produce at least 1,000 km^3 of erupted material (Miller & Wark, 2008). Based on volume calculations of Michalski and Bleacher (2013), the proposed calderas could have produced more than 4,600—7,200 km^3 of erupted material (using mafic magma densities for dense rock equivalents), supporting the claim that the proposed calderas can produce enough material to be considered supervolcanoes.

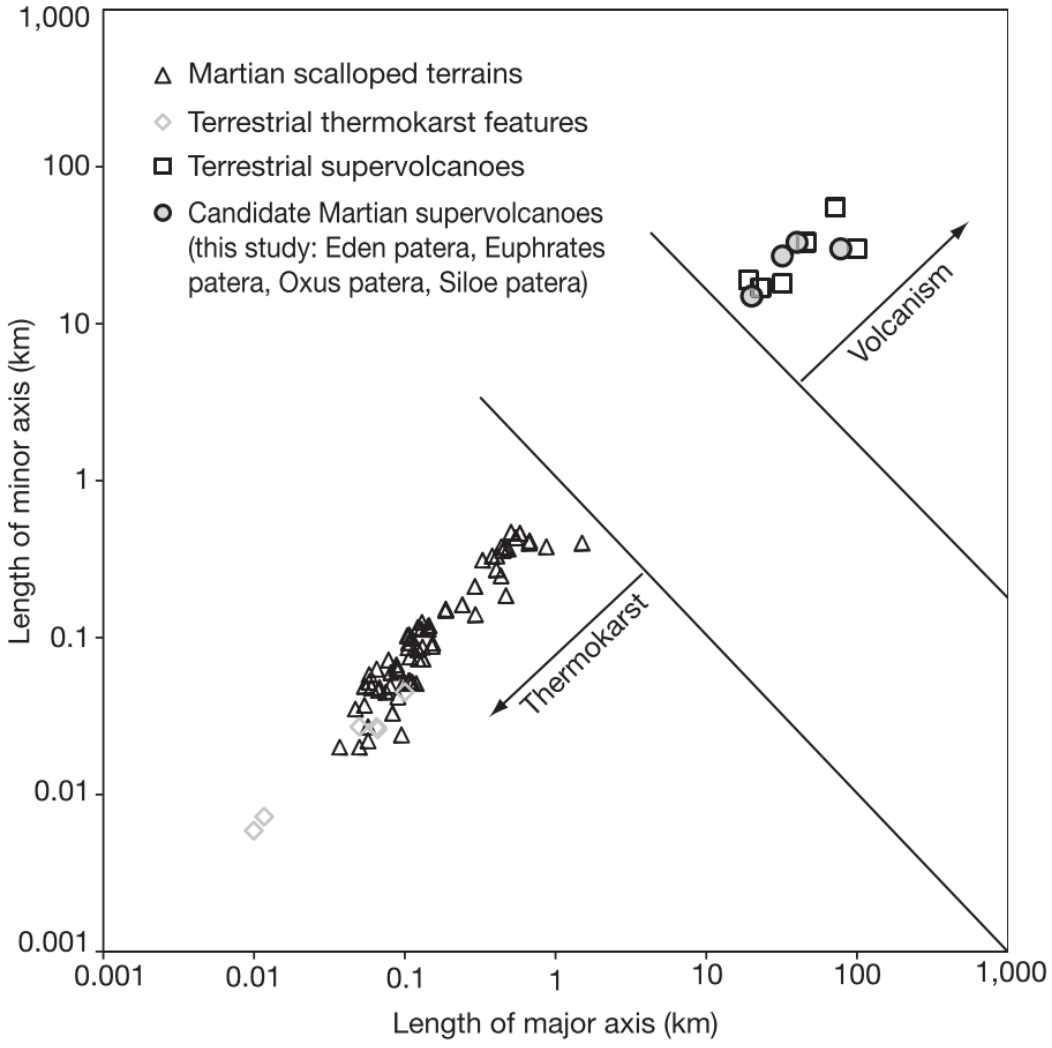

Figure 3.6 Areal comparison of martian and terrestrial collapse features (thermokarsts, calderas, and martian scalloped terrains and proposed calderas). Figure adapted from Michalski and Bleacher (2013).

3.2.1.5 Alternative formation mechanism

Michalski and Bleacher (2013) also test the possibility of collapse resulting from the excavation of subsurface ice (at Eden Patera) based on their initial volume estimations. Using a model that describes the amount and distribution of subsurface ice, they suggest the observed collapse depth is possible if all pore space beneath Eden Patera (down to a depth of 10 km) is filled with ice. They argue that such a requirement is extreme and is unlikely to be the sole factor for collapse.

3.3 Research questions and approach

Michalski and Bleacher (2013) present evidence for regional volcanism with ridge plains (wrinkle ridges) and size similarities between terrestrial and proposed calderas. However, wrinkle ridges have been shown to occur within faulted layered material of a variety of origins (Plescia & Golombek, 1986), and many impact craters in northwestern Arabia Terra display high depth-to-diameter ratios. Without large scale morphologies consistent with volcanism (i.e., volcanic edifices), I question the volcanic nature of the proposed calderas. Collapse morphologies are a common feature in Arabia Terra (i.e., chaos terrain, fretted terrain, concentric fracturing features), and Michalski and Bleacher (2013) have already shown that collapse of Eden Patera by removal of subsurface ice is possible, though they rule it unlikely. The research questions that I will address in this chapter are: (1) Can the evidence for explosive volcanism identified on Apollinaris Mons be used as a framework for identifying explosive volcanism in Arabia Terra? (2) Without strong regional evidence for volcanism, is there other strong evidence that the proposed calderas are volcanic features? (3) Are chaotic style collapse features due to removal of subsurface water a better morphologic match to the proposed calderas?

My results first describe the morphologic and thermophysical observations of the Eden Patera complex, since Michalski and Bleacher (2013) suggest this depression has the most evidence for volcanism. I will discuss the large-scale morphologies observed at Eden Patera in MOLA data and THEMIS image mosaics, and follow up with the fine-scale observations made in CTX and HiRISE datasets. I then compare intra-depression features of Eden Patera with Siloe Patera and Ismenia Patera. Ismenia Patera is included in this study because it is similar in size to Eden Patera. Siloe Patera is included because of the proposed volcanic flow beyond its southern rim. Finally, I describe regional features surrounding Eden, Ismenia, and Siloe Paterae to determine if the proposed calderas are morphologically distinct from other depressions and morphologies in the surrounding terrain.

The morphologic and thermophysical characteristics of Eden, Ismenia, and Siloe Paterae are evaluated with respect to known volcanic calderas on Earth and Mars. As an alternative formation mechanism, I also compare the characteristics of the proposed calderas to those of dewatering collapse features within a region of Mars that is dominated by large outflow channels, and characterized by chaotic and fretted terrains.

3.4 Results

3.4.1 Eden Patera

3.4.1.1 Overview

The Eden Patera complex (Figure 3.7), located at 11° W, 34° N, consists of three nested depressions that reach a maximum depth of ~2 km relative to the surrounding plains. The depression is emplaced in uneven topography, with the elevation of the rim varying between -3 and -4 km. Concentric fractures border the western and eastern rims

of Depressions 1 and 2 (Figure 3.7), while Depression 3 appears as a broad, northwest to southeast trending, region 500 m below the surrounding topography. The terrain immediately inside the rim of Eden Patera slopes into the depression in discrete blocks along regions of concentric fractures (Figure 3.7). The only exception is along the eastern portion of the rim in Depression 1, which is raised and slopes outward at ~3°. Depression 3 slopes into Depression 2 at ~2°. The terrain between Depression 2 and 3 lacks a defined wall, but is marked by a curvilinear fracture. A similar shallow depression feature is present along the southern wall of Eden Patera (Figure 3.7).

Two extensive, dissected plateau structures are present in Depressions 1 and 2 (Figure 3.7). Dissected plateau 1 is ~500 km^2 in area. The plateau slopes towards the east at ~6°, and its surface is dissected by ~3 km wide valleys. Linear ridge features are visible on the surface of Dissected plateau 1 (Figure 3.3c). The highest elevation of plateau 1 is 400 m below the elevation of the western rim of Depression 1.

Dissected plateau 2 is 34 km long, ~11 km wide (spanning nearly the entire diameter of Depression 2), and ~200 km^2 in area. This plateau has a peak on the north side of the feature and is bound by two 1.5 km wide valleys that dissect the plateau into two sections. The plateau slopes ~9° both to the north and south from the northern ridge. The peak of Dissected plateau 2 is at the same elevation as the northern rim of Eden Patera (Figure 3.7).

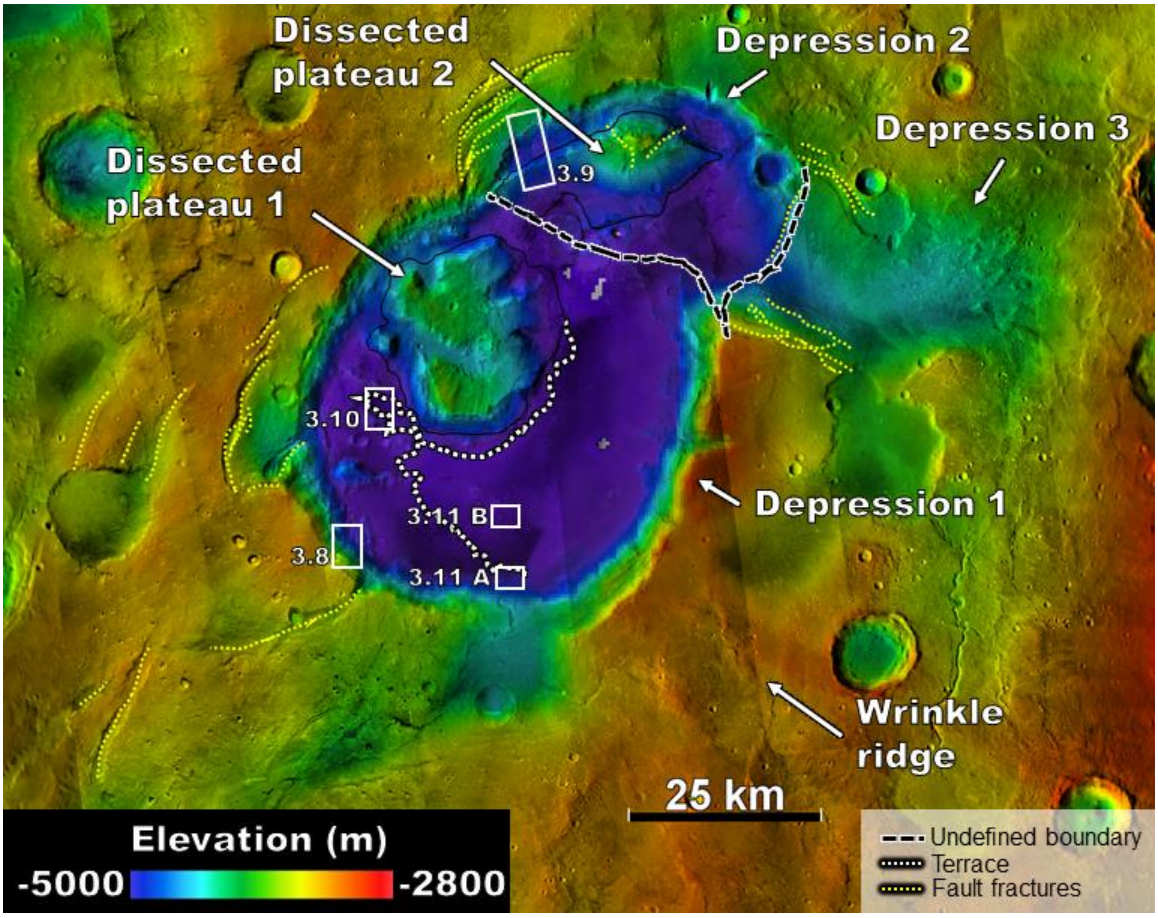

Figure 3.7 Colorized MOLA elevation data draped over CTX mosaic of Eden Patera. The complex consists of three nested depressions bound by concentric fractures. Wrinkle ridges are observed southeast of Depression 1 and along the surface of Dissected plateau 1. The eastern edge of Depression 2 lacks a defined wall; instead, the terrain of Depression 3 slopes into Depression 2 at ~2°. A depression similar to Depression 3 is present along the southern rim of Depression 1. The dissected plateaus are outlined by solid black lines. CTX image ID's: B03_010842_2142_XN_34N010W, P18_007915_2150_XN_35N012W, B17_016288_2131_XI_33N010W, B21_017989_2140_XN_34N011W, B20_017277_2139_XN_33N011W, B16_016077_2144_XN_34N010W, G01_018767_2143_XN_34N011W, D22_035764_2120_XN_32N010W.

3.4.1.2 Bedding in Eden Patera

Bedding is visible in CTX and HiRISE visible wavelength images along the southwestern wall of Eden Patera in Depression 1 (Figure 3.8), and occurs ~700 m below the surrounding plains near an elevation of -4.1 km. HiRISE coverage of this deposit is not available, but the bedding appears friable because linear rills dissecting the bedding

layer are not ridge-forming, a feature often found within coherent bedding layers (Chuang et al., 2016). THEMIS derived thermal inertia of the bedding layer in Figure 3.8 is between 200 – 400 TIU (THEMIS image ID: I05799005).

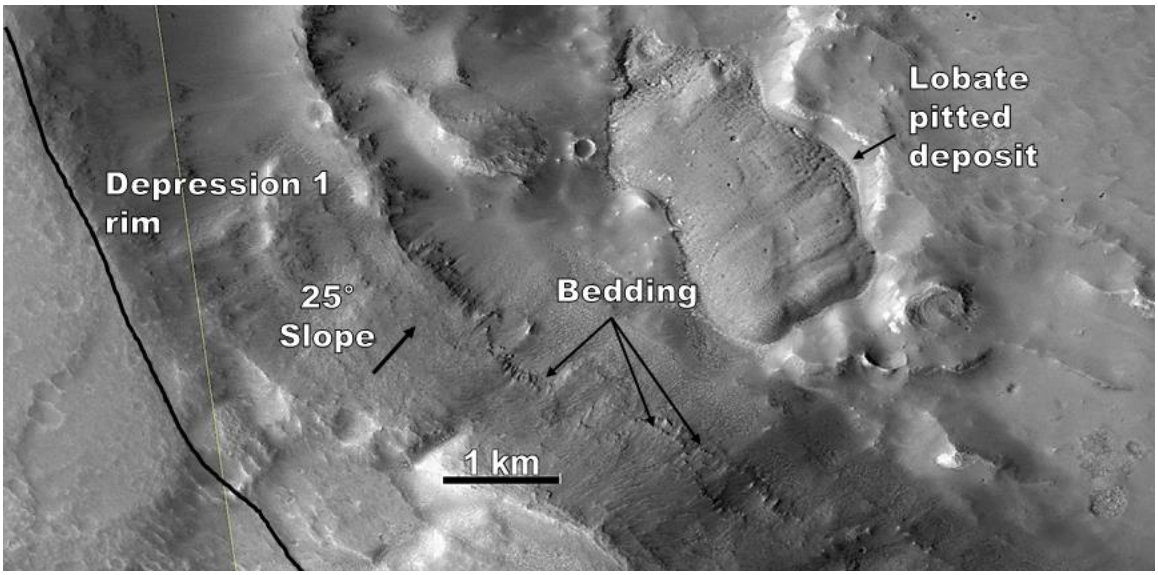

Figure 3.8 Image location labeled in Figure 3.7. Planar bedding is visible along the southwestern wall of Eden Patera. The slope of the wall here is 25°. CTX image ID: ID: B20_017277_2139_XN_33N011W.

Along the northern wall of Eden Patera, in Depression 2, three separate layers are visible in HiRISE images (Figures 3.9). The lowermost layer is the most prominent and is ~200 m below the elevation of the rim (elevation of -4.1 km), reflecting the uneven surface topography in northwestern Arabia Terra. THEMIS derived thermal inertia of the bedding along the northern wall is ~250—300 TIU (THEMIS image ID: I03140003), and appears friable due to a lack of resistant ridges along the layer. Few boulders are present within the layer, with some boulders persisting ~500 m down the ~25° slope, and stopping where the slope of the wall drops to ~10°. Planar bedding is also visible below the peak of Dissected plateau 2, along the northern slope (Figure 3.9). No boulders are observed within or below the bedding along the plateau.

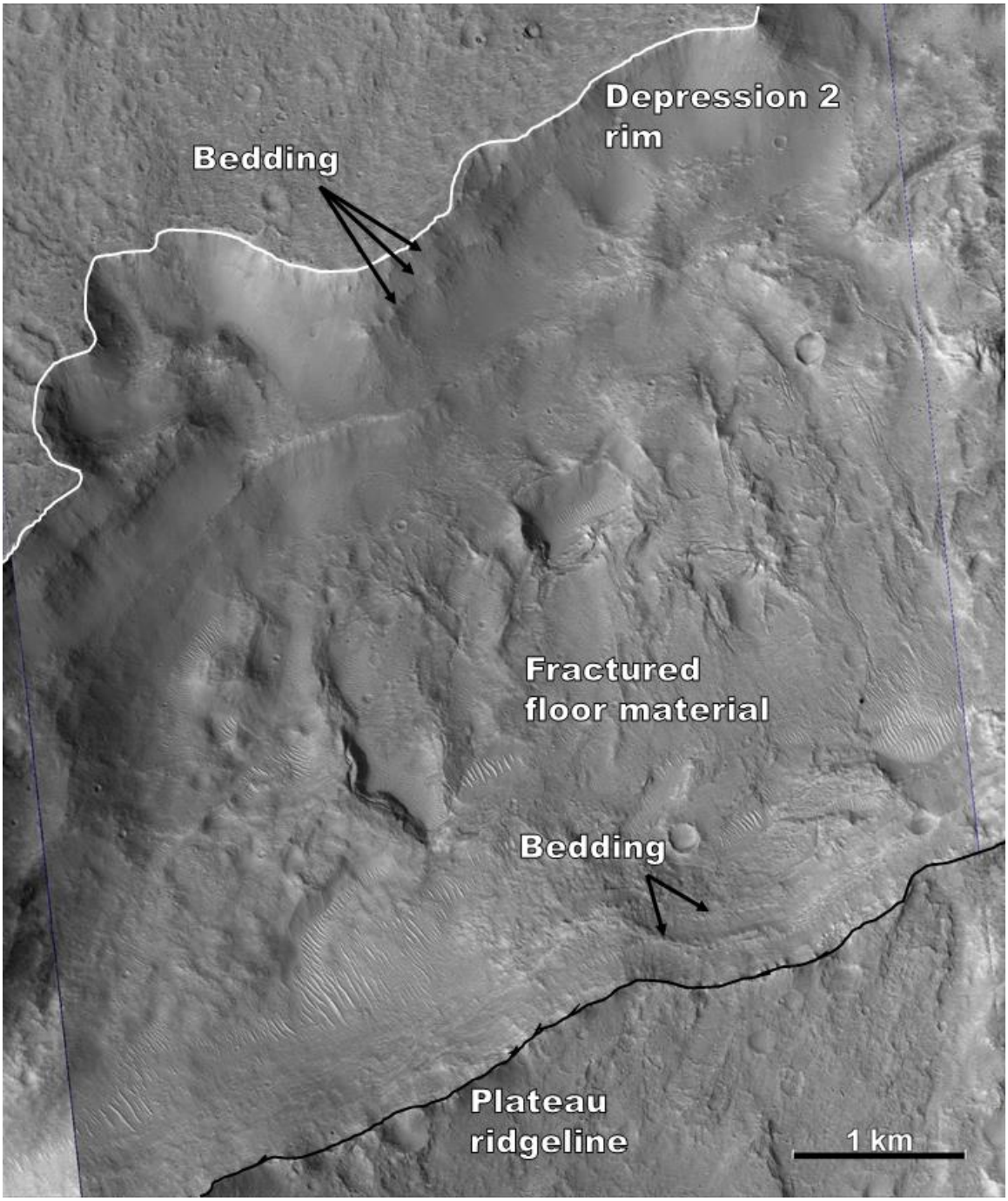

Figure 3.9 Image location labeled in Figure 3.7. Bedding is visible along the northern wall of Eden Patera and along the northern aspect of the dissected plateau in Depression 2. Rectilinear and curvilinear fractured terrain is found along the floor of Depression 2, between the rim and plateau ridge. HiRISE image ID: ESP_029092_2145.

3.4.1.3 Floor characteristics at Eden Patera

A terrace feature borders the southern and western edges of the Depression 1 floor (Figure 3.7). The terrace is ~50 m tall (measured using cast shadow lengths in HiRISE data), and has a rectilinear fractured surface texture (Figure 3.10). Boulders appear to break off the edges of the terrace, and collect at the foot of the ~70 m long terrace slopes. The thermal inertia of the terrace is ~400—500 TIU based on THEMIS data (THEMIS image ID's I05799005, I03140003, I10879005). The floor of Depression 1 that is bordered by the terrace feature has a thermal inertia value of ~300 TIU (THEMIS image ID's: I03140003, I10879005). Meter-scale layering is observed along the western extent of the terrace (Figure 3.10). The southern extent of the terrace is comprised of dissected ridges and mesa structures (Figures 3.11).

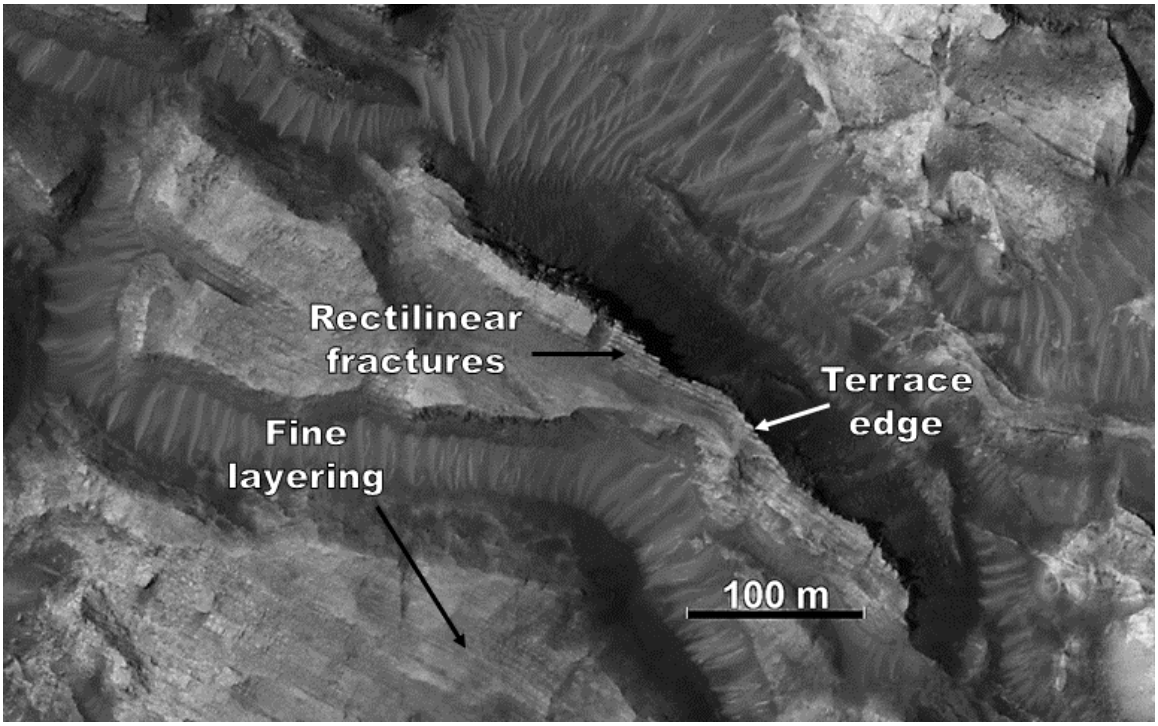

Figure 3.10 Image location labeled in Figure 3.7. The terrace feature that borders the floor of Depression 1 shows a fractured edge. Boulders are seen down the slopes of the terrace edge. Fine meter-scale layering is observed along the ridges. HiRISE image ID: ESP_030371_2140.

The southern region of Depression 1 contains a low albedo material at the base of the terrace in Figure 3.11A, which has a thermal inertia value of ~500 – 600 TIU (THEMIS image ID: I03140003, I10879005). Where visible in HiRISE datasets, the floor in the low albedo region is littered with boulders; impact craters in this low albedo material have blocky crater ejecta (Figure 3.11A).

The south-central region of the floor includes ~50 m tall mesas (Figures 3.11B). Impact craters in this region lack the blocky ejecta observed within the low albedo material. The morphology of the mesas resembles the terrace that borders the floor, and like the terrace, boulders persist down the 70 m long slopes of the mesa (Figure 3.11B).

The floor of Depression 2 is limited in extent since the dissected plateau structure occupies most of the area, but rectilinear and curvilinear fracturing features occupy the region between the plateau and the northern wall (Figures 3.9). The thermal inertia of these fractured terrains is ~200 – 300 TIU (THEMIS image ID: I05025006, I10879005). There are no observed boulders associated with these fractured terrains in HiRISE images.

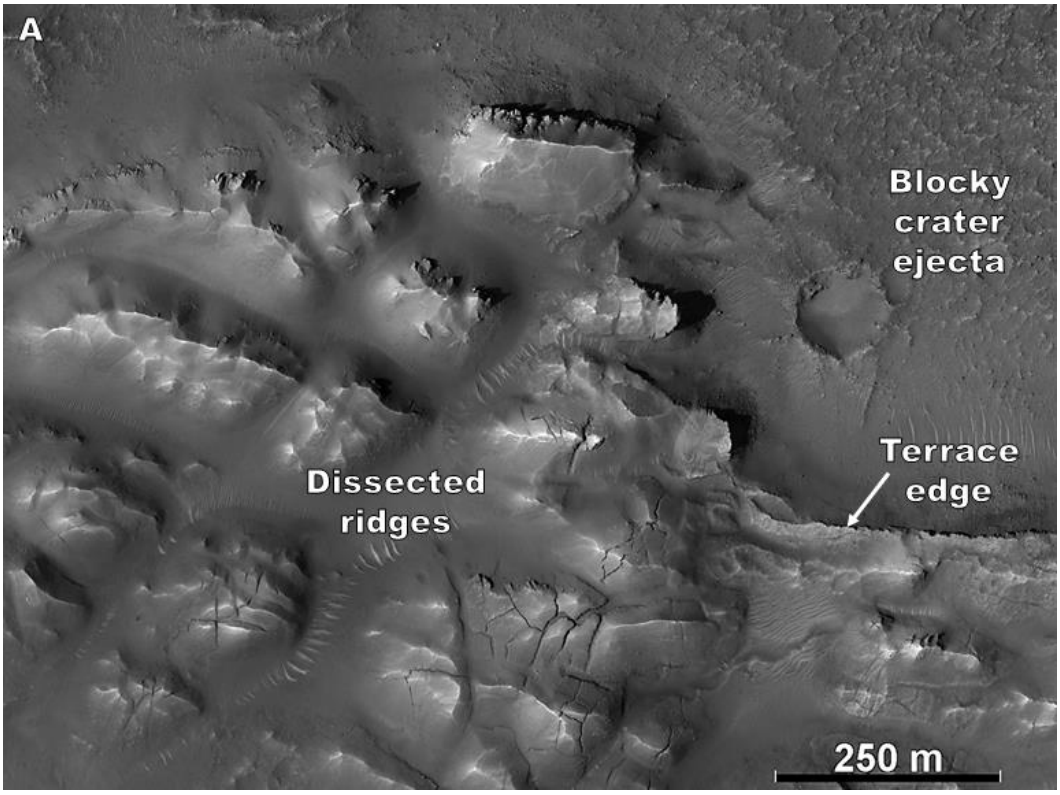

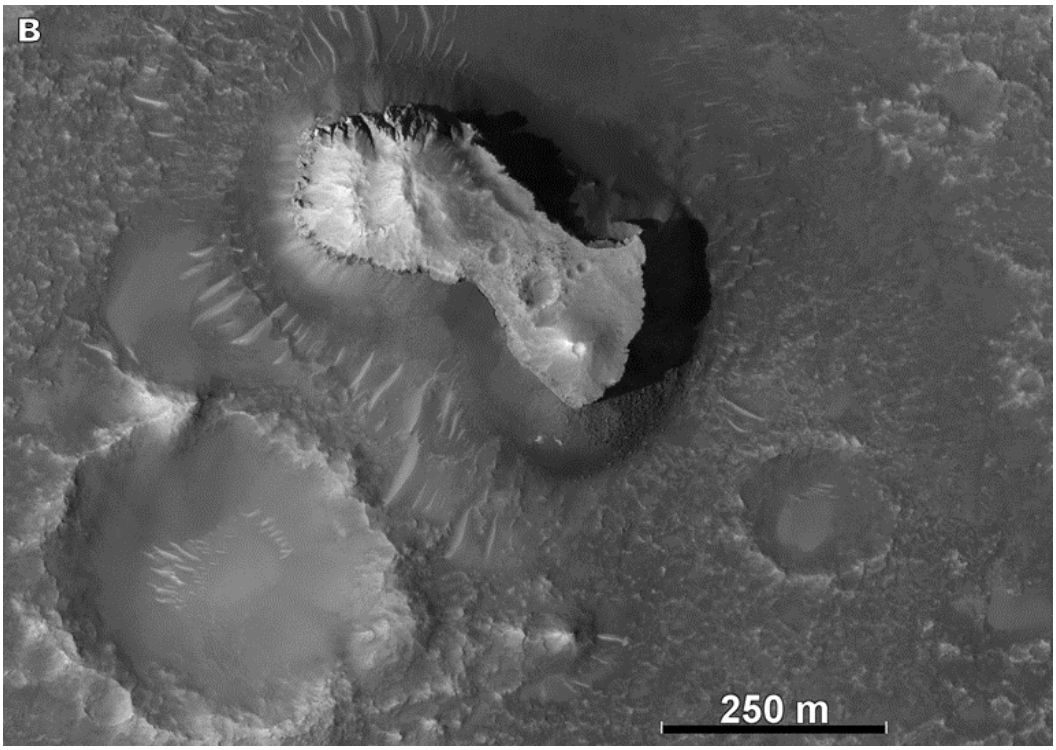

Figure 3.11 Image locations labeled in Figure 3.7. (A) The southern edge of the terrace in Depression 1 shows dissected ridges above a blocky interior floor. (B) The south-central region of the floor preserves ~50 m tall mesas with boulders along the slopes. The floor in (B) lacks boulders. HiRISE image ID: ESP_028525_2135.

3.4.2 Siloe Patera

3.4.2.1 Overview

Siloe Patera is a 39 by 34 km, sub-circular depression located 850 km east of Eden Patera at 6.6° E, 35.2° N (Figure 3.2 and 3.12). The rim elevation of Siloe Patera varies by ~900 m, which is similar to the one-kilometer variance observed at Eden Patera. Unlike Eden Patera, concentric fracturing is not present around the rim of Siloe Patera. The slope of the walls also varies between 10° and 32° with the steepest slopes along the eastern wall.

Two large, kilometer-long valleys cut through the northern and southern portion of the rim of Siloe Patera. The valley dissecting the southern rim, the larger of the two, is sinuous with a length of 15 km and widens from ~0.4 to 2 km toward the rim. Bedding, including three, 20 m thick layers, is visible along the walls of the valley in HiRISE images. Boulders are not visible within or below the bedding, and the average slope of the wall is ~14°. A 3 km wide mound of material is present at the mouth of the valley, along the base of the wall in Siloe Patera. The valley dissecting the northern wall shows many similar features, but is only 3 km long and ~500 m wide.

In addition to the two large valleys, the northwestern portion of the wall is characterized by numerous 100 m wide valleys (Figure 3.12). The slopes of these dissected walls are less than 15°. Many similar-scale, sinuous valleys are also present just outside the rim of the depression (Figure 3.12).

3.4.2.2 Bedding in Siloe Patera

Planar bedding is present along the northern and eastern walls of Siloe Patera. HiRISE coverage of the eastern wall shows three block rick layers, each ~30 m thick.

Boulders within these bedded layers visibly persist only 100 m down slope. A few boulders are present at the base of the 2.5 km long wall, but it is unclear if they are sourced from the bedded layers. Thermal inertia of the bedded layers is between 200—300 TIU (THEMIS image ID: I07546014).

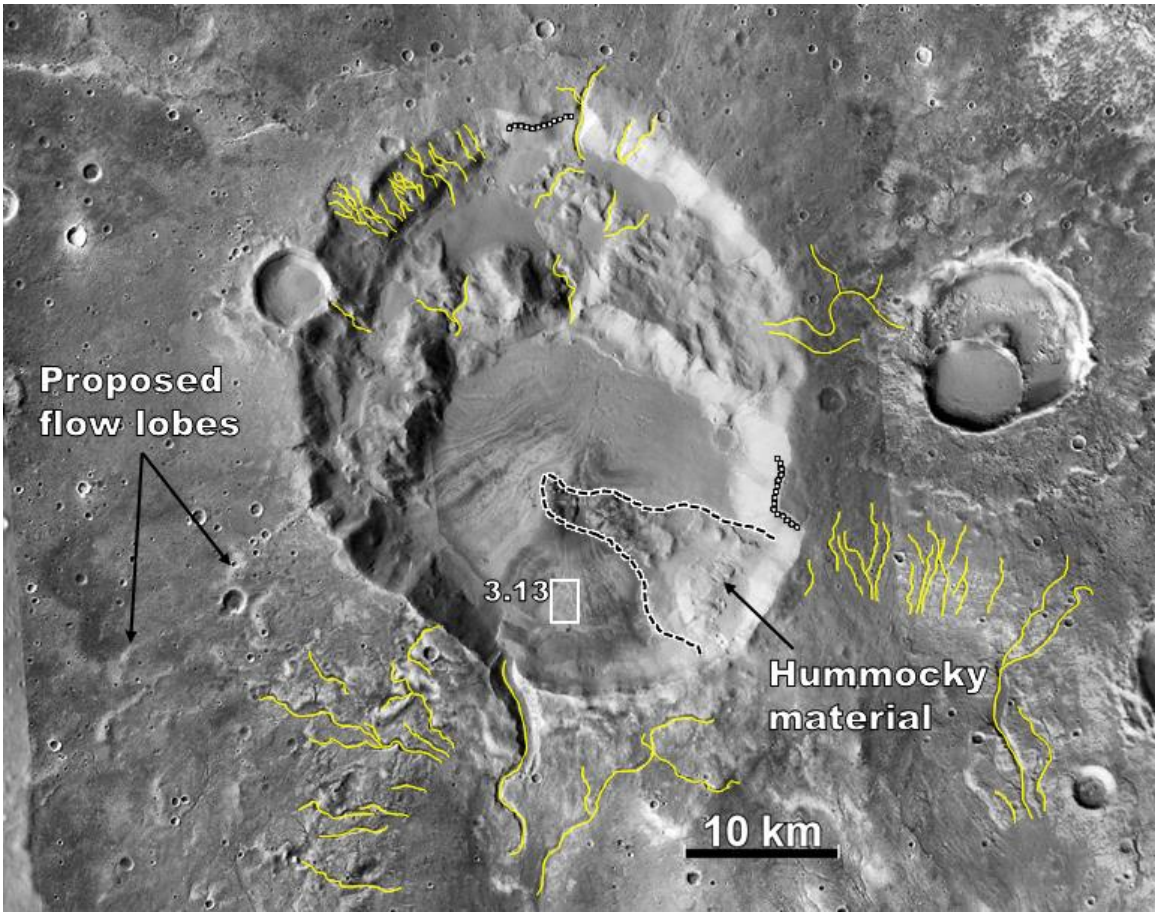

Figure 3.12 CTX mosaic of Siloe Patera. Bedding (dashed white lines) is present along the northern and eastern wall. A hummocky deposit emanating from the southwestern portion of the wall is outlined by dashed black lines. Sinuous valley features within and around Siloe Patera are represented by yellow lines. CTX image ID: J03_045891_2151_XI_35N353W, J11_048950_2149_XN_34N352W, D15_033047_2171_XI_37N353W, P21_009325_2160_XN_36N354W.

3.4.2.3 Floor characteristics of Siloe Patera

A ~300 km^2 crescent-shaped plateau extends across the northern region of Siloe Patera (Figure 3.12). The plateau has an irregular, hummocky surface that varies in

elevation between -2700 and -3500 m (average depth of the plateau below the rim is ~1 km). The low elevation regions of the plateau are smooth and level surfaces in CTX images, and display a surface texture of discontinuous linear and curvilinear ridges in HiRISE images. A series of sinuous valleys extend down from the northern wall to the basal floor of Siloe Patera (Figure 3.12). The valleys are 0.5 km wide and dissect the hummocky terrain of the plateau.

A circular, low relief floor encompasses the southern region of Siloe Patera (Figure 3.12). The area of this deeper floor is ~330 km^2 and the crater rim-to-floor depth is ~2 km. A hummocky deposit (with a surface roughness on the order of 100's of meters) extends from the southeastern wall across the low relief floor, with a slope of ~5° dipping towards the depression center (Figure 3.12). A wall scarp aligned with the hummocky deposit extends 2 km beyond the rest of the rim of Siloe Patera. The floor texture of the southern depression is similar to the flat surfaces on the plateau, displaying disconnected linear and curvilinear ridges on the order of 10's of meters (Figure 3.13). Some shallow valleys within this terrain show linear fracture features that trend parallel to the valley (Figure 3.13).

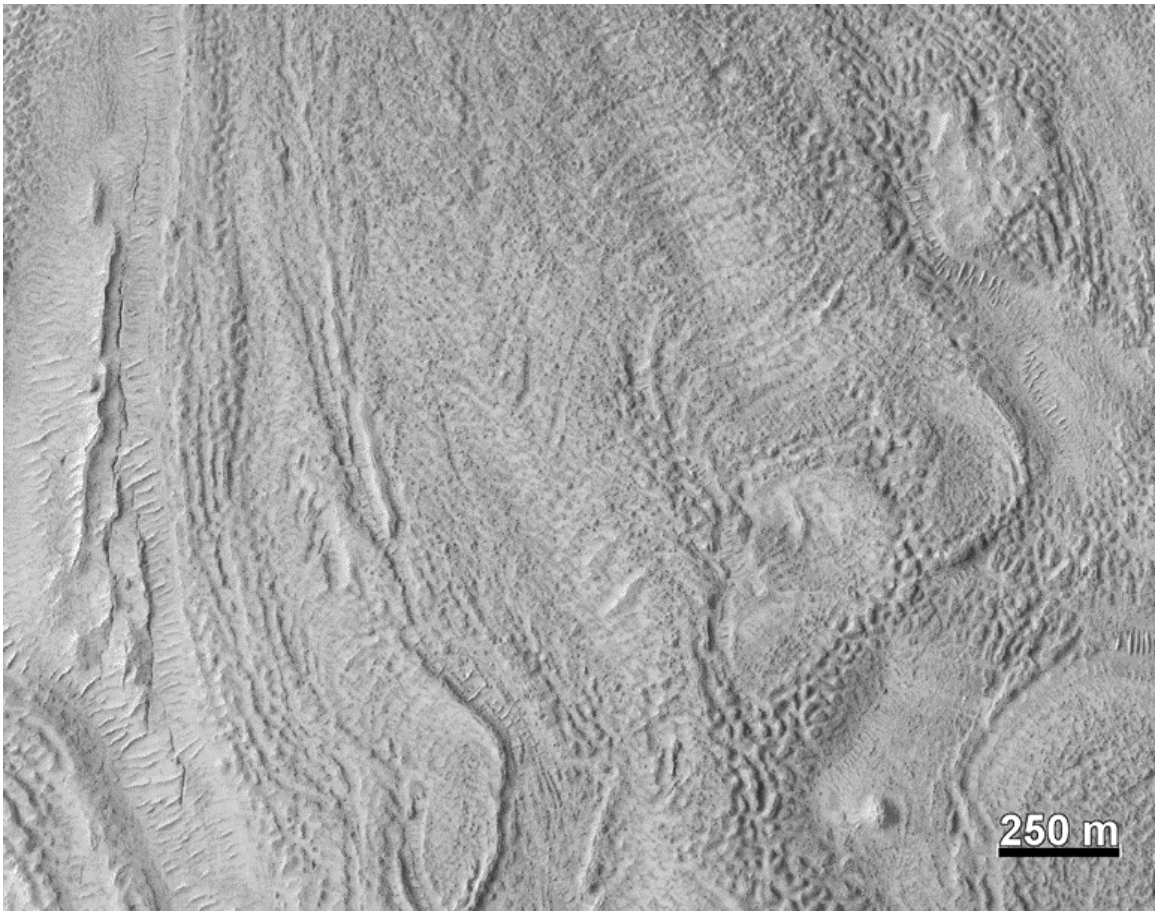

Figure 3.13 Image location labeled in Figure 3.12. The floor of Siloe Patera shows discontinuous linear ridges, and curvilinear valleys, that contain parallel fractures within the center. HiRISE image ID: ESP_036726_2155.

3.4.3 Ismenia Patera

Ismenia Patera is located 600 km northeast of Eden Patera along the dichotomy boundary at 2° E, 38.5° N (Figure 3.2 and 3.14). Ismenia Patera is 82 by 73 km in size and has a maximum depth of 1.9 km. The southern and western portion of the rim are slightly raised and slope outward by 1.5°. The rim interior is characterized by concentric fractures, creating disconnected terraces (Figure 3.14). The slope of the wall varies between 3° and 26°, with the steepest slopes present along the southern rim.

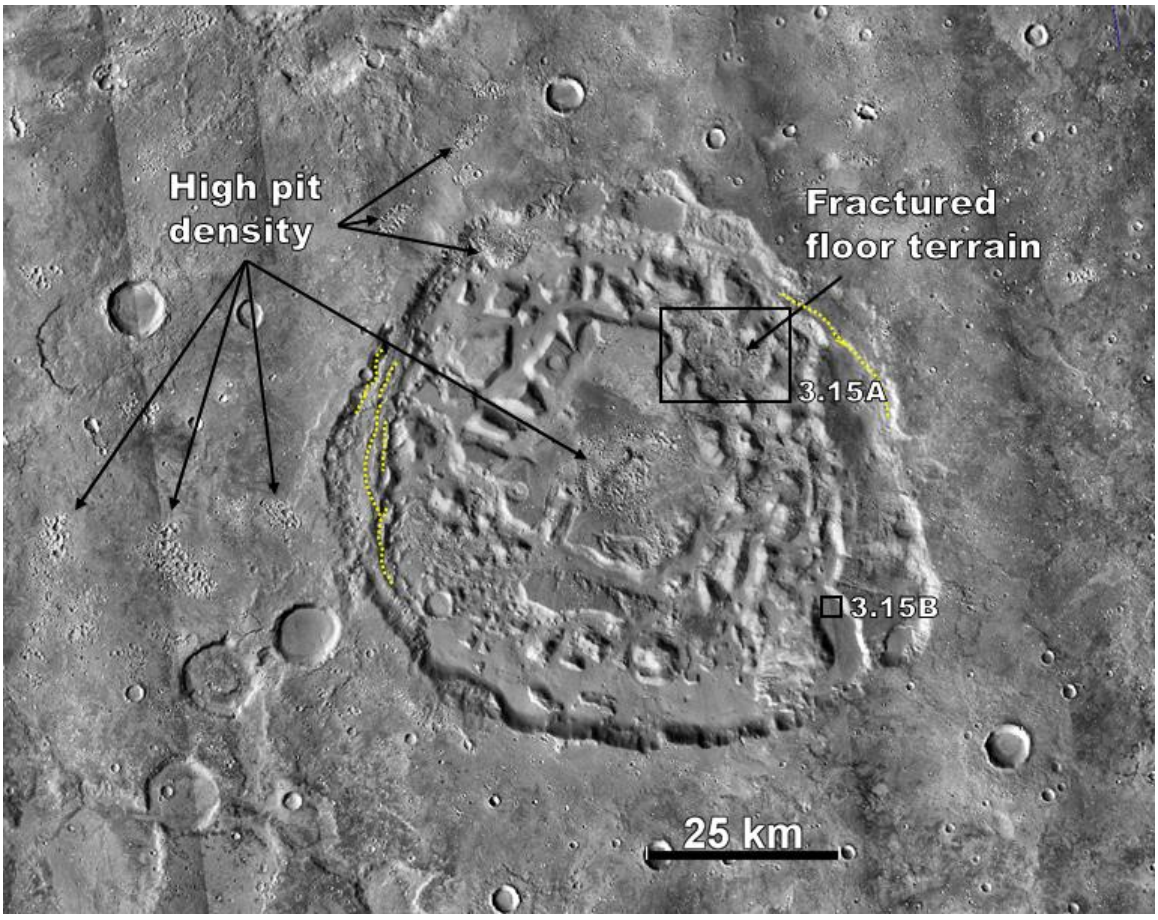

Figure 3.14 CTX mosaic of Ismenia Patera. The rim of the depression is characterized by terraces and concentric fracturing (dashed yellow lines). The interior of the depressions is dominated by polygonal plateau structures. The floor between the plateaus shows rectilinear fracturing features (3.15A) and disconnected linear ridges (3.15B). The central plateau has a high pit density that resembles similar pit clusters outside of the depression. CTX image ID: P20_008956_2197_XN_39N000W, P15_006952_2201_XN_40N357W, P22_009602_2210_XN_41N357W, D16_033390_2180_XI_38N356W, P21_009312_2208_XN_40N359W, G23_027153_2179_XN_37N359W, G20_025953_2199_XN_39N359W, J05_046656_2186_XN_38N358W, P15_006807_2187_XN_38N358W.

The interior of Ismenia Patera is dominated by tens of kilometers wide polygonal plateaus (Figure 3.14), which resemble the polygonal plateaus associated with chaos terrain (e.g., Circum-Chryse region of Mars; Chapman & Tanaka, 2002). The plateaus have rounded edges and are dissected by kilometer wide valleys. While most of the plateau surfaces are flat, many are tilted towards the center of the depression with slopes

of less than 6°. The plateaus are ~500 m tall on average. The tallest plateau is located along the southeastern portion of the rim, and has a peak height 100 m above the elevation of the adjacent southeastern rim. The central plateau is the largest, and occupies 15% of Ismenia Pateras area. The middle of the central plateau has an unusual dense pit cluster (pitted terrain) that is unique relative to the rest of the depression. This pitted terrain shows no evidence of crater ejecta, and is also present northwest of the depression extending to tens of kilometers beyond the rim of Ismenia Patera (Figure 3.14).

Bedding, mesas, and fractured terrain similar to those found in Eden Patera are present in Ismenia Patera. Planar bedding is visible along the slopes of some plateaus, but is not observed along the walls of Ismenia Patera. Between the plateaus, portions of the crater floor show rectilinear fracturing and morphologies similar to other chaos terrains (Figures 3.15A). In HiRISE images, the fractured terrain shows mesas with a knobby surface texture; some of the mesas show flat topped surfaces with linear fracture patterns, and angular edges with boulders persisting down the ~70 m long slopes (similar to the terrace height in Eden Patera). The rest of the depression floor between the plateaus appears smooth in CTX images, but disconnected linear ridges on the order of 10's of meters are apparent in HiRISE images (Figures 3.15B). The linear ridge structures are oriented parallel to the edge of the plateaus, and become more discontinuous and curvilinear closer to the plateau. Thermal inertia of the fractured terrain is ~200—300 TIU (THEMIS image ID: I09044011, I06173010).

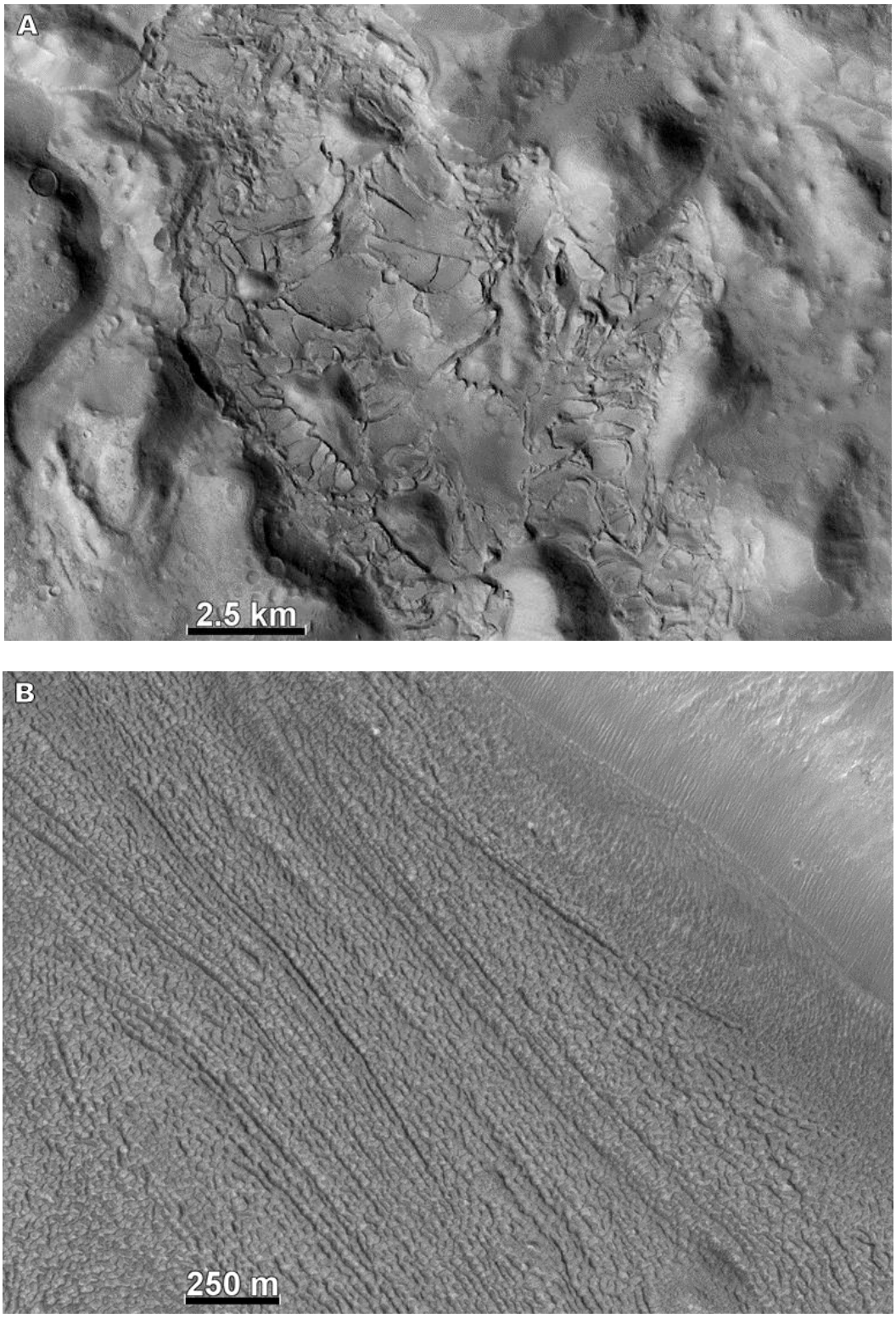

Figure 3.15 Image location labeled in Figure 3.14. (A) Patches of fractured terrain on the floor of Ismenia. Mounds within the terrain have fractured plateaus sloping up along their sides. (B) Disconnected linear ridges in the intra-plateau terrain. The ridges are oriented parallel to the edge of the plateau. CTX image ID (A): P15_006807_2187_XN_38N358W. HiRISE image ID (B): ESP_050137_2185.

3.4.4 Regional morphologies surrounding Eden, Ismenia and Siloe Patera

The regional topography around Eden Patera slopes towards the dichotomy boundary to the northwest at less than 1° (Figure 3.16). At the dichotomy boundary, the elevation drops by 600 m over 6 km as the terrain transitions to the northern lowlands. Northwest of Eden Patera, the dichotomy boundary is characterized by polygonal plateaus and rectilinear fracturing similar to other chaotic terrains along the dichotomy boundary (e.g., Circum-Chryse; Tanaka et al., 2003) (Figure 3.16). This fractured terrain is extensive, covering ~4700 km^2 (by comparison, the Eden Patera complex is ~3000 km^2). Wide channel features similar to fretted terrain are present southwest of Eden Patera, along the dichotomy boundary (Figure 3.16).

The plains around Eden Patera are uneven and characterized by sinuous channels, fractures, and wrinkle ridges (Figure 3.16). Many of the channels and depressions appear connected and trend towards the northern lowlands. For example, a 40 km wide, 450 m deep depression extends from the southwestern rim of Eden Patera, abutting against the head of a 2 km wide, 100 km long sinuous channel (Figure 3.16). The channel extends southeast to northwest, crossing the dichotomy boundary before diffusing into the basin. Similar sinuous channels are present throughout the plateau surrounding Eden Patera, and generally trend in a northwestern and western direction. Of the smaller channel features, one leads into Depression 3 of Eden Patera (Figure 3.7 and 3.16).

Much like the region of Arabia Terra surrounding Eden Patera, the regions surrounding Ismenia and Siloe Patera contain chaotic-like fracturing features, sinuous channels that extend into the northern lowlands, fretted terrain, and wrinkle ridges. Channels and valleys are present, with many of them dissecting multiple craters. Also,

similar to the Eden Patera region, many of the channels and depressions appear connected, and trend toward the northern lowlands with the topography.

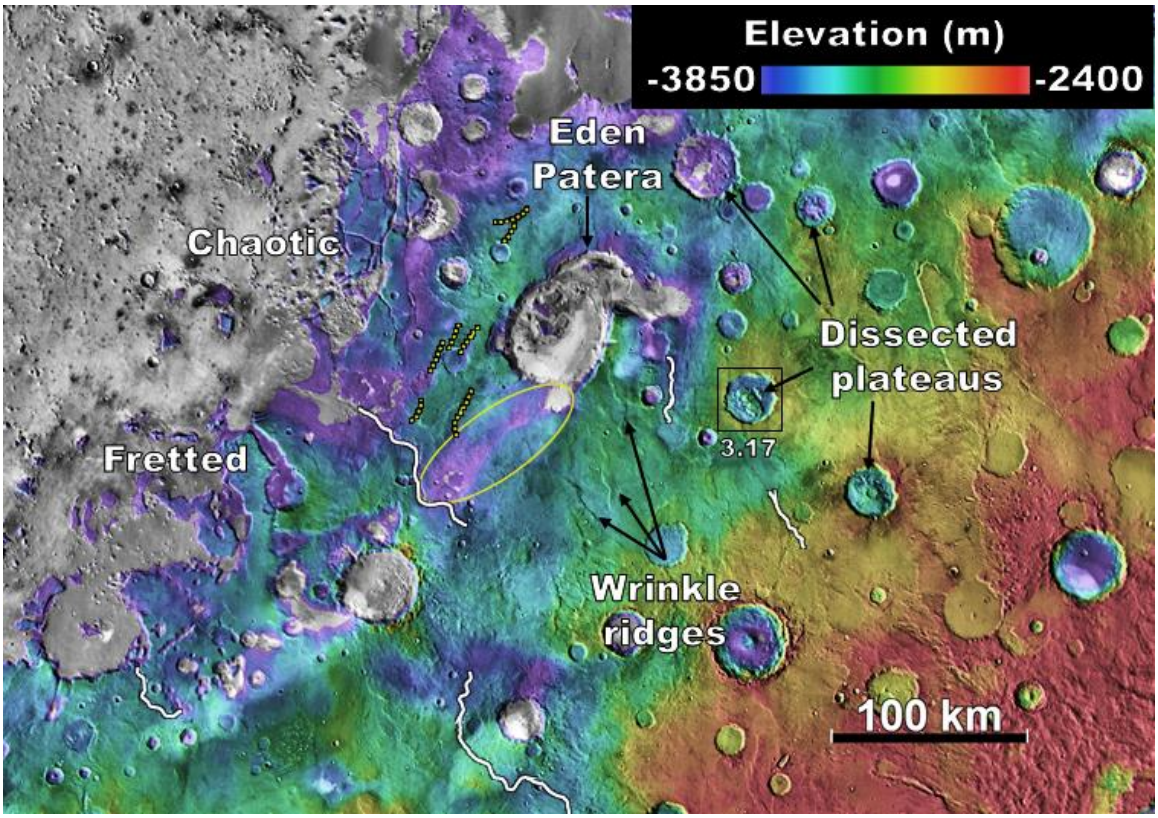

Figure 3.16 Colorized MOLA data draped over THEMIS daytime global mosaic of northwestern Arabia Terra, surrounding Eden Patera. Fracturing not associated with Eden Patera is also present (dashed yellow lines). The terrain beyond Eden Patera is composed of sinuous channels (while lines), wrinkle ridges, and chaotic and fretted terrain along the dichotomy boundary. Dissected plateaus are visible in regional craters around Eden Patera. The broad depression adjacent to Eden Patera and the 100 km long channel are outlined in yellow.

3.4.5 Morphology of other craters and depressions in northwestern Arabia Terra

Within northwestern Arabia Terra, many of the craters lack morphological features associated with an impact origin, such as raised rims, ejecta blankets, or central peaks. Some of these modified craters show dissected plateau structures similar in morphology to the dissected plateaus within Eden Patera (Figure 3.17). The surfaces of these plateaus are irregular, with kilometer wide valleys dissecting them (Figure 3.17).

For example, fractured terrain characterized by dissected and curvilinear ridge structures is present in the northern region of an unnamed crater in Figure 3.17.

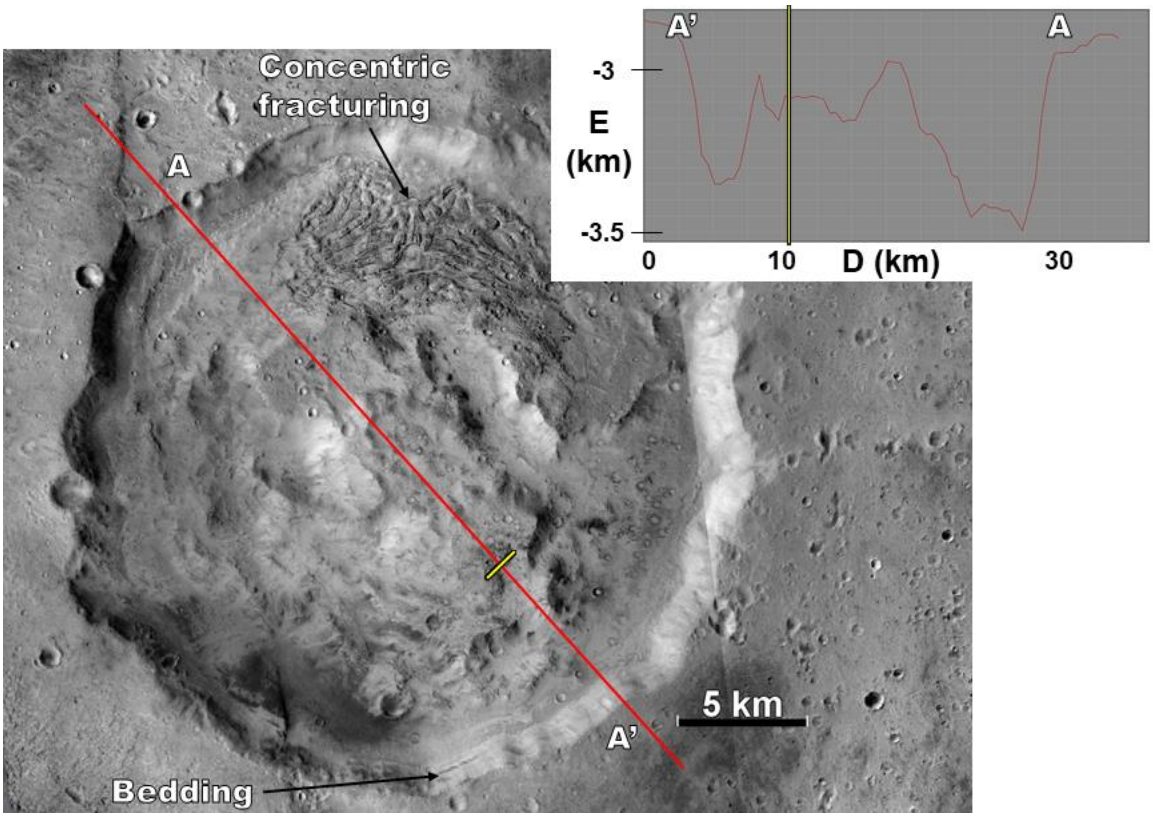

Figure 3.17 Image location labeled in Figure 3.16. An example of the dissected plateau structures within craters around Eden Patera. An elevation versus distance plot (upper right) shows the cross section through the plateau. Curvilinear fracturing features are present in the northern region of the crater floor, and bedding is observed along the wall of the crater. CTX image ID: B20_017356_2134_XN_33N008W, B17_016222_2128_XN_32N009W.

In addition to dissected plateaus, some craters in northwestern Arabia Terra contain intra-crater terrace features and curvilinear fracturing that resemble the terrace in Eden Patera. A crater adjacent to the heart-shaped basin, south of Oxus Cavus (Figure 3.2 and 3.18), shows an example of an intra-crater terrace. The terrace is ~30 m tall, occupies the southern region of the crater floor, and shows rectilinear fracturing features on the surface and along the edges in HiRISE datasets (Figure 3.18). Boulders are visible along

the slopes of the terrace, but are not present on the smooth crater floor. Thermal inertia of the terrace walls is ~300—400 TIU (THEMIS image ID: I05886007). On the opposite side of the basin, curvilinear fracturing features are present within a circular depression, similar to those found on the floor of Eden Patera and the unnamed crater in Figure 3.18.

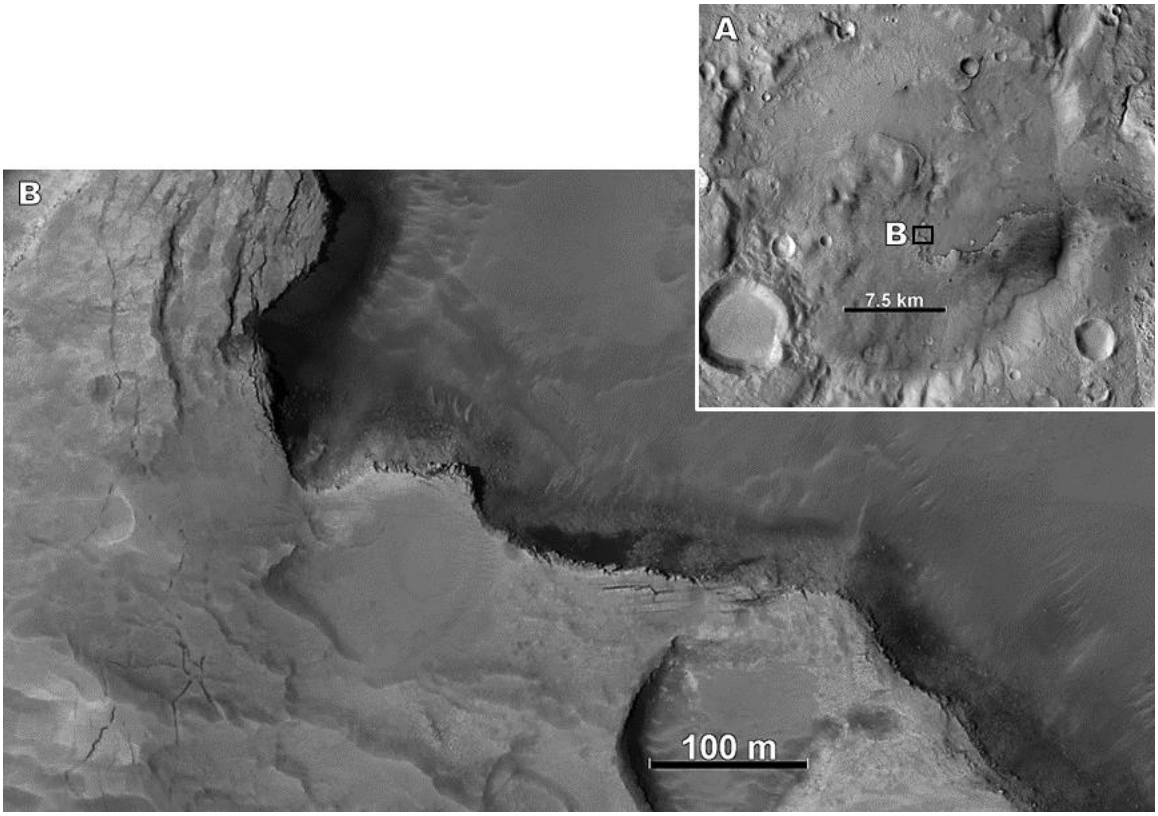

Figure 3.18 Image located labeled in Figure 3.2. A terrace feature similar to the one in Eden Patera is present around the floor of a crater near Oxus Cavus (Figure 3.2). The terrace is ~30 m tall, and shows similar fracturing features along the terrace edge, as those preserved by the Eden Patera terrace feature. The floor of this terrace is smooth, in contrast to the block rich floor of Eden Patera. HiRISE image ID: PSP_008877_2165.

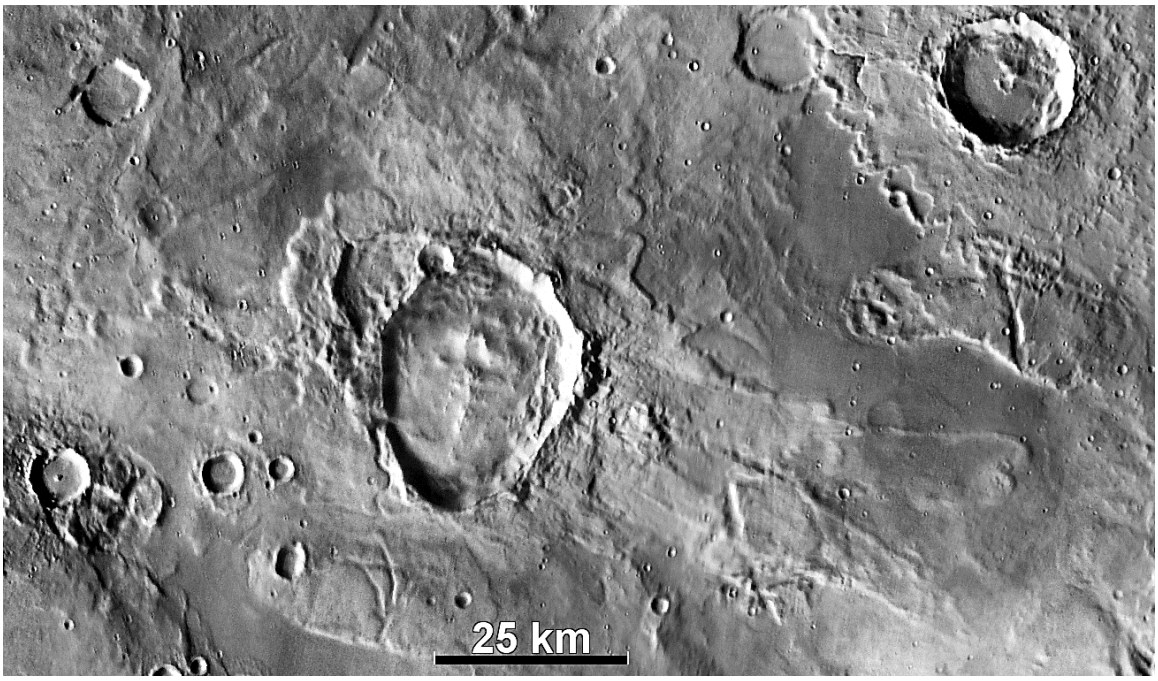

Figure 3.19 An unnamed impact crater (6° E, 32° N) 160 km south of Siloe Patera displays lobate rampart ejecta, off its eastern rim, in a similar elongated extent as Siloe Patera. THEMIS daytime global mosaic.

3.5 Discussion

3.5.1 Morphologic comparison between Eden, Ismenia, and Siloe Paterae

Because Arabia Terra is an ancient landscape nearly 4 billion years old, erosional processes can greatly affect the preservation state of landforms (e.g., impact craters). Previous works have suggested that northwestern Arabia Terra experienced episodes of resurfacing and denudation based on remnants of layered deposits, and topographically high inliers, the latter of which are considered isolated segments of older terrains (e.g., Hynek & Phillips, 2001). The source of the erosion is attributed to surface runoff during an early, wetter, Mars that maintained a thicker atmosphere (Davis et al., 2016; Hynek & Phillips, 2001; Zabrusky et al., 2012). Through these modification processes, impact craters in the landscape are infilled, rims and peaks are eroded, and ejecta blankets are erased and/or exhumed after prior burial (e.g., Craddock et al., 1997).

As discussed in Section 3.2.1.1, the proposed calderas in Arabia Terra were recognized because they exhibit high depth-to-diameter ratios relative to other modified craters in Arabia Terra (Michalski & Bleacher, 2013). To further assess the difference between the proposed calderas and modified craters, Figure 3.20 shows the diameter of the proposed Arabia Terra calderas (except Oxus Cavus because of its linear shape), and both their maximum depth and average plateau depth. Examples of depressions caused by dewatering style collapse are also included.

All depressions aside from Semeykin crater occur between class 1 and class 2 craters, or highly to moderately modified craters for plateau surface depth (Semeykin crater plots as class 1; Figure 3.20). The maximum depth of the proposed calderas plot between class 2 and class 4 craters, or moderately modified to near pristine. The observed discrepancy between surface morphology and high depth-to-diameter ratio can be explained by post-impact crater collapse. The proposed calderas are likely modified impact-craters based on the modified morphologies the depressions preserve. This suggests that the observed plateau depth is near the original depth of the crater, with the maximum crater depth reflecting the modified depth, post-collapse.

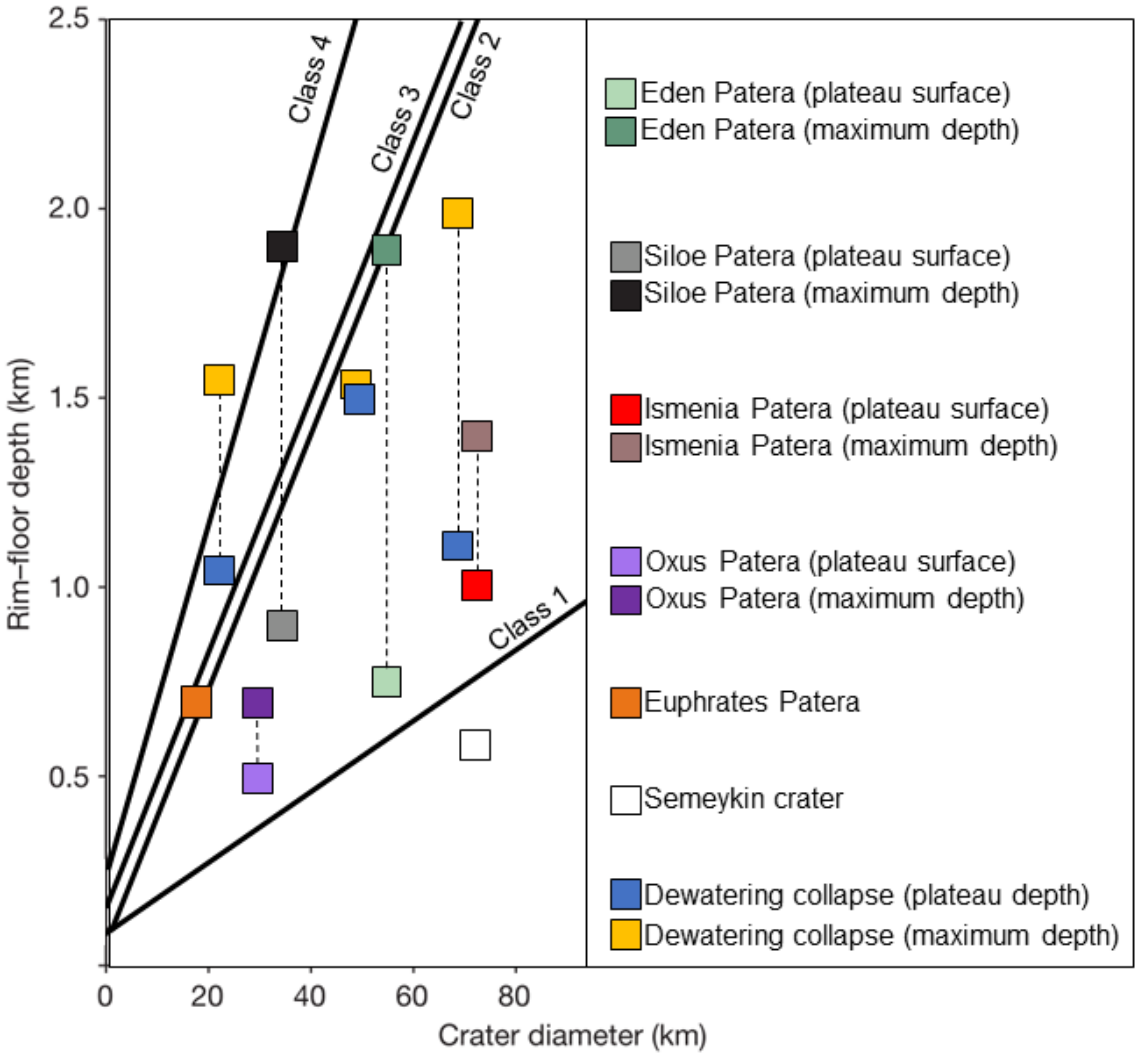

Figure 3.20 Depth-to-Diameter plot for all the proposed calderas in Arabia Terra (except for Oxus Cavus), and three examples of dewatering collapse craters in the Circum-Chryse region of Mars. Dashed lines connect the plateau depth and maximum depth for corresponding depressions. Trendlines are fit to the data in four classes: class 1 represents the most degraded and class 4 represents the least degraded (Robbins & Hynek, 2012).

Furthermore, while most of the impact craters in Arabia Terra appear modified, many of them still preserve evidence for an impact origin. For example, an impact crater 160 km south of Siloe Patera displays rampart ejecta with portions of the ejecta more prominently spread in a single direction (Figure 3.19). Similar unidirectional, lobate ejecta, commonly referred to as butterfly ejecta, results from low-angle impacts. It is

interpreted that the matching ejecta on the other side of the unnamed impact crater has been eroded or modified by later impacts or other aeolian or fluvial processes.

Likewise, the lobate deposit extending from the southern rim of Siloe Patera, interpreted by Michalski and Bleacher (2013) as lobate impact crater ejecta, closely resembles rampart butterfly ejecta, and should display a similar lobate deposit on the opposite side of the depression. It is possible that the lobate deposit has the same impact origin as is interpreted for the unnamed crater in Figure 3.19, implying the possibility that an ejecta blanket on the other side of Siloe Patera is obscured by subsequent impacts and erosion. Further, both Siloe Patera and the unnamed crater in Figure 3.19 exhibit a long axis diameter perpendicular to the ejecta, as is common for shallow impacts (Herrick & Hessen, 2006). While evidence such as the dissected plateau and high depth-to-diameter ratio suggest that Siloe Patera experienced collapse at some point, the similarities between butterfly ejecta patterns and the lobate deposit supports the idea that Siloe Patera could be a modified impact crater that experienced post-cratering collapse and erosion.

The presence of fractured floor terrains in Eden (Figure 3.9), Siloe (Figure 3.13), and Ismenia Paterae (3.15A), and the presence of discontinuous linear ridge structures in Siloe and Ismenia Paterae, is further evidence for surface modification in Arabia Terra. The fractured floor materials could be the result of partial collapse of the surface. For example, mesas preserved along the floor of Eden Patera (Figure 3.11B) are likely to be remnants of the terrace after subsequent erosion or later collapse. While thermal inertia of fractured surfaces are likely reflective of mantling dust, a lack of any high-strength floor materials suggests the fracture features are not emplaced in competent bedrock. Discontinuous linear ridge such as those found within Eden Patera are more likely

associated with recent (~1—100 Ma) peri-glacial reworking of the surface and can contribute to valley formation (Levy et al., 2009). The hummocky plateau texture in Siloe Patera may also be the result peri-glacial surface modification.

The proposed calderas are not the only features in Arabia Terra with high depth-to-diameter ratios. Examples of craters from all four crater modification classes (Robbins & Hynek, 2012) with depth-to-diameter ratios greater than the proposed calderas are present in Arabia Terra. This suggests that both fresh and modified craters can display high depth-to-diameter ratios. The most logical way to increase the depth-to diameter ratio of a modified crater is by structural collapse after impact. The mechanism for such collapse could be volcanic caldera collapse, or collapse by removal of subsurface material.

3.5.2 Comparison of proposed calderas to known calderas on Mars and Earth

The most direct way to test the hypothesis for proposed calderas in Arabia Terra is to compare the morphologies of the depressions to known calderas on Earth and Mars. First, the proposed calderas in Arabia Terra all lack a surrounding, positive edifice. Michalski and Bleacher (2013) make the argument that the proposed calderas are similar in morphology to terrestrial supervolcanoes, but many terrestrial supervolcanoes typically preserve some edifice structure (Chesner, 2012; Delgado & Pavez, 2015; Tizzani et al., 2007). While not every caldera on Earth has an edifice, there is usually some positive volcanic construct surrounding the caldera that represents the rim and volcanic slopes (Miller & Wark, 2008). On Mars, all known volcanoes also preserve edifice structures. While most of the volcanoes on Mars are characterized by effusive morphologies, Apollinaris Mons represents a likely explosive volcano with an edifice. With examples of

both effusive and explosive caldera-forming volcanoes preserving edifice structures, the interpretation for proposed calderas that lack an edifice is inconsistent with known volcanism on Earth and Mars.

Concentric fracturing, or ring faults, is a morphologic indicator of structural collapse common to volcanic calderas (Table 3.1; Cole et al., 2005; Lipman, 1997). However, such concentric fracturing is also common around depressions with alternative collapse mechanisms, such as subsurface dewatering (Branney, 1995). As such, concentric fracturing alone is not sufficient evidence for a volcanic collapse origin.

Michalski and Bleacher (2013) propose Eden Patera to represent a possible piecemeal collapse. This style of collapse is defined as having block faulted floors, or unconsolidated floor materials from chaotic subsidence (Branney & Kokelaar, 1994; Cole et al., 2005). Piecemeal collapse is associated with the eruption of multiple, overlapping magma chambers, or where tectonically-controlled faults break the caldera floor into separate blocks (Cole et al., 2005). A piecemeal collapse origin is inferred from the large fault-blocks present within Eden Patera, bound by curvilinear fracturing. However, intra-caldera fault-blocks are not common features in terrestrial or martian calderas.

The morphology and low thermal inertia of the depression floors and (where exposed) outcrops in the proposed calderas is consistent with unconsolidated floor materials. Most calderas on Earth (and Mars) collapse through an edifice, exposing older volcanic materials from the eruptive center. In Arabia Terra, there is no edifice, and it appears that the collapse features are exposing regional stratigraphy rather than stratigraphy associated with a volcanic center. While the stratigraphy resembles that found in Apollinaris Mons, the lack of an edifice makes it impossible to associate the

stratigraphy exposed within the depression with the mechanism for forming the depression. However, I recognize that while no younger volcanic constructs (cones or effusive flows) were identified at any of the proposed Arabia Terra calderas, the ancient modified nature of the region might not preserve such evidence of volcanism.

The southern floor region of Eden Patera has elevated thermal inertia values consistent with the presence of high-strength blocks. Ejecta material produced from impact craters in this region produce coherent boulders, and not friable particulate debris (Figure 3.11A). While it is difficult to assess the source of the high- thermal inertia material, it does not appear to be related to volcanism. The deposit is not laterally extensive, and likely not related to lava fill. Instead, it seems more likely that the floor of Eden Patera is characterized by high-strength rock in the substrate, exposed and reworked during collapse of the depression.

If the high-strength blocky deposit is volcanic in nature, the terrace feature that borders the floor of Depression 1 in Eden Patera, proposed to be a lava lake high stand (Figure 3.10 and 3.11; Michalski and Bleacher, 2013), would have similar thermal inertia values, which is not the case. The terrace is also not a morphologic feature unique to Eden Patera and the other proposed calderas. Other craters in northwestern Arabia Terra also preserve terrace deposits around the crater floor (Figure 3.18), and have thermal inertia values consistent with poorly consolidated materials that are not consistent with lava flows. As such, the terrace deposits are likely remnants of partial crater in-filling, which were subsequently modified by erosion, evident by the presence of isolated mesas within the southern portion of the floor (Figure 3.11B).

Table 3.1 Comparison between proposed calderas and other collapse features on Mars

	Arabia Terra proposed calderas					Circum-Chryse dewatering craters			Known martian calderas		
	Ismenia Patera	Eden Patera	Siloe Patera	Oxus Patera	Euphrates Patera	Collapse Crater A	Collapse Crater B	Collapse Crater C	Apollinaris Mons	Alba Mons	Ascraeus Mons
Dimensions (km)	75	51	37x32	30	15x20	73x76	47	77x90	84x72	63x43	57x40
Curvilinear fracturing	YES	YES	NO	NO	NO	YES	YES	NO	YES	YES	YES
Rectilinear fracturing	YES	YES	NO	NO	NO	YES	YES	NO	NO	NO	NO
Terraces	YES	YES	NO	YES	YES	NO	NO	NO	YES	YES	YES
Dissected plateaus	YES	YES	NO	NO	NO	YES	YES	NO	NO	NO	NO

In Table 3.1, I directly compare the presence of fracturing features, dissected plateaus, and chaotic terrains between the proposed calderas in Arabia Terra and known volcanic calderas on Mars (Apollinaris, Ascraeus, and Alba Mons). While all the known volcanic calderas in Table 3.1 show evidence for concentric fracturing, only two of the five proposed calderas in Arabia Terra preserve concentric fractures. However, concentric fracturing also commonly occurs in impact craters (Kumar & Kring, 2008), and from ice-melt collapse pits, and mining subsidence on Earth (Branney, 1995). Because this morphologic feature occurs in a wide variety of collapse structures it is not helpful in distinguishing between possible volcanic calderas, subsidence features, or impact craters and should not be used as diagnostic evidence for caldera formation.

Another key difference between the known and proposed volcanoes on Mars is the presence of chaos terrain and dissected plateau structures within the Arabia Terra depressions (Table 3.1). The large dissected plateaus within Eden, Ismenia, and Siloe Paterae are not consistent with morphologies found in either effusive or explosive calderas on Earth or Mars. For example, Apollinaris Mons contains a plateau structure within the caldera, but the plateau is not dissected to the same degree as those in the proposed calderas. The plateau within Apollinaris Mons is above the level of the surrounding caldera rim, and is likely remnant pyroclastic debris that has been modified by erosion (Krysak, 2011). The plateaus in the proposed calderas are likely fault blocks related to piecemeal structural collapse of the depressions, and not volcanic in nature. Finally, while silicic supervolcanoes on Earth do often contain resurgent domes after an explosive eruption, volcanism on Mars is primarily basaltic (Basaltic Volcanism Study

Project, 1981; Carr, 1973; Greeley and Spudis, 1981; Robinson et al., 1993); as such, lava domes are not expected on Mars.

Regional evidence for volcanism in Arabia Terra was primarily derived from the presence of wrinkle ridges around the proposed calderas (Michalski & Bleacher, 2013). Wrinkle ridges were interpreted to represent volcanic terrains because they were believed to form from the compressional tectonism associated with cooling lavas (Watters, 1993). However, studies show wrinkle ridges can form in a wide variety of materials from thrust faulting activity along bedding planes of differing rock strength (e.g., Schultz, 2000; Tanaka et al., 2003). For example, wrinkle ridges have been observed within terrestrial, non-volcanic, materials from deformed shallow thrust faults (Plescia & Golombek, 1986). Without evidence for volcanism in the form of lobate flows or edifice structures, the presence of wrinkle ridges in Arabia Terra is instead attributed to thrust faulting likely caused by discontinuities in underlying rock strength between bedded layers (Okubo & Schultz, 2002).

3.5.3 Applying the framework for identifying explosive volcanism at Apollinaris Mons to the proposed Arabia Terra calderas

The first question posed in this chapter is, can the evidence for explosive volcanism identified at Apollinaris Mons be used as diagnostic criteria for identifying explosive volcanism within the proposed calderas of Arabia Terra? The evidence for explosive volcanism identified at Apollinaris Mons includes: (1) an edifice composed primarily of friable deposits, both on the surface, and within exposed layers of the edifice and debris apron, (2) evidence for lateral grading of boulders down the flank of the edifice, indicative of volcanic or non-volcanic mass flows, (3) bedded deposits of poorly

consolidated, low thermal inertia materials, some instances of which preserve truncated bedding (features not typically found in bedded lavas), (4) and brecciated deposits within the caldera that may suggest pyroclastic activity or explosive brecciation of buried, coherent lavas.

As stated in section 3.5.2, a key difference between the proposed calderas and Apollinaris Mons caldera is the dissected plateau structures within the Arabia Terra depressions (Table 3.1). The large dissected plateaus within Eden, Ismenia, and Siloe Paterae are not consistent with morphologies found in either effusive or explosive calderas on Earth or Mars, including Apollinaris Mons. The plateaus in the proposed calderas are thus more likely fault blocks related to chaotic structural collapse of the depressions, and not volcanic in nature.

Of the four lines of evidence for explosive volcanism identified at Apollinaris Mons, only bedded layering was identified at the proposed calderas. Bedding identified at Apollinaris Mons occurs within the caldera and along the flanks, both of which expose stratigraphy associated with a prominent edifice; whereas, the bedding in the proposed Arabia Terra calderas is within the collapse feature that exposes older, regional stratigraphy. Alone, the presence of bedding does little to suggest volcanic activity, since bedded layering is a common landform preserved by many sedimentary processes. It is only by the presence of an identifiable edifice structure that bedding can be related to volcanic processes. Bedding found within the proposed Arabia Terra caldera walls and plateaus likely represents older, regional stratigraphy exposed during collapse, and cannot be directly related to the mechanism that formed the depressions.

In the case of Ismenia patera, bedding observed along the dissected plateau walls are likely the result of crater fill material resulting from regional resurfacing events in Arabia Terra (Tanaka et al., 2003), and not volcanic in origin. This hypothesis is strengthened by the presence of dense pit clusters along the dissected plateau surfaces (Figure 3.14), and regionally around Ismenia Patera. Similar pit clusters have been identified along crater floors elsewhere on Mars and are associated with water-related degassing pipes (Tornabene et al., 2012), similar to degassing fumaroles. While fumaroles are the result of gasses present within a recently deposited pyroclastic deposit, the gasses (primarily water vapor) necessary for degassing pipes as proposed by Tornabene et al. (2012) were present within the crust prior to crater formation. Should the pit clusters within and around Ismenia Patera be sourced from the same event, as Ismenia Patera likely represents a modified impact crater, regional resurfaced by volatile-rich material seems plausible.

3.5.4 Comparison of Eden, Ismenia, and Siloe Paterae with dewatering terrains on Mars

In total, the proposed calderas all lack an edifice structure, regional evidence for volcanism, and local geomorphologic and thermophysical characteristics consistent with known volcanoes. As little to no supporting evidence exists for a volcanic interpretation, alternative causes for collapse are investigated.

Collapse features resulting from the removal of subsurface ice or liquid water are common on Mars, and are concentrated near the dichotomy boundary. For example, the Circum-Chryse Planitia region of Mars is characterized by chaotic collapse terrain (Figure 3.21; Sharp, 1973). Features associated with dewatering collapse are listed for comparison in Table 3.1. The landscape in the Circum-Chryse region is dominated by

large outflow channels and chaos terrain that displays arrays of fractured polygonal plateau structures (Chapman & Tanaka, 2002; Sharp, 1973). The chaos terrains are preserved both within the channels, and within isolated circular depressions, interpreted to represent modified craters that experienced subsequent collapse (Roda et al., 2016). These channels and chaotic terrains can reach depths greater than one kilometer, rivaling the depths observed in the chaos terrains of northern Arabia Terra and the proposed calderas (average maximum depth of the proposed calderas is ~1.5 km).

The general process of formation of the Circum-Chryse outflow channels and chaos terrains is interpreted as catastrophic flooding from the discharge of subsurface water (e.g., Zegers et al., 2010). While the triggers of these overland flows is debated, the main theories include: (1) melting of subsurface ice by near-surface magmatism (Chapman & Tanaka, 2002; Leask et al., 2006; Meresse et al., 2008; Ogawa, 2003; Rodriguez et al., 2005; Sharp, 1973), (2) release of subsurface water from a pressurized aquifer (Andrews-Hanna & Phillips, 2007; Carr, 1979; Clifford, 1993; Harrison & Grimm, 2009), (3) dewatering of subsurface gas-hydrates or evaporite minerals (Max & Clifford, 2001; Montgomery & Gillespie, 2005), (4) and melting of near-surface buried ice sheets (Roda et al., 2014; Zegers et al., 2010).

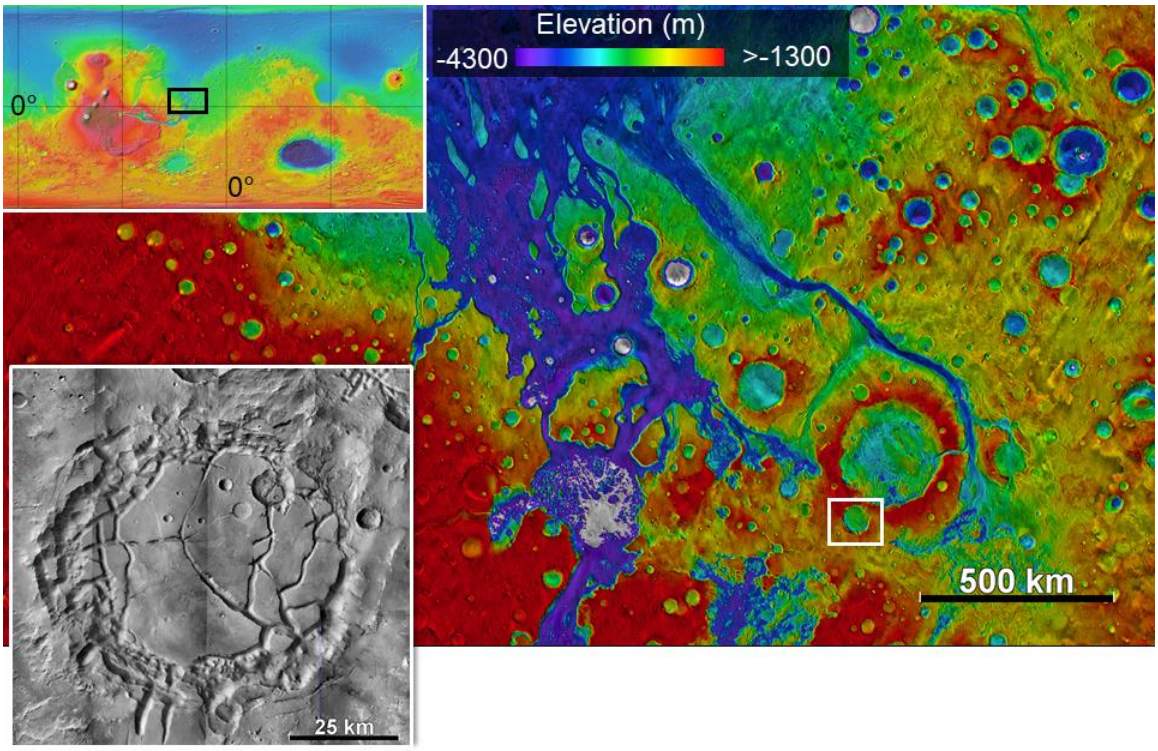

Figure 3.21 Colorized MOLA elevation data draped over THEMIS daytime global mosaic of the Xanthe and Margaritifer Terra (Circum-Chryse) region of Mars. The terrain is dominated by large outflow channels, chaotic and fretted terrain within the valleys, and collapse craters beyond the channels. The white box corresponds to the image on the bottom left, which shows the rectilinear fracturing and polygonal plateaus associated with chaos terrain. CTX image ID: P17_007731_1815_XN_01N023W, P06_003472_1823_XI_02N022W, P06_003327_1815_XN_01N023W, B05_011792_1800_XN_00N022W.

Chaos terrain-floored craters are common in these dewatering regions, and form due to the release of subsurface groundwater, resulting in the fracturing and subsidence of overlying rock (Rodriguez et al., 2005). Intra-crater chaotic terrains are interpreted as modified impact craters that collapsed by dewatering of the substrate. The dissected plateaus of the proposed Arabia Terra calderas closely resemble these chaos terrain-floored craters (see comparison in Table 3.1). The interior of both Eden and Ismenia Paterae preserve rectilinear and curvilinear fracturing features that are similar in morphology to dewatering style collapse features of the Circum-Chryse region (Figure 3.22 A-C). Of the proposed calderas, Ismenia Patera is morphologically the most similar

to the chaotic collapse craters around the Circum-Chryse region. Compared to Arabia Terra, the chaotic plateaus in the Circum-Chryse region preserve sharper edges, are more widespread within the Xanthe and Margaritifer Terra region (Circum-Chryse), and usually occupy the entire crater interior. While the proposed Arabia Terra calderas and the dewatering craters show distinctions between the types of fractured terrains they preserve, the presence of dissected plateau structures and chaos-like terrain makes them morphologically distinct from martian calderas (Table 3.1). Thus, Eden, Ismenia, and Siloe Patera share more morphologic similarities with dewatering collapse craters than volcanic calderas on Earth or Mars.

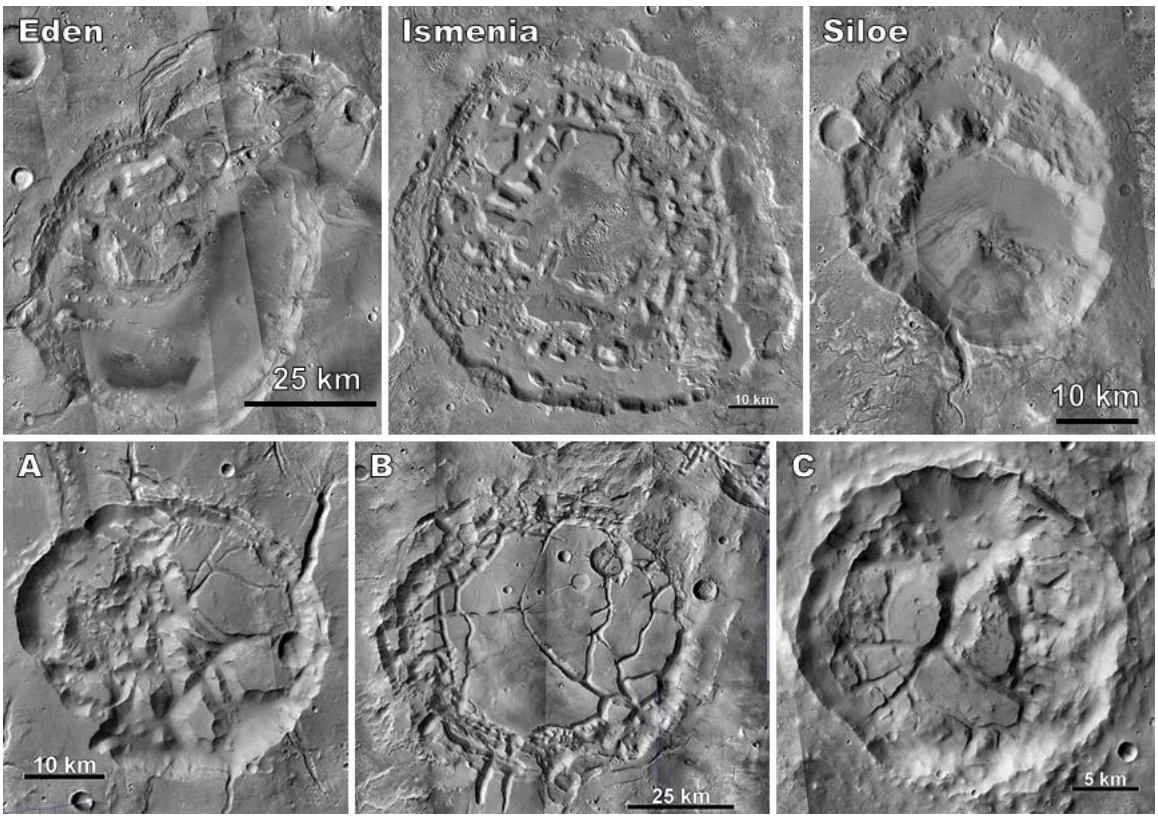

Figure 3.22 A direct morphologic comparison between Eden, Ismenia, and Siloe Paterae, and three unnamed dewatering collapse craters in Xanthe and Margaritifer Terra (A, B, and C). A, B, and C correspond to the same unnamed dewatering features in Table 3.1. The dewatering collapse craters and the Arabia Terra depressions show similar sizes, depths, and intra-crater plateau structures. Regional evidence for dissecting channels and valleys is also observed.

Roda et al. (2016) conducted a statistical analysis of the chaotic terrains in the Circum-Chryse region, based on the depth and diameter of the dewatering collapse craters, and depth of collapse. They found that the dewatering collapse craters were indistinguishable from the chaotic terrains present within the large outflow channels, and along the dichotomy boundary, suggesting similar formation processes. While the presence of large channels and valleys is not as widespread in northwestern Arabia Terra, the modified collapse craters present likely formed in a similar manner as those in the Circum-Chryse region. With less extensive channels and chaos features, possible flooding from dewatering of the Arabia Terra subsurface may have just been a milder

version of the catastrophic floods that shaped the Circum-Chryse region. Based on morphologies that more closely resemble dewatering collapse features in the Circum-Chryse region, the proposed calderas in Arabia Terra are likely modified craters that experienced similar formation processes, namely collapse by the removal of subsurface water.

3.6 Conclusion

Michalski and Bleacher (2013) proposed several depressions in Arabia Terra to be volcanic calderas based on their morphologic similarities to terrestrial calderas. However, the thermophysical and geomorphologic data presented here show inconsistencies between terrestrial and martian calderas and the proposed Arabia Terra features. All proposed calderas within Arabia Terra lack a surrounding edifice, which are typically found at caldera-style volcanoes. Concentric fracturing is a common structure surrounding different types of collapse features (e.g., calderas, dewatering pits), and as such the concentric fracturing surrounding some of the proposed Arabia Terra calderas cannot be directly associated with a volcanic collapse origin. Dissected plateau structures within the Arabia Terra depression interiors are consistent with large, fractured fault blocks, which are not found within known collapse calderas. Proposed lava lakes and vent structures lack the morphology and thermal inertia associated with coherent bedrock or lavas. Bedding found within the paterae walls and plateaus likely represents older deposits exposed by the collapse paterae, and cannot be directly related to the paterae themselves.

The proposed calderas more closely resemble dewatering style collapse features present within the Circum-Chryse region of Mars. These dewatering collapse features are

characterized by polygonal plateau structures that resemble the dissected plateaus within Eden, Ismenia, and Siloe Paterae. While the detailed nature of collapse in the Circum-Chryse region is still debated, the morphologic similarities between Circum-Chryse and Arabia Terra would suggest the anomalous depressions likely resulted from the removal of subsurface water, resulting in the chaotic terrains present in Arabia Terra today.

CHAPTER FOUR: CONCLUSION

The objectives of this thesis were to investigate morphologic and thermophysical properties at the regional and outcrop scale to identify explosive volcanic deposits on Mars. This work sought to accomplish three main objectives:

(1) Identify possible distinguishing characteristics of explosive volcanic deposits on Mars using remote sensing data of Apollinaris Mons.

(2) Investigate local morphologies within the Arabia Terra proposed calderas by using volcaniclastic evidence from Apollinaris Mons as a framework.

(3) Investigate large-scale morphologies beyond the proposed calderas to identify evidence for regional volcanism, or other formation mechanisms, responsible for the proposed calderas.

To address these objectives, geomorphologic and thermophysical characteristics of possible explosive volcanic deposits on Apollinaris Mons were compared to terrestrial volcanic analogs to more accurately identify evidence for explosive volcanism on Mars. Deposits that best characterize evidence for explosive volcanism were compared to morphological features and outcrops within the proposed calderas in Arabia Terra to determine the likelihood for a volcanic origin. Table 4.1 lists distinguishing characteristics of effusive versus explosive volcanism. These features are based on terrestrial examples of effusive and explosive volcanism, and observed morphologies of proposed effusive and explosive volcanism on Mars.

Apollinaris Mons is characterized by a caldera and edifice complex that rises ~5 km above the surrounding terrain. The average slope of the volcanic flanks is ~7°, consistent with terrestrial composite volcanoes. Thermal inertia of the volcano is consistently low, average at 90 TIU, consistent with weakly-consolidated, particulate materials. Valleys dissect the flanks of the edifice and suggest a primarily friable nature. Within exposed valley and crater walls on the edifice, evidence for explosive volcanism on Apollinaris Mons includes planar and truncated bedding, and lateral size grading of breccia blocks with distance from the caldera rim, and brecciated deposits that are all suggestive of volcanic mass flows.

Planar bedding is consistent with fall deposits, or discrete lateral flow events. Truncated bedding is consistent with traction transport in dilute mass flows, such as dilute pyroclastic density currents. However, such truncations could also be formed by later erosive flows through earlier deposits. Breccias also form during mass flows, such as concentrated pyroclastic density currents or debris flows. Gradation of blocks down slope is further evidence for lateral transport since heavier blocks are dropped out of the flow at more proximal regions due to decreasing carrying capacity with distance from source. The combined evidence of a caldera with a prominent edifice, the regional low thermal inertia, and presence of extensive friable deposits with evidence of lateral transport away from the caldera supports an explosive volcanic history for Apollinaris Mons. This study revealed no evidence for past effusive activity (high strength materials), although I recognize that current data limitations prevent access to the entire volcanic history.

Evidence for explosive volcanism on Apollinaris Mons cannot be easily applied to the proposed calderas in Arabia Terra because, unlike Apollinaris Mons, the proposed calderas are at the same level as the surrounding topography and lack a positive edifice. The proposed calderas in Arabia Terra were identified based on their high depth-to-diameter ratios relative to other modified craters in Arabia Terra (Michalski & Bleacher, 2013). However, examples of both fresh and modified impact craters with depth-to-diameter ratios greater than the proposed calderas are present in Arabia Terra. The most logical way to increase the depth-to diameter ratio of a modified crater is by structural collapse after impact. Concentric fracturing around some of the proposed calderas, though consistent with ring-fractures at volcanic calderas, is not unique to volcanic collapse. As such, while there is evidence that Arabia Terra depressions experienced collapse, the mechanism for collapse cannot be tied directly to volcanism.

Another key difference from known volcanoes on Mars is the presence of rectilinear fracturing and dissected plateau structures within the proposed Arabia Terra calderas. The dissected plateaus are not consistent with morphologies found in either effusive or explosive calderas on Earth or Mars, and are likely fault blocks related to chaotic collapse of the depressions, and not volcanic in nature.

Bedding found within the proposed Arabia Terra caldera walls and plateaus likely represents older stratigraphy exposed by collapse. Without being emplaced on a volcanic construct, the observed bedding cannot be directly related to a volcanic origin either, since bedded deposits are common sedimentary structures. Terraces that border the floor of Eden Patera (proposed to be lava lake high-stands) maintain low thermal inertias, and are not a morphologic feature unique to the proposed calderas. Other craters in

northwestern Arabia Terra also preserve terrace deposits around the crater floor, and have thermal inertia values consistent with poorly consolidated materials, and not high-strength lavas. As such, the terrace deposits are likely remnants of crater in-filling, which were subsequently modified by partial collapse and erosion.

Instead of a volcanic interpretation, the proposed Arabia Terra calderas are morphologically consistent with dewatering collapse craters in Circum-Chryse. Both collapse craters and the proposed calderas contain dissected plateau structures, and rectilinear floor fracturing consistent with chaos terrain. Sinuous valleys and channels both in Circum-Chryse and Arabia Terra suggest water was removed from the subsurface towards the northern lowlands. Additionally, Siloe Patera preserves evidence for impact-cratering, further implicating the proposed calderas as being impact craters that experienced later collapse due to loss of subsurface groundwater.

This research demonstrates that geomorphologic and thermophysical observations of large-scale and fine-scale features can be combined to determine the origin of both volcanic and non-volcanic Martian structures. However, without sufficient geologic context such as a volcanic edifice, distinguishing volcaniclastic materials from other sedimentary deposits on Mars remains a challenge. It is possible that the bedded, friable deposits exposed within Arabia Terra have a volcanic origin; however, the source has yet to be identified. This work demonstrates that careful and detailed geologic mapping, when compared with terrestrial analogs, provides insight into the geologic history of Mars.

Table 4.1: A list of distinguishing characteristics for identifying effusive versus explosive volcanic deposits

Style	Necessity to be emplaced on volcanic edifice	Thermal Inertia	Surface flow	Bedding	Outcrop scale evidence	
Explosive	Yes	Low	Lobate morphologies	Planar and truncated	Boulders do not persist more than a few hundred meters below bedding	Evidence for lateral transport (i.e., lateral grading)
Effusive	No*	High	Lobate morphologies	Planar	Boulders Persist more than 1 km down slope	Coherent, block rich layers

*Evidence for effusive volcanism can be identified without the presence of a volcanic edifice. Lobate lava flows have a characteristic morphology that can be identified beyond a volcanic edifice.

REFERENCES

Andrews-Hanna, J. C., & Phillips, R. J. (2007). Hydrological modeling of outflow channels and chaos regions on Mars. *Journal of Geophysical Research*, *112*(E08001). https://doi.org/10.1029/2006JE002881

Anguita, F., Anguita, J., Castilla, G., De La Casa, M. A., Domínguez, J. M., Herrera, R., et al. (1997). Arabia Terra, Mars: Tectonic and palaeoclimatic evolution of a remarkable sector of Martian lithosphere. *Earth, Moon and Planets*, *77*(1), 55–72. https://doi.org/10.1023/A:1006143106970

Assaad, F. A., & LaMoreaux, P. E. (2004). Geology of Indurated Rocks, Unconsolidated Sedimentary Deposits and Karst Terrains. In T. H. Hughes (Ed.), *Field Methods for Geologists and Hydrogeologists* (pp. 7–30). Berlin, Heidelberg: Springer Berlin Heidelberg. https://doi.org/10.1007/978-3-662-05438-3_2

Bailey, J. E., Self, S., Wooller, L. K., & Mouginis-Mark, P. J. (2007). Discrimination of fluvial and eolian features on large ignimbrite sheets around La Pacana Caldera, Chile, using Landsat and SRTM-derived DEM. *Remote Sensing of Environment*, *108*(1), 24–41. https://doi.org/10.1016/j.rse.2006.10.018

Baird, A. K., Toulmin, P., Clark, B. C., Rose, H. J., Keil, K., Christian, R. P., & Gooding, J. L. (1976). Mineralogic and petrologic implications of viking geochemical results from Mars: interim report. *Science*, *194*(4271), 1288–93. https://doi.org/10.1126/science.194.4271.1288

Bandfield, J. L. (2002). Global mineral distributions on Mars. *Journal of Geophysical Research*, *107*(E6), 5042. https://doi.org/10.1029/2001JE001510

Bandfield, J. L. (2008). High-silica deposits of an aqueous origin in western Hellas Basin, Mars. *Geophysical Research Letters*, *35*(12), 1–5. https://doi.org/10.1029/2008GL033807

Bandfield, J. L., Hamilton, V. E., & Christensen, P. R. (2000). A global view of Martian surface compositions from. *Science*, *287*(March), 1626–1630.

Bandfield, J. L., Hamilton, V. E., Christensen, P. R., & McSween, H. Y. (2004). Identification of quartzofeldspathic materials on Mars. *Journal of Geophysical Research*, *109*(10), 1–14. https://doi.org/10.1029/2004JE002290

Bandfield, J. L., Edwards, C. S., Montgomery, D. R., & Brand, B. D. (2013). The dual nature of the martian crust: Young lavas and old clastic materials. *Icarus*, *222*(1), 188–199. https://doi.org/10.1016/j.icarus.2012.10.023

Banin, A., Clark, B. C., & Waenke, H. (1992). Surface chemistry and mineralogy. In *In: Mars (A93-27852 09-91)* (pp. 594–625).

Basaltic Volcanism Study Project (1981). *Basaltic Volcanism on the Terrestrial Planets*. *Pergamon Press, Inc.* New York: Pergamon Press. https://doi.org/10.1016/0031-9201(84)90072-4

Bourke, M. C., Wilson, S. A., & Zimbelman, J. R. (2003). The variability of TARs in troughs on Mars. In *34th Lunar and Planetary Science Conference* (Vol. 2090).

Bradley, B. A., Sakimoto, S. E. H., Frey, H., & Zimbelman, J. R. (2002). Medusae Fossae Formation : New perspectives from Mars Global Surveyor. *Journal of Geophysical Research*, *107*(E8), 5058. https://doi.org/10.1029/2001JE001537

Brand, B. D., & Heiken, G. (2009). Tuff cones, tuff rings, and maars of the Fort Rock–Christmas Valley Basin, Oregon: Exploring the vast array of pyroclastic features that record violent hydrovolcanism at Fort Rock and the Table Rock Complex. *Volcanoes to Vineyards: Geologic Field Trips Through the Dynamic Landscape of the Pacific Northwest* (Vol. 15). https://doi.org/10.1130/2009.fl

Brand, B. D., Mackaman-Lofland, C., Pollock, N. M., Bendana, S., Dawson, B., & Wichgers, P. (2014). Dynamics of pyroclastic density currents: Conditions that promote substrate erosion and self-channelization - Mount St Helens, Washington (USA). *Journal of Volcanology and Geothermal Research*, *276*, 1–26. https://doi.org/10.1016/j.jvolgeores.2014.01.007

Branney, M. J. (1995). Downsag and extension at calderas: new perspectives on collapse geometries from ice-melt, mining, and volcanic subsidence. *Bulletin of Volcanology*, *57*(5), 303–318. https://doi.org/10.1007/BF00301290

Branney, M. J., & Kokelaar, P. (1994). Volcanotectonic faulting, soft-state deformation, and rheomorphism of tuffs during development of a piecemeal caldera, English Lake District. *Geological Society of America Bulletin*, *106*(4), 507–530. https://doi.org/10.1130/0016-7606(1994)106<0507:VFSSDA>2.3.CO;2

Carr, M. H. (1973). Volcanism on Mars. *Journal of Geophysical Research*, *78*(20), 4049–4062.

Carr, M. H. (1979). Formation of Martian flood features by release of water from confined aquifers. *Journal of Geophysical Research*, *84*(B6), 2995–3007. https://doi.org/10.1029/JB084iB06p02995

Chapman, M. G., & Tanaka, K. L. (2002). Related magma-ice interactions: Possible origins of chasmata, chaos, and surface materials in Xanthe, Margaritifer, Meridiani Terrae, Mars. *Icarus*, *155*(2), 324–339. https://doi.org/10.1006/icar.2001.6735

Chesner, C. A. (2012). The Toba Caldera Complex. *Quaternary International*, *258*, 5–18. https://doi.org/10.1016/j.quaint.2011.09.025

Christensen, P. R., Anderson, D. L., Chase, S. C., Clark, R. N., Kieffer, H. H., Malin, M. C., et al. (1992). Thermal emission spectrometer experiment: Mars Observer mission. *Journal of Geophysical Research*, *97*(E5), 7719. https://doi.org/10.1029/92JE00453

Christensen, P. R., Bandfield, J. L., Bell, J. F. I., Gorelick, N., Hamilton, V. E., Ivanov, A., et al. (2003). Morphology and Composition of the Surface of Mars:Mars Odyssey THEMIS Results. *Science*, *300*(27 June), 2056–2061. https://doi.org/10.1126/science.1080885

Christensen, P. R., Jakosky, B. M., Kieffer, H. H., Malin, M. C., McSween, Jr., H. Y., Nealson, K., et al. (2004). The Thermal Emission Imaging System (THEMIS) for the Mars 2001 Odyssey Mission. *Space Science Reviews*, *110*, 85–130. https://doi.org/10.1023/B:SPAC.0000021008.16305.94

Christensen, P. R., McSween, H. Y., Bandfield, J. L., Ruff, S. W., Rogers, A. D., Hamilton, V. E., et al. (2005). Evidence for magmatic evolution and diversity on Mars from infrared observations. *Nature*, *436*(7050), 504–509. https://doi.org/10.1038/nature03639

Christensen, P. R., Engle, E., Anwar, S., Dickenshied, S., Noss, D., Gorelick, N., & Weiss-Malik, M. (2009). JMARS – A Planetary GIS. In *American Geophysical Union, Fall Meeting 90* (p. IN22A-06).

Chuang, F. C., Crown, D. A., & Tornabene, L. L. (2016). Zumba crater, Daedalia Planum, Mars: Geologic investigation of a young, rayed impact crater and its secondary field. *Icarus*, *269*, 75–90. https://doi.org/10.1016/j.icarus.2016.01.005

Clifford, S. M. (1993). A model for the hydrologic and climatic behavior of water on Mars. *Journal of Geophysical Research*, *98*(E6), 10973. https://doi.org/10.1029/93JE00225

Cole, J. W., Milner, D. M., & Spinks, K. D. (2005). Calderas and caldera structures: A review. *Earth-Science Reviews*, *69*, 1–26. https://doi.org/10.1016/j.earscirev.2004.06.004

Costard, F. M., & Kargel, J. S. (1995). Outwash plains and thermokarst on mars. *Icarus*, *114*(1), 93–112. https://doi.org/10.1006/icar.1995.1046

Craddock, R. A., Maxwell, T. A., & Howard, A. D. (1997). Crater morphometry and modification in the Sinus Sabaeus and Margaritifer Sinus regions of Mars. *Journal of Geophysical Research*, *102*(E6), 13321–13340. https://doi.org/10.1029/97JE01084

Crown, D. A., & Greeley, R. (1993). Volcanic Geology of Hadriaca Patera and the Eastern Hellas Region of Mars. *Journal of Geophysical Research*, *98*(E2), 3431–3451. https://doi.org/10.1029/92JE02804

Davis, J. M., Balme, M., Grindrod, P. M., Williams, R. M. E., & Gupta, S. (2016). Extensive Noachian fluvial systems in Arabia Terra: Implications for early Martian climate. *Geology*, *44*(10), 847–850. https://doi.org/10.1130/G38247.1

Delgado, F., & Pavez, A. (2015). New insight into La Pacana caldera inner structure based on a gravimetric study (central Andes, Chile). *Andean Geology*, *42*(3), 313–328. https://doi.org/10.5027/andgeoV42n3-a02

Edgett, K. S., & Parker, T. J. (1997). Water on early Mars: Possible subaqueous sedimentary deposits covering ancient cratered terrain in western Arabia and Sinus Meridiani. *Geophysical Research Letters*, *24*(22), 2897–2900. https://doi.org/10.1029/97GL02840

El Maarry, M. R., Dohm, J. M., Marzo, G. A., Fergason, R., Goetz, W., Heggy, E., et al. (2012). Searching for evidence of hydrothermal activity at Apollinaris Mons, Mars. *Icarus*, *217*(1), 297–314. https://doi.org/10.1016/j.icarus.2011.10.022

Farrell, A., & Lang, N. (2010). Distribution of Explosive and Effusive Volcanic Deposits at Apollinaris Patera, Mars. In *41st Lunar and Planetary Science Conference*.

Fassett, C. I., & Head, J. W. (2007). Layered mantling deposits in northeast Arabia Terra, Mars: Noachian-Hesperian sedimentation, erosion, and terrain inversion. *Journal of Geophysical Research E: Planets*, *112*(8), 1–19. https://doi.org/10.1029/2006JE002875

Fergason, R. L., & Christensen, P. R. (2008). Formation and erosion of layered materials: Geologic and dust cycle history of eastern Arabia Terra, Mars. *Journal of Geophysical Research*, *113*(12), 1–22. https://doi.org/10.1029/2007JE002973

Fergason, R. L., Christensen, P. R., & Kieffer, H. H. (2006). High-resolution thermal inertia derived from the Thermal Emission Imaging System (THEMIS): Thermal model and applications. *Journal of Geophysical Research*, *111*(12), 1–22. https://doi.org/10.1029/2006JE002735

Francis, P. (1993). *VOLCANOES. A PLANETARY PERSPECTIVE.* Oxford (UK): Clarendon Press.

Francis, P. W., & Wood, C. A. (1982). Absence of Silicic Volcanism on Mars: Implications for Crustal Composition and Volatile Abundance. *Journal of Geophysical Research*, *87*(30), 9881–9889. https://doi.org/10.1029/JB087iB12p09881

Gardner, J. E., Hilton, M., & Carroll, M. R. (1999). Experimental constraints on degassing of magma: Isothermal bubble growth during continuous decompression from high pressure. *Earth and Planetary Science Letters*, *168*, 201–218. https://doi.org/10.1016/S0012-821X(99)00051-5

Giordano, G., De Rita, D., Fabbri, M., & Rodani, S. (2002). Facies associations of rain-generated versus crater lake-withdrawal lahar deposits from Quaternary volcanoes, central Italy. *Journal of Volcanology and Geothermal Research*, *118*(1–2), 145–159. https://doi.org/10.1016/S0377-0273(02)00254-8

Grant, J. A., & Schultz, P. H. (1990). Gradational epochs on Mars: Evidence from West-Northwest of Isidis Basin and Electris. *Icarus*, *84*(1), 166–195. https://doi.org/10.1016/0019-1035(90)90164-5

Greeley, R., & Crown, D. A. (1990). Volcanic Geology of Tyrrhena Patera, Mars. *Journal of Geophysical Research*, *95*(B5), 7133–7149. https://doi.org/10.1029/JB095iB05p07133

Greeley, R., & Guest, J. E. (1987). Geologic map of the eastern equatorial region of Mars (1:15,000,000). USGS Misc. Inv. Ser.

Greeley, R., & Spudis, P. D. (1981). Volcanism on Mars. *Reviews of Geophysics*, *19*(1), 13–41. https://doi.org/10.1029/RG019i001p00013

Greeley, R., Foing, B. H., McSween, H. Y., Neukum, G., Pinet, P., van Kan, M., et al. (2005). Fluid lava flows in Gusev crater, Mars. *Journal of Geophysical Research E: Planets*, *110*(5), 1–6. https://doi.org/10.1029/2005JE002401

Gregg, T. K. P., & de Silva, S. L. (2009). Tyrrhena Patera and Hesperia Planum, Mars: New insight (and old interpretations) from high-resolution imagery. In *40th Lunar and Planetary Science Conference* (pp. 1–2). https://doi.org/10.1029/2008JE003076.

Gulick, V., & Baker, V. (1990). Origin and evolution of valleys on Martian volcanoes. *Journal of Geophysical Research*, *95*(B9), 14325–14344. https://doi.org/10.1029/JB095iB09p14325

Harrison, K. P., & Grimm, R. E. (2009). Regionally compartmented groundwater flow on Mars. *Journal of Geophysical Research*, *114*(4), n/a-n/a. https://doi.org/10.1029/2008JE003300

Hartmann, W. K. (2005). Martian cratering 8: Isochron refinement and the chronology of Mars. *Icarus*, *174*(2 SPEC. ISS.), 294–320. https://doi.org/10.1016/j.icarus.2004.11.023

Herrick, R. R., & Hessen, K. K. (2006). The planforms of low-angle impact craters in the northern hemisphere of Mars. *Meteoritics and Planetary Science*, *41*(10), 1483–1495. https://doi.org/10.1111/j.1945-5100.2006.tb00431.x

Hulme, G. (1974). The interpretaion of lava flow morphology. *Geophys. J. R. Astr. Soc.*, *39*(February), 361–383.

Hynek, B. M., & Phillips, R. J. (2001). Evidence for extensive denudation of the Martian highlands. *Geology*, *29*(5), 407–410. https://doi.org/10.1130/0091-7613(2001)029<0407:EFEDOT>2.0.CO

Hynek, B. M., Phillips, R. J., & Arvidson, R. E. (2003). Explosive volcanism in the Tharsis region: Global evidence in the Martian geologic record. *Journal of Geophysical Research*, *108*(E9), 5111. https://doi.org/10.1029/2003JE002062

Ivanov, M. A., & Head, J. W. (2006). Alba Patera, Mars: Topography, structure, and evolution of a unique late Hesperian-early Amazonian shield volcano. *Journal of Geophysical Research*, *111*(9), 1–31. https://doi.org/10.1029/2005JE002469

Jaupart, C., & Allègre, C. J. (1991). Gas content, eruption rate and instabilities of eruption regime in silicic volcanoes. *Earth and Planetary Science Letters*, *102*, 413–429. https://doi.org/10.1016/0012-821X(91)90032-D

Kadish, S. J., Head, J. W., Barlow, N. G., & Marchant, D. R. (2008). Martian pedestal craters: Marginal sublimation pits implicate a climate-related formation mechanism. *Geophysical Research Letters*, *35*(16), 1–5. https://doi.org/10.1029/2008GL034990

Keller, J. M., Boynton, W. V., Karunatillake, S., Baker, V. R., Dohm, J. M., Evans, L. G., et al. (2007). Equatorial and midlatitude distribution of chlorine measured by Mars Odyssey GRS. *Journal of Geophysical Research*, *112*(3), 1–18. https://doi.org/10.1029/2006JE002679

Kerber, L., & Head, J. W. (2010). The age of the Medusae Fossae Formation: Evidence of Hesperian emplacement from crater morphology, stratigraphy, and ancient lava contacts. *Icarus*, *206*(2), 669–684. https://doi.org/10.1016/j.icarus.2009.10.001

Kerber, L., & Head, J. W. (2012). A progression of induration in Medusae Fossae Formation transverse aeolian ridges: Evidence for ancient aeolian bedforms and extensive reworking. *Earth Surface Processes and Landforms*, *37*, 422–433. https://doi.org/10.1002/esp.2259

Kerber, L., Head, J. W., Madeleine, J. B., Forget, F., & Wilson, L. (2011). The dispersal of pyroclasts from Apollinaris Patera, Mars: Implications for the origin of the Medusae Fossae Formation. *Icarus*, *216*(1), 212–220. https://doi.org/10.1016/j.icarus.2011.07.035

Kerber, L., Head, J. W., Madeleine, J. B., Forget, F., & Wilson, L. (2012). The dispersal of pyroclasts from ancient explosive volcanoes on Mars: Implications for the friable layered deposits. *Icarus*, *219*(1), 358–381. https://doi.org/10.1016/j.icarus.2012.03.016

Krysak, D. J. (2011). *The geologic history of Apollinaris Mons, Mars*. University of Buffalo, State University of New York.

Kumar, P. S., & Kring, D. A. (2008). Impact fracturing and structural modification of sedimentary rocks at Meteor Crater, Arizona. *Journal of Geophysical Research*, *113*(9), 1–17. https://doi.org/10.1029/2008JE003115

Leask, H. J., Wilson, L., & Mitchell, K. L. (2006). Formation of Aromatum Chaos, Mars: Morphological development as a result of volcano-ice interactions. *Journal of Geophysical Research*, *111*(8). https://doi.org/10.1029/2005JE002549

Levy, J. S., Head, J. W., & Marchant, D. R. (2009). Concentric crater fill in Utopia Planitia: History and interaction between glacial "brain terrain" and periglacial mantle processes. *Icarus*, *202*(2), 462–476. https://doi.org/10.1016/j.icarus.2009.02.018

Lipman, P. W. (1976). Caldera-collapse breccias in the western San Juan Mountains, Colorado. *Bulletin of the Geological Society of America*, *87*(10), 1397–1410. https://doi.org/10.1130/0016-7606(1976)87<1397:CBITWS>2.0.CO;2

Lipman, P. W. (1997). Subsidence of ash-flow calderas: relation to caldera size and magma-chamber geometry. *Bulletin of Volcanology*, *59*(3), 198–218. https://doi.org/10.1007/s004450050186

Mackaman-Lofland, C., Brand, B. D., Taddeucci, J., & Wohletz, K. (2014). Sequential fragmentation/transport theory, pyroclast size-density relationships, and the emplacement dynamics of pyroclastic density currents - A case study on the Mt. St. Helens (USA) 1980 eruption. *Journal of Volcanology and Geothermal Research*, *275*, 1–13. https://doi.org/10.1016/j.jvolgeores.2014.01.016

MacLeod, N. S., Sherrod, D. R., Chitwood, L. A., & Jensen, R. A. (1995). Geologic map of Newberry Volcano, Deschutes, Klamath, and Lake counties, Oregon. Imap.

Malin, M. C. (1979). Mars: Evidence of indurated depositsof fine materials. In *Mars, Abstracts from the Second International Colloquium* (p. 54).

Malin, M. C., & Edgett, K. S. (2000). Sedimentary rocks of early Mars. *Science*, *290*(5498), 1927–1937. https://doi.org/10.1126/science.290.5498.1927

Malin, M. C., Bell, J. F., Cantor, B. A., Caplinger, M. A., Calvin, W. M., Clancy, R. T., et al. (2007). Context Camera Investigation on board the Mars Reconnaissance Orbiter. *Journal of Geophysical Research*, *112*(5), 1–25. https://doi.org/10.1029/2006JE002808

Mandt, K. E., de Silva, S. L., Zimbelman, J. R., & Crown, D. A. (2008). Origin of the Medusae Fossae Formation, Mars: Insights from a synoptic approach. *Journal of Geophysical Research*, *113*(12), E12011. https://doi.org/10.1029/2008JE003076

Masursky, H. (1973). An overview of geological results from Mariner 9. *Journal of Geophysical Research*, *78*(20), 4009–4030. https://doi.org/10.1029/JB078i020p04009

Max, M. D., & Clifford, S. M. (2001). Initiation of Martian outflow channels: Related to the dissociation of gas hydrate? *Geophysical Research Letters*, *28*(9), 1787–1790. https://doi.org/10.1029/2000GL011606

Mccauley, J. F. (1973). Mariner 9 evidence for wind erosion in the equatorial and mid-latitude regions of Mars. *Journal of Geophysical Research*, *78*(20), 4123–4137. https://doi.org/10.1029/JB078i020p04123

McEwen, A. S., Eliason, E. M., Bergstrom, J. W., Bridges, N. T., Hansen, C. J., Delamere, W. A., et al. (2007). Mars reconnaissance orbiter's high resolution imaging science experiment (HiRISE). *Journal of Geophysical Research*, *112*(5), 1–40. https://doi.org/10.1029/2005JE002605

McSween, H. Y. (1985). SNC meteorites - Clues to Martian petrologic evolution? *Reviews of Geophysics*, *23*(4), 391–416. https://doi.org/10.1029/RG024i001p00141

Mellon, M. T., Jakosky, B. M., Kieffer, H. H., & Christensen, P. R. (2000). High-Resolution Thermal Inertia Mapping from the Mars Global Surveyor Thermal Emission Spectrometer. *Icarus*, *148*(2), 437–455. https://doi.org/10.1006/icar.2000.6503

Meresse, S., Costard, F., Mangold, N., Masson, P., & Neukum, G. (2008). Formation and evolution of the chaotic terrains by subsidence and magmatism: Hydraotes Chaos, Mars. *Icarus*, *194*(2), 487–500. https://doi.org/10.1016/j.icarus.2007.10.023

Michael, G. G. (2013). Planetary surface dating from crater size-frequency distribution measurements: Multiple resurfacing episodes and differential isochron fitting. *Icarus*, *226*(1), 885–890. https://doi.org/10.1016/j.icarus.2013.07.004

Michalski, J. R., & Bleacher, J. E. (2013). Supervolcanoes within an ancient volcanic province in Arabia Terra, Mars. *Nature*, *502*(7469), 47–52. https://doi.org/10.1038/nature12482

Miller, C. F., & Wark, D. A. (2008). Supervolcanoes and their explosive supereruptions. *Elements*, *4*, 11–16. https://doi.org/10.2113/GSELEMENTS.4.1.11

Montgomery, D. R., & Gillespie, A. (2005). Formation of Martian outflow channels by catastrophic dewatering of evaporite deposits. *Geology*, *33*(8), 625–628. https://doi.org/10.1130/G21270.1

Moore, J. M. (1990). Nature of the mantling deposit in the heavily cratered terrain of northeastern Arabia, Mars. *Journal of Geophysical Research*, *95*(B9), 14279. https://doi.org/10.1029/JB095iB09p14279

Mouginis-Mark, P. J. (1992). Emplacement of long lava flows at Elysium Mons, Mars. In *23rd Lunar and Planetary Science Conference* (Vol. 23, p. 939).

Mouginis-Mark, P. J., Wilson, L., & Head III, J. W. (1982). Explosive Volcanism on Hecates Tholus, Mars' Investigation of Eruption Conditions. *Journal of Geophysical Research*, *87*(30), 9890–9904. https://doi.org/10.1029/JB087iB12p09890

Mouginis-Mark, P. J., Wilson, L., & Zimbelman, J. R. (1988). Polygenic Eruptions on Alba-Patera, Mars. *Bulletin of Volcanology*, *50*(6), 361–379.

Ogawa, Y. (2003). Correction to "Evaluation of melting process of the permafrost on Mars: Its implication for surface features" by Yoshiko Ogawa, Yasuko Yamagishi, and Kei Kurita. *Journal of Geophysical Research*, *108*(E7), 5071. https://doi.org/10.1029/2003JE002118

Okubo, C. H., & Schultz, R. A. (2002). Fault geometry below wrinkle ridges based on slope asymmetry and implications for mechanical stratigraphy. In *33rd Lunar and Planetary Science Conference* (p. 1708, [Abst.]).

Palladino, D. M., & Valentine, G. A. (1995). Coarse-tail vertical and lateral grading in pyroclastic flow deposits of the Latera Volcanic Complex (Vulsini, central Italy): origin and implications for flow dynamics. *Journal of Volcanology and Geothermal Research*, *69*(3–4), 343–364. https://doi.org/10.1016/0377-0273(95)00036-4

Platz, T., Byrne, P. K., Massironi, M., & Hiesinger, H. (2015). Volcanism and tectonism across the inner solar system: an overview. *Geological Society, London, Special Publications*, *401*(1), 1–56. https://doi.org/10.1144/SP401.22

Plescia, J. B., & Golombek, M. P. (1986). Origin of planetary wrinkle ridges based on the study of terrestrial analogs. *Geological Society of America Bulletin*, *97*(11), 1289–1299. https://doi.org/10.1130/0016-7606(1986)97<1289:OOPWRB>2.0.CO

Presley, M. A. (2002). What Can Thermal Inertia Do for You? In *33rd Lunar and Planetary Science Conference* (pp. 18–19).

Reimers, C. E., & Komar, P. D. (1979). Evidence for explosive volcanic density currents on certain Martian volcanoes. *Icarus*, *39*(1), 88–110. https://doi.org/10.1016/0019-1035(79)90103-9

Robbins, S. J., & Hynek, B. M. (2012). A new global database of Mars impact craters ≥1 km: 1. Database creation, properties, and parameters. *Journal of Geophysical Research*, *117*(5), 1–18. https://doi.org/10.1029/2011JE003966

Robbins, S. J., Di Achille, G., & Hynek, B. M. (2011). The volcanic history of Mars: High-resolution crater-based studies of the calderas of 20 volcanoes. *Icarus*, *211*(2), 1179–1203. https://doi.org/10.1016/j.icarus.2010.11.012

Robinson, M. S., Mouginis-Mark, P. J., Zimbelman, J. R., Wu, S. S. C., Ablin, K. K., & Howington-Kraus, A. E. (1993). Chronology, Eruption Duration, and Atmospheric Contribution of the Martian Volcano Apollinaris Patera. *Icarus*, *104*(2), 301–323. https://doi.org/10.1006/icar.1993.1103

Roda, M., Kleinhans, M. G., Zegers, T. E., & Oosthoek, J. H. P. (2014). Catastrophic ice lake collapse in Aram Chaos, Mars. *Icarus*, *236*, 104–121. https://doi.org/10.1016/j.icarus.2014.03.023

Roda, M., Kleinhans, M. G., Zegers, T. E., & Govers, R. (2016). Origin of circular collapsed landforms in the Chryse region of Mars. *Icarus*, *265*, 70–78. https://doi.org/10.1016/j.icarus.2015.10.020

Rodriguez, J. A. P., Sasaki, S., Kuzmin, R. O., Dohm, J. M., Tanaka, K. L., Miyamoto, H., et al. (2005). Outflow channel sources, reactivation, and chaos formation, Xanthe Terra, Mars. *Icarus*, *175*(1), 36–57. https://doi.org/10.1016/j.icarus.2004.10.025

Ruff, S. W., Christensen, P. R., Blaney, D. L., Farrand, W. H., Johnson, J. R., Michalski, J. R., et al. (2006). The rocks of Gusev Crater as viewed by the Mini-TES instrument. *Journal of Geophysical Research*, *111*(12), 1–36. https://doi.org/10.1029/2006JE002747

Sagan, C., Veverka, J., Fox, P., Dubisch, R., Lederberg, J., Levinthal, E., et al. (1972). Variable features on Mars: Preliminary mariner 9 television results. *Icarus*, *17*(2), 346–372. https://doi.org/10.1016/0019-1035(72)90005-X

Schultz, P. H., & Lutz, A. B. (1988). Polar wandering of Mars. *Icarus*, *73*(1), 91–141. https://doi.org/10.1016/0019-1035(88)90087-5

Schultz, R. A. (2000). Localization of bedding plane slip and backthrust faults above blind thrust faults: Keys to wrinkle ridge structure. *Journal of Geophysical Research*, *105*(E5), 12035–12052. https://doi.org/10.1029/1999JE001212

Schultz, R. A. (2002). Stability of rock slopes in Valles Marineris, Mars. *Geophysical Research Letters*, *29*(19), 38-1-38–4. https://doi.org/10.1029/2002GL015728

Scott, D. H., & Tanaka, K. L. (1982). Ignimbrites of Amazonis Planitia region of Mars. *Journal of Geophysical Research*, *87*(1), 1179–1190. https://doi.org/10.1029/JB087iB02p01179

Scott, D. H., & Tanaka, K. L. (1986). Geologic map of the western equatorial region of Mars. U. S. Geological Survey Misc.

Scott, D. H., Dohm, J. M., & Applebee, D. J. (1993). Geologic map of science study area 8, Apollinaris Patera region of Mars. Reston, VA.

Séjourné, A., Costard, F., Gargani, J., Soare, R. J., Fedorov, A., & Marmo, C. (2011). Scalloped depressions and small-sized polygons in western Utopia Planitia, Mars: A new formation hypothesis. *Planetary and Space Science*, *59*(5–6), 412–422. https://doi.org/10.1016/j.pss.2011.01.007

Self, S. (2006). The effects and consequences of very large explosive volcanic eruptions. *Philosophical Transactions of the Royal Society A: Mathematical, Physical and Engineering Sciences*, *364*(1845), 2073–2097. https://doi.org/10.1098/rsta.2006.1814

Sharp, R. P. (1973). Mars: Fretted and chaotic terrains. *Journal of Geophysical Research*, *78*(20), 4073–4083. https://doi.org/10.1029/JB078i020p04073

Sheridan, M. F. (1970). Fuarmolic mounds and ridges of the bishop tuff, california. *Bulletin of the Geological Society of America*, *81*(3), 851–868. https://doi.org/10.1130/0016-7606(1970)81[851:FMAROT]2.0.CO;2

de Silva, S. L., & Bailey, J. E. (2017). Some unique surface patterns on ignimbrites on Earth: A "bird's eye" view as a guide for planetary mappers. *Journal of Volcanology and Geothermal Research*, *342*, 47–60. https://doi.org/10.1016/j.jvolgeores.2017.06.009

de Silva, S. L., Bailey, J. E., Mandt, K. E., & Viramonte, J. M. (2010). Yardangs in terrestrial ignimbrites: Synergistic remote and field observations on Earth with applications to Mars. *Planetary and Space Science*, *58*(4), 459–471. https://doi.org/10.1016/j.pss.2009.10.002

Smith, D. E., Zuber, M. T., Frey, H. V., Garvin, J. B., Head, J. W., Muhleman, D. O., et al. (2001). Mars Orbiter Laser Altimeter: Experiment summary after the first year of global mapping of Mars. *Journal of Geophysical Research*, *106*(E10), 23689–23722. https://doi.org/10.1029/2000JE001364

Tanaka, K. L. (2003). Resurfacing history of the northern plains of Mars based on geologic mapping of Mars Global Surveyor data. *Journal of Geophysical Research*, *108*(E4), 8043. https://doi.org/10.1029/2002JE001908

Tanaka, K. L., Carr, M. H., Skinner, J. A., Gilmore, M. S., & Hare, T. M. (2003). Geology of the MER 2003 “Elysium” candidate landing site in southeastern Utopia Planitia, Mars. *Journal of Geophysical Research*, *108*(E12). https://doi.org/10.1029/2003JE002054

Tanaka, K. L., Skinner, J. A., Dohm, J. M., Irwin, R. P., Kolb, E. J., Fortezzo, C. M., et al. (2014). *Geologic Map of Mars*. *U.S. Geological Survey Scientific Investigations*. Reston, VA. https://doi.org/10.3133/sim3292

Theilig, E., & Greeley, R. (1986). Lava flows on Mars: analysis of small surface features and comparisons with terrestrial analogs. *Journal of Geophysical Research*, *v. 91*(B13), E193–E206.

Tizzani, P., Berardino, P., Casu, F., Euillades, P., Manzo, M., Ricciardi, G. P., et al. (2007). Surface deformation of Long Valley caldera and Mono Basin, California, investigated with the SBAS-InSAR approach. *Remote Sensing of Environment*, *108*(3), 277–289. https://doi.org/10.1016/j.rse.2006.11.015

Tornabene, L. L., Osinski, G. R., McEwen, A. S., Boyce, J. M., Bray, V. J., Caudill, C. M., et al. (2012). Widespread crater-related pitted materials on Mars: Further evidence for the role of target volatiles during the impact process. *Icarus*, *220*(2), 348–368. https://doi.org/10.1016/j.icarus.2012.05.022

Vergniolle, S., & Jaupart, C. (1986). Separated two-phase flow and basaltic eruptions. *Journal of Geophysical Research*, *91*(B12), 842–860.

Ward, A. W. (1979). Yardangs on Mars: Evidence of recent wind erosion. *Journal of Geophysical Research*, *84*(9), 8147. https://doi.org/10.1029/JB084iB14p08147

Watters, T. R. (1993). Compressional tectonism on Mars. *Journal of Geophysical Research*, *98*(E9), 17049. https://doi.org/10.1029/93JE01138

West, M. (1974). Martian volcanism: Additional observations and evidence for pyroclastic activity. *Icarus*, *21*(1), 1–11. https://doi.org/10.1016/0019-1035(74)90085-2

Wilhelms, D. E., & Baldwin, R. J. (1988). The role of Igneous sills in shaping the martian uplands. In *19th Lunar and Planetary Science Conference* (pp. 355–365). https://doi.org/10.1017/CBO9781107415324.004

Williams, D. A., Greeley, R., Werner, S. C., Michael, G., Crown, D. A., Neukum, G., & Raitala, J. (2008). Tyrrhena Patera: Geologic history derived from Mars Express High Resolution Stereo Camera. *Journal of Geophysical Research*, *113*(11), 1–14. https://doi.org/10.1029/2008JE003104

Williams, H., Soediono, B., & Williams, H. (1942). The geology of Crater Lake National Park, Oregon, with a reconnaissance of the Cascade Range southward to Mount Shasta. Carnegie Institution of Washington publication (Vol. 540). Washington, D.C.: [Carnegie Institution of Washington?]. https://doi.org/10.1017/CBO9781107415324.004

Wilson, L., & Head, J. W. (1983). A comparison of volcanic eruption processes on Earth, Moon, Mars, Io and Venus. *Nature*, *302*(5910), 663–669. https://doi.org/10.1038/302663a0

Wilson, L., & Mouginis-Mark, P. J. (1987). Volcanic input to the atmosphere from Alba Patera on Mars. *Nature*, *330*(26 November 1987), 354–357.

Woods, A. W. (1995). The dynamics of explosive volcanic eruptions. *Reviews of Geophysics*, *33*(4), 495–530. https://doi.org/10.1029/95rg02096

Wrobel, K., Schultz, P., & Crawford, D. (2006). An atmospheric blast/thermal model for the formation of high-latitude pedestal craters. *Meteoritics and Planetary Science*, *41*(10), 1539–1550. https://doi.org/10.1111/j.1945-5100.2006.tb00434.x

Zabrusky, K., Andrews-Hanna, J. C., & Wiseman, S. M. (2012). Reconstructing the distribution and depositional history of the sedimentary deposits of Arabia Terra, Mars. *Icarus*, *220*(2), 311–330. https://doi.org/10.1016/j.icarus.2012.05.007

Zegers, T. E., Oosthoek, J. H. P., Rossi, A. P., Blom, J. K., & Schumacher, S. (2010). Melt and collapse of buried water ice: An alternative hypothesis for the formation of chaotic terrains on Mars. *Earth and Planetary Science Letters*, *297*, 496–504. https://doi.org/10.1016/j.epsl.2010.06.049

Zimbelman, J. R., & Griffin, L. J. (2010). HiRISE images of yardangs and sinuous ridges in the lower member of the Medusae Fossae Formation, Mars. *Icarus*, *205*(1), 198–210. https://doi.org/10.1016/j.icarus.2009.04.003